Research supported by the National Science Foundation under grant ATM-0071371, and by a one-year AMS Graduate Fellowship

CLIMATOLOGICAL AND RADAR-INDICATED CHARACTERISTICS OF UNITED STATES EXTREME RAIN EVENTS

by

Russ Schumacher

Richard H. Johnson, P.I.

Colorado State University

DEPARTMENT OF ATMOSPHERIC SCIENCE

PAPER NO. 743

CLIMATOLOGICAL AND RADAR-INDICATED CHARACTERISTICS OF UNITED STATES EXTREME RAIN EVENTS

by

Russ Schumacher

Department of Atmospheric Science
Colorado State University
Fort Collins, CO 80523-1371

Fall 2003

Atmospheric Science Paper # 743

ABSTRACT

CLIMATOLOGICAL AND RADAR-INDICATED CHARACTERISTICS OF UNITED STATES EXTREME RAIN EVENTS

This study examines the radar-indicated structures and other features of extreme rain events in the United States over a three-year period. A rainfall event is defined as "extreme" when the 24-h precipitation total at one or more stations surpasses a threshold that varies spatially based on the frequency of heavy rain in that location. Using the National Weather Service high-resolution rain gauge network, and eliminating bad precipitation data, this definition yields 193 such events from 1999 to 2001 in the area east of the Rocky Mountains, excluding Florida.

The monthly frequency distribution of extreme rain events generally agrees with previous studies of precipitation systems. There is an overall maximum in June, July, and August, though events occur in every month of the year. In the northern part of the country, extreme rainfall is almost exclusively confined to the warm season. In contrast, the distribution in the south indicates that extreme rainfall there is less dependent on season.

Two-km national composite radar reflectivity data are used to examine the structure and evolution of each extreme rain event. In the northern and Great Plains states, almost all of the extreme rain events are associated with mesoscale convective systems (MCSs), while in the northeast and southeast, synoptic-scale weather systems and tropical cyclones play a much greater role. In total, 59% of the total number of events are associated with MCSs. The heavy rain from extreme-rain-producing MCSs typically begins in the evening, peaks sometime after dark, and dissipates or moves away in the early morning hours.

While a wide variety of organizational structures (as indicated by the reflectivity data) were seen among the MCS cases, two patterns of organization were observed most frequently. The first pattern has a line with "training" convective elements and an adjoining region of stratiform rain. The second has a backbuilding convective line/cluster with a parallel region of stratiform rain downstream. The organization of each type of MCS is conducive to large rainfall accumulations.

Composite analysis of RUC–2 model analyses reveals that training line/adjoining stratiform (TL/AS) systems typically form under deep atmospheric moisture on the cool side of a pre-existing slow-moving surface boundary, while backbuilding with parallel stratiform (BPS) MCSs also occur in a very moist environment but are more dependent on mesoscale and storm-scale processes than on pre-existing synoptic boundaries. Two case studies are also presented that further reinforce the conclusions drawn from the composite analysis.

Russ Stanley Schumacher
Department of Atmospheric Science
Colorado State University
Fort Collins, Colorado 80523-1371
Fall 2003

ACKNOWLEDGEMENTS

This research was supported by National Science Foundation grant ATM–0071371 and by a one-year American Meteorological Society Graduate Fellowship.

The national composite radar data were provided by the Global Hydrology Resource Center (GHRC) at the Global Hydrology and Climate Center, Huntsville, Alabama. Precipitation data were provided by the National Climatic Data Center. RUC–2 analyses were obtained from the Atmospheric Radiation Measurement (ARM) Program sponsored by the U.S. Department of Energy, Office of Science, Office of Biological and Environmental Research, Environmental Sciences Division.

I would like to thank the members of my graduate committee, Drs. David Thompson and Jorge Ramirez, for their service in reviewing my work and providing valuable suggestions. I would especially like to thank my advisor, Dr. Richard Johnson, for all of his guidance, suggestions, and encouragement in the process of performing the analysis and writing this manuscript, as well as for the many conversations about the importance and relevance of this work.

I would also like to thank Dr. Matt Parker for his insights into the issue of classifying MCSs and Dr. David Schultz of the National Severe Storms Laboratory for discussions about this work and for continuing to motivate my research in the atmospheric sciences. Thanks go to the members of the Johnson research group—Rick Taft, Paul Ciesielski, Gail Cordova, Crystal Pettet, and Brian McNoldy—for their assistance in all areas of completing this project. Finally, I would like to thank my family and friends for supporting me in this and all of my endeavors.

CONTENTS

FIGURES

TABLES

Chapter 1

INTRODUCTION

Flash flooding, defined as flooding that occurs within six hours of its causative rainfall, is responsible for more fatalities in the United States each year than any other convective storm-related phenomenon, including tornadoes, hurricanes, and lightning (NOAA 2003). After several especially destructive events in the 1970s, flash floods and extreme rain events received increased attention from the research and operational forecasting communities. Since then, many advances have been made toward understanding the processes that lead to flash flooding. However, predicting such events remains a difficult task, in part because they often occur on very small scales and can result from a wide variety of storm types. In addition, successful forecasting of a flash flood requires not only an accurate meteorological prediction (i.e., the location and amount of rainfall), but a hydrological prediction as well. As put by Doswell et al. (1996), "a flash flood event is the concatenation of a meteorological event with a particular hydrological situation."

When initiating a study of flash floods, one must then decide whether to consider the meteorological or hydrological aspects of the event(s), or both. As noted by Droegemeier et al. (2000), "in the educational, research, and operational frameworks, meteorology and hydrology have evolved along independent and even divergent paths." At the current time, this makes investigating both the meteorology and hydrology of a large number of flash flood events next to impossible. This study, then, will focus on meteorological aspects of weather systems that often produce flash flooding, which, using the terminology of Bradley and Smith (1994) and others, will be called "extreme rain events." For the most part,

the events considered here will be selected and evaluated using meteorological observations (i.e., rain gauge data) without regard for the magnitude of flash flooding. The hydrological aspects of these events will not be ignored, but are for the most part beyond the scope of this study.

The best example of a flash flood "climatology" in the scientific literature is the study by Maddox et al. (1979). They examined the synoptic and mesoscale atmospheric conditions during 151 flash flood events in all parts of the United States and pinpointed four surface and upper-air patterns in which the events typically formed. Chappell (1986) reviewed the state of the science regarding quasi-stationary convection and provided several examples of such convective events. More recently, Doswell et al. (1996) and Davis (2001) described techniques that can be used to forecast extreme rainfall and made mention of the storm structures often responsible for producing it. Several gaps remain in the understanding of extreme-rain-producing weather systems, however. There is very little quantitative information about whether extreme rainfall is most often produced by synoptic weather systems, mesoscale convective systems (MCSs), tropical cyclones, or other types of weather systems. In addition, such characteristics are not likely to be uniform throughout the country, so information about the spatial and temporal variations in the types of weather systems that produce extreme rainfall would also be valuable. While the atmospheric conditions conducive to extreme rainfall have been relatively well-documented, the organizational structures of the storms that form in these conditions have not been thoroughly explored. A radar-based analysis of a large sample of extreme rain events will be presented herein, which will help to answer these questions and to further clarify where, when, how often, and in what form extreme rain events are most likely to occur in the United States.

In the chapters to follow, rain gauge data from a three-year period are used to select extreme rain events and to analyze the annual and diurnal characteristics of these events in different regions of the United States. Then, composite radar reflectivity data

are used to observe the type of weather system responsible for the extreme rainfall in each case. Over half of the events are associated with mesoscale convective systems (MCSs), and two patterns of convective organization are most frequently observed. These patterns are described, and the synoptic and mesoscale conditions in which they typically occur are presented. Finally, two extreme rain events are examined in greater detail to provide further insight into the processes responsible for extreme local rainfall and the destructive flash flooding that it often causes.

Chapter 2

BACKGROUND AND MOTIVATION

2.1 Events motivating past studies

As with other areas involving convective storms, much of the published research on the subject of flash floods has been motivated by particularly damaging or otherwise notable events. Two such events that received much attention in the literature (and sparked even further flash flood research) were the Big Thompson Canyon, Colorado flood of 31 July 1976 (Maddox et al. 1978, Caracena et al. 1979, Yoshizaki and Ogura 1988), and the Johnstown, Pennsylvania flood of 19-20 July 1977 (Hoxit et al. 1978, Bosart and Sanders 1981, Zhang and Fritsch 1986, 1987, and 1988). These floods were responsible for 139 and 77 fatalities, respectively, and emphasized that extreme damage and loss of life from intense convective rainfall can occur in all parts of the country and in widely varying conditions.

Some more recent examples of valuable case studies are those of Schwartz et al. (1990), who studied the 1987 Minneapolis flash flood; Petersen et al. (1999) on the 1997 Fort Collins flash flood; Pontrelli et al. (1999) on the 1995 Madison County, Virginia flash flood; and Smith et al. (2001) on flash flood-producing supercells in Texas, Florida, Nebraska, and Pennsylvania.

2.2 Flash flood and extreme rain climatology

While case studies provide great insights into the form and function of weather systems, the climatological characteristics of such events are also important to ascertain. As

Table 2.1: Thresholds for determining extreme rainfall used in some past studies.

Reference	Study area	Terminology	Definition
Changnon and Vogel (1981)	Illinois	"isolated severe rainstorm"	75 mm in 1-4 h over less than 1000 km^2
Crysler et al. (1982)	Central and Eastern U.S.	"heavy precipitation event"	102 mm in 8 h
Belville and Stewart (1983)	Louisiana	"extreme rain event"	storm total > 200 mm
Winkler (1988)	Minnesota	"extreme rainstorm"	76 mm in 24 h
Foufoula-Georgiou and Wilson (1990)	Midwest U.S.	"extreme rainstorm"	storm total > 230 mm
Houze et al. (1990)	Oklahoma	"major rain event"	25 mm over 12500 km^2 in 24 h
Giordano and Fritsch (1991)	mid-Atlantic region	"intense rainstorm"	190 mm in 12 h
Bradley and Smith (1994)	Southern Plains	"extreme rainstorm"	125 mm in 24 h
Konrad (1997)	Southeastern U.S.	"heavy rain event"	50 mm in 6 h
Junker et al. (1999)	Midwest U.S.	"heavy rainfall event"	50 mm in 24 h
Brooks and Stensrud (2000)	Entire U.S.	"heavy rain event"	25 mm in 1 h, and 100 mm in 3 h

such, many investigators have attempted to determine the climatological characteristics of flash flood and extreme rain events. One problem in this endeavor, which will be discussed again later, is that there is no accepted definition of such an event. As mentioned in chapter 1, the National Weather Service (NWS) defines a flash flood as one which occurs within six hours of the causative rainfall. However, there is no consistent way to "measure" this, aside from the flooding and damage reports in the National Atmospheric and Oceanic Administration (NOAA) *Storm Data* publication and other eyewitness reports. While some investigators have used the flood reports to create flash flood climatologies (e.g., Maddox et al. 1979, hereafter MCH79), many others have used rainfall totals as measured by rain gauges to select events for their studies. Table 2.1 offers a sampling of the different criteria used in the past to define such events.

Certain atmospheric ingredients must be in place for extreme rainfall to occur, regardless of how it is defined. Doswell et al. (1996, hereafter DBM96) describe these ingredients using a simple formula for any point on the earth:

$$P = \overline{R}D \tag{2.1}$$

where P is the total precipitation, $\overline{R}$ is the average rainfall rate, and D is the duration of the rainfall. Thus, for large precipitation totals, either the rainfall rate or the rain duration (or both) must be large. Further, since precipitation results from lifting moist air to condensation,

$$R = Ewq \tag{2.2}$$

where E is the precipitation efficiency, w the ascent rate in an updraft, and q the mixing ratio of the air. This means that rapidly ascending air with large water vapor content (i.e., large vertical moisture flux) is necessary to produce a significant rainfall rate. The rainfall rate is also limited by the precipitation efficiency, the proportion of water going into the system that actually falls out as precipitation. DBM96 also point out that rainfall duration is related to the system size and speed and the variations in rainfall intensity within a storm. Slow-moving storms increase the rainfall duration at a given point, and are thus conducive to extreme rainfall totals.

MCH79 listed four characteristics of the atmosphere that were common to almost all of the flash floods they studied, regardless of their location:

(1) Heavy rains were produced by convective storms,

(2) Surface dewpoint temperatures were very high,

(3) Large moisture contents were present through a deep tropospheric layer,

(4) Vertical wind shear was weak to moderate through the cloud depth,

In other words, satisfying the above equations, the necessary moisture and ascent were in place for large rainfall rates, and weak to moderate vertical shear allowed for organized but

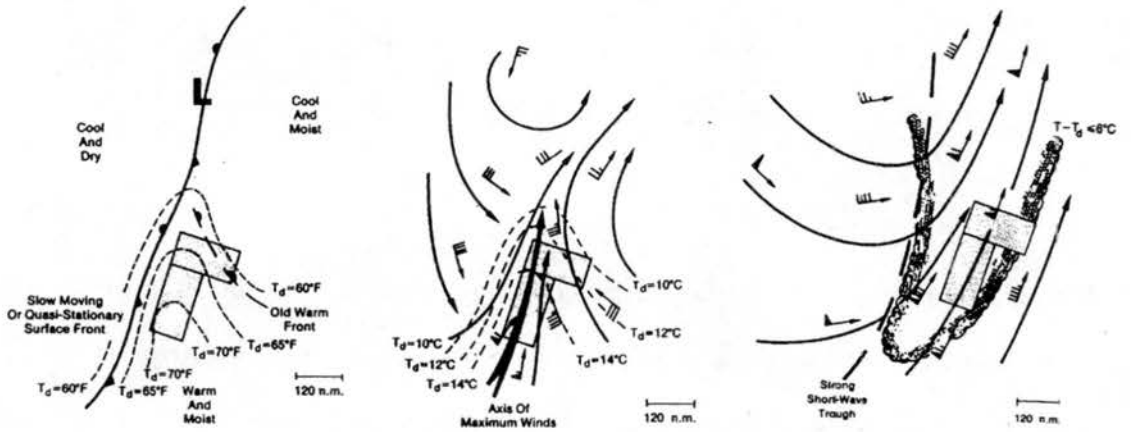

(a) Surface (b) 850 hPa (c) 500 hPa

Figure 2.1: (a) Surface, (b) 850-hPa, and (c) 500-hPa patterns for a typical synoptic type flash flood event. Potential for heavy rains and flash flooding exists in the shaded areas. Winds are in knots with full barb representing 10 kt and flag representing 50 kt. From Maddox et al. (1979).

slow-moving storms.

2.2.1 Synoptic and mesoscale environments of extreme rain events

Once the necessary ingredients for extreme rainfall have been determined, it is important to know more about the synoptic and mesoscale atmospheric conditions most often responsible for bringing these ingredients together. These conditions as they relate to extreme rain events and flash floods have been well-documented in the literature. MCH79 examined 151 flash flood events and determined that one of four patterns described each event: synoptic, frontal, mesohigh, or western. (Western events will not be discussed in detail here, because the events being considered in the present study are limited to the part of the United States east of the Rocky Mountains.)

Synoptic events comprised 20% of their sample, and are associated with synoptic-scale cyclones or frontal systems. In these events, the flash flooding typically occurs ahead of a strong upper-level trough and an associated slow-moving surface front (Fig. 2.1).

The frontal and mesohigh patterns are distinctly different from the synoptic pattern,

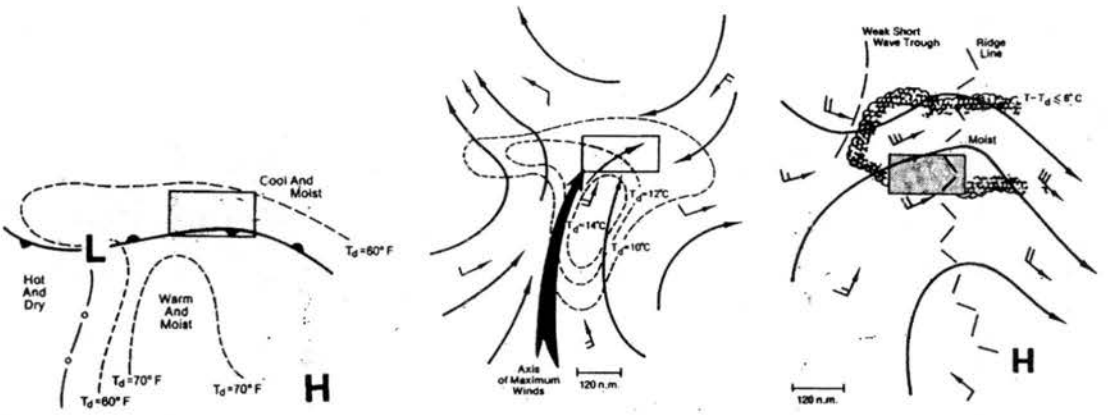

(a) Surface (b) 850 hPa (c) 500 hPa

Figure 2.2: As in Fig. 2.1, except for a typical frontal event. From Maddox et al. (1979)

and are likely associated with mesoscale convective systems (MCSs) in most cases, though this is not discussed by MCH79. While synoptic type flash floods typically occur in the warm sector of the weather system (i.e., on the warm side of a cold front), frontal and mesohigh flash floods occur on the cool side of a boundary.

Frontal events (comprising 25% of their sample) are typically triggered by a surface boundary oriented west-to-east, usually in the form of a stationary or warm front (Fig. 2.2a). Warm, moist air from the south flows over the boundary, leading to convection on the cool side (Fig. 2.2b). Winds aloft are approximately parallel to the boundary, and the heavy rains often occur near the large-scale ridge position (Fig. 2.2c) with a weak midlevel shortwave trough upstream. This arrangement leads to the development of new storms upstream, while mature cells are carried downstream by the upper-level winds. Trier and Parsons (1993) further described such a frontal situation as a forcing mechanism for MCSs.

Mesohigh events (comprising 34% of their sample) are triggered by a quasi-stationary outflow boundary left behind by previous convection, with the heaviest rain falling on the cool side of the boundary and to the south or southwest of a convectively-generated mesohigh pressure center (Fig. 2.3a). The surface pattern is less defined for this type of event; MCH79 noted that some events occurred with a slow-moving surface front to the

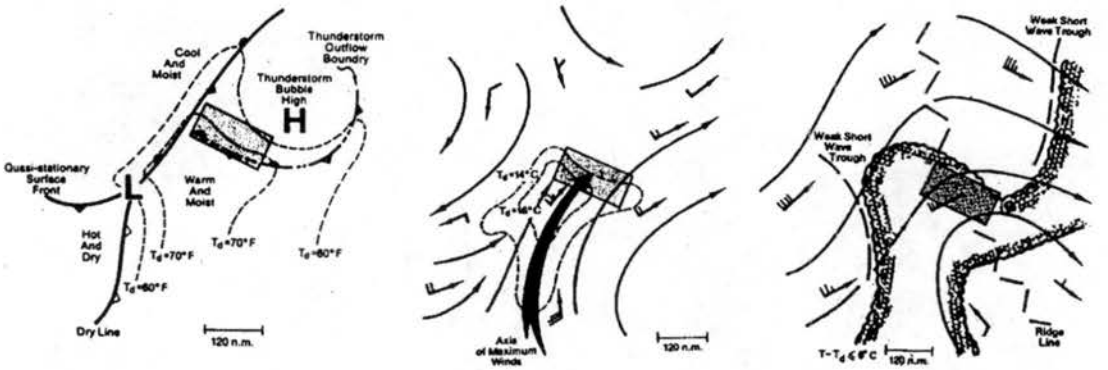

(a) Surface (b) 850 hPa (c) 500 hPa

Figure 2.3: As in Fig. 2.1, except for a typical mesohigh event. From Maddox et al. (1979)

west, while for others there were no nearby fronts. As with the frontal type, the upper-level winds are approximately parallel to the outflow boundary (Fig. 2.3c), allowing storms to repeatedly develop and move over the same area.

Others have expanded upon the ideas presented by MCH79 and introduced additional patterns that are often observed in conjunction with extreme rainfall. Giordano and Fritsch (1991) found that synoptic conditions during warm season extreme rain events in the Mid-Atlantic region are very similar to the mean conditions for that time of year. (DBM96 elaborated on this point: "flash flood event days are often not manifestly different from the nonevent days that preceded them. The difference between a rather nondescript day and a terrible flash flood situation many not be obvious even at the time of the morning soundings on the fateful day.") However, Giordano and Fritsch noted two important exceptions: that the dew point temperatures in the surface–850-hPa layer are well above average and that there is increased directional wind shear at low levels, which agree with the findings of MCH79.

Winkler (1988), Bradley and Smith (1994), and Konrad (1997) presented common synoptic patterns during extreme rain events in Minnesota, the Southern Plains, and the southeastern United States, respectively. Each study found, as did MCH79, that while

several different synoptic environments can be conducive to extreme rainfall, each pattern somehow brings together the ingredients discussed by DBM96. Additionally, they found that the synoptic pattern in place for a particular event can have a direct impact on the magnitude, location, and duration of the precipitation. For instance, Winkler (1988) found that extreme rain events in Minnesota with southwest flow aloft, a 500-hPa trough, and a defined surface boundary were typically more widespread and persisted longer than those downstream of an upper-level ridge with northwest flow aloft.

Glass et al. (1995) and Junker et al. (1999) used composite analysis to further elucidate the synoptic and mesoscale conditions associated with extreme precipitation, especially in Midwest events resulting from MCSs. In addition, a very recent paper by Moore et al. (2003) presented results of composite analysis for MCS-related heavy rain events that occur on the cool sides of surface boundaries. These three papers emphasized the importance of strong low-level winds (often in the form of a low-level jet) advecting warm, moist air into the region where the heavy rainfall occurs. Glass et al.'s (1995) conceptual model (Fig. 2.4) applies to both the frontal and mesohigh-type events described by MCH79, as air with high equivalent potential temperature (θ_e) is advected over a quasi-stationary surface boundary by the low-level jet. The highest potential for extreme rainfall is on the cool side of the boundary and coincides partially with the maximum of θ_e advection. Junker et al. (1999) also found that a maximum of positive θ_e advection is typically located near the rainfall maximum (Fig. 2.5).

The equivalent potential temperature is the potential temperature that a parcel of air would have if all its moisture were condensed and the resulting latent heat used to warm the parcel (Holton 1992). In other words, it is a measure of both the temperature and moisture of a parcel. For a saturated parcel, it is approximated by:

$$\theta_e \approx \theta \exp(L_c q_s / c_p T) \tag{2.3}$$

where θ is the potential temperature, L_c is the latent heat of condensation, q_s is the saturation mixing ratio, c_p is the specific heat of air at constant pressure, and T is the

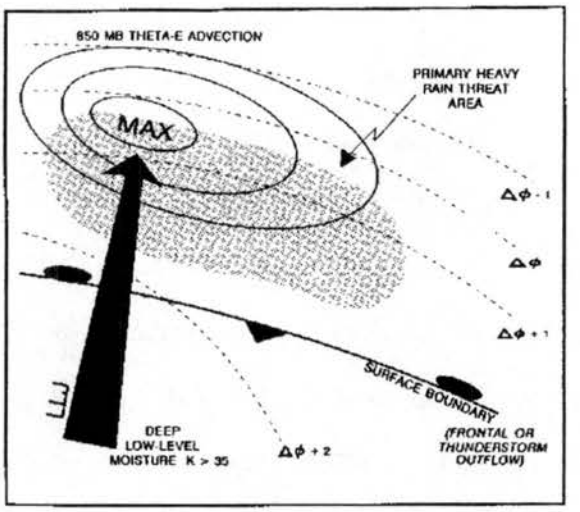

Figure 2.4: Conceptual model to highlight areas favorable for heavy convective rainfall. Dashed lines represent 850–300 hPa thickness contours. From Glass et al. (1995).

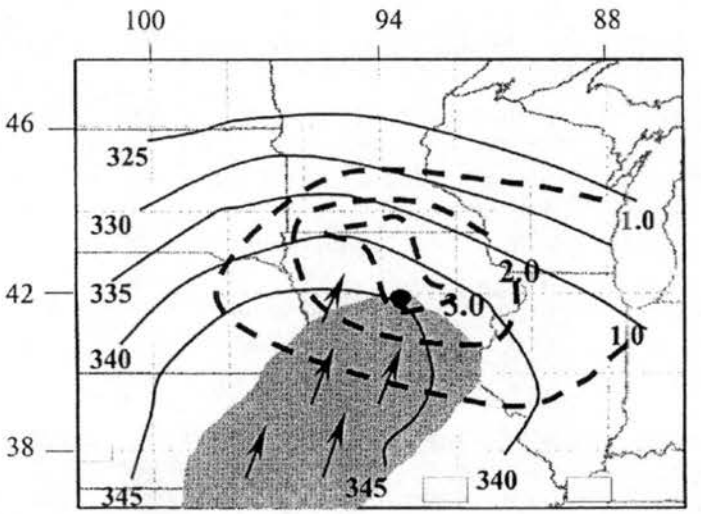

Figure 2.5: Composite of 850-hPa wind direction (arrows) and isotachs (shaded area $\geq$ 20 kt), equivalent potential temperature (solid lines, interval = 5 K), and advection of equivalent potential temperature by the wind (dashed lines, values $\geq 1 \times 10^{-4}$ K s^{-1} are contoured with a contour interval of 1×10^{-4} K s^{-1}) for 12 heavy rainfall events. The grid is centered on the location of the center of the heaviest observed isohyet. The composite has been normalized to a point in Iowa (the small black circle). From Junker et al. (1999)

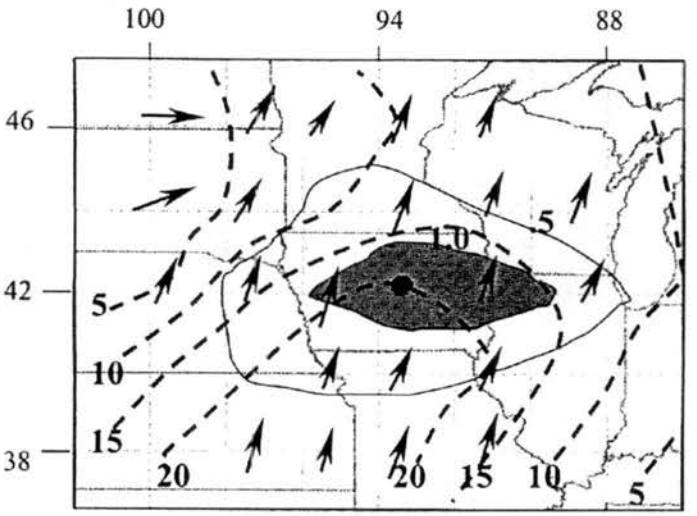

Figure 2.6: As in Fig. 2.5, except for 850-hPa wind direction (arrows), isotachs (dashed, contour interval = 5 kt), and temperature advection (solid line depicts values $\geq 0.5 \times 10^{-4}$ K s^{-1} and shaded area depicts values $\geq 1.0 \times 10^{-4}$ K s^{-1}). From Junker et al. (1999).

air temperature. The advection of θ_e is important physically because it represents the advection of both warm air *and* moisture. By the quasi-geostrophic omega equation (Holton 1992), warm-air advection results in large-scale ascent. In addition, warm air advection at low levels can increase the atmospheric instability because the temperature at low levels will increase more rapidly than the air above (i.e., an increased lapse rate.) Finally, the moisture advection may result in an increase in vertical moisture flux, which in turn may increase the amount of precipitation that falls (Eqn. 2.2).

Junker et al. (1999) found that extreme rain events often occur at the northern edge of the 850-hPa wind speed maximum (Fig. 2.6) and in a region of 850-hPa moisture flux convergence (Fig. 2.7). All three types of flash floods described by MCH79 were shown to occur to the north of the low-level wind maximum, and Augustine and Caracena (1994) also showed that MCS development is favored in this region. Low-level jets are often important to the development of extreme precipitation because they can provide a source of moisture that replenishes the moisture falling out as rain in convective storms.

Hulson (1971) demonstrated that low-level moisture convergence is often a precursor to convective initiation, and the southwest to northeast-oriented axis of moisture conver-

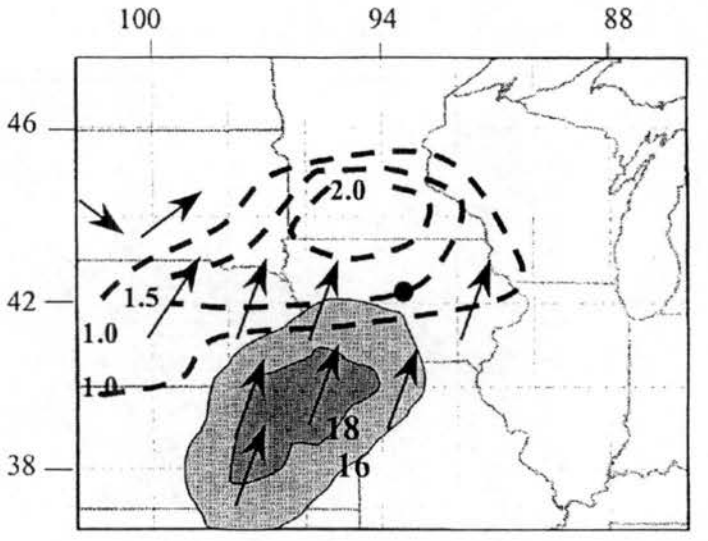

Figure 2.7: As in Fig. 2.5, except for magnitude and direction of 850-hPa moisture flux (light shaded area represents the magnitudes $\geq 16 \times 10^{-2}$ m s^{-1} and dark shaded area values $\geq 18 \times 10^{-2}$ m s^{-1}; the arrows represent the direction of the moisture flux vector) and 850-hPa moisture flux convergence. The magnitude of the moisture flux convergence is shown for values $\geq 1.0 \times 10^{-7}$ m s^{-1} contoured every 0.5×10^{-7} m s^{-1}. From Junker et al. (1999)

gence seen in Fig. 2.7 may point to the area where new cell formation is most likely. Somewhat curiously, the maximum values of 850-hPa moisture flux convergence are to the north and west of the heaviest rainfall. Junker et al. (1999) speculate that two factors are responsible for this: first, that the initial convection associated with the heavy rainfall is often rooted in the boundary layer in an area of surface moisture convergence south of the 850-hPa maximum, and second, that new convective cells may form to the north and west and then move eastward with the mean flow as they mature.

Another tool for discerning the environments of extreme rain events is to analyze representative atmospheric soundings. Figure 2.8 (from Davis 2001) shows the characteristics of such a sounding. Davis discusses how rainfall can be produced by two distinct microphysical processes: warm rain (collision-coalescence) and cold rain (ice). Warm rain processes occur in the lower levels of a storm cloud, at parcel temperatures greater than 0 °C. Mixed ice and water processes occur between 0 °C and −20 °C, and ice processes (especially hail production) occur at temperatures colder than −20 °C.

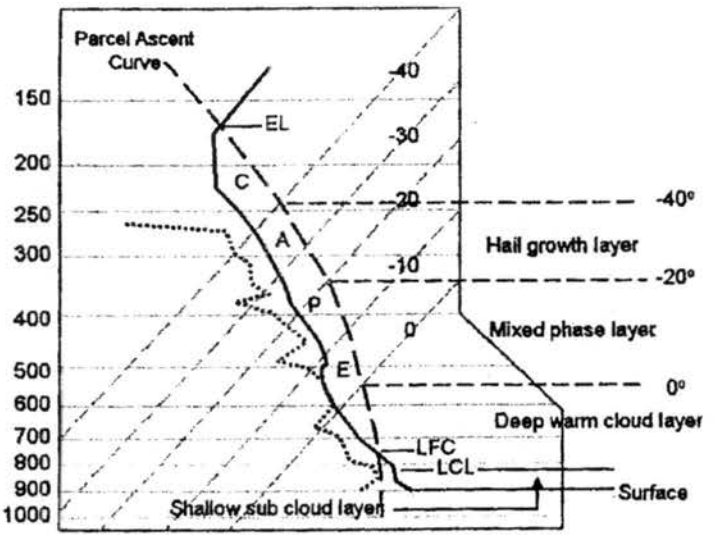

Figure 2.8: Representative skew-T log p plot for flash floods. The sounding is broken down into layers based on the microphysical processes responsible for rainfall production. The depth of the subcloud layer, warm cloud layer, mixed phase layer, and hail growth layer can be important parameters for rainfall production with warm or cold rain processes. The mean precipitable water, relative humidity, and CAPE in each layer also greatly impact the rainfall production processes. From Davis (2001).

Warm rain processes are capable of generating higher rainfall rates than cold rain processes, because they promote rapid condensation of water vapor into raindrops at low levels of the cloud, maximizing the precipitation efficiency. When the LCL is low and the freezing level is high (i.e., a deep warm cloud layer, Fig. 2.8), the potential for extreme precipitation is even greater because warm rain processes can operate in a large part of the cloud. Flash flood situations typically have warm cloud layers that are 3-4 km thick (Chappell 1993).

Chappell (1993) also notes that moderate (as opposed to very high) values of convective available potential energy (CAPE), and high values of relative humidity (RH) through a deep layer are also favorable for extreme rainfall production. High values of CAPE are usually associated with strong updrafts, which limit the amount of time that water vapor spends at low levels. These circumstances are more conducive to large hail production than heavy rainfall. A deep moist layer is important because entrainment of dry air into the

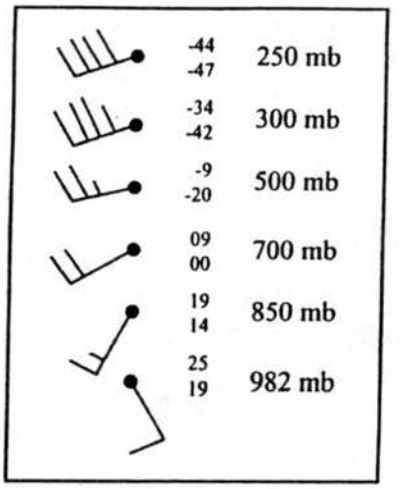

Figure 2.9: Mean vertical wind, temperature, and dewpoint profile for 85 cases of 2 in day^{-1} rainfall. Long barbs = 10 kt, short barbs = 5 kt, the top number is temperature (°C), and the bottom is dewpoint (°C). From Junker et al. (1999).

convective cloud (and thus reduction of precipitation efficiency) will be minimized. Deep moisture also limits evaporation of rainfall in the storm. Evaporation can lead to strong downdrafts and fast storm motion, which are not ideal for extreme local precipitation. (Supercell thunderstorms seem to be an exception to this rule, since they typically have a significant dry layer at midlevels, but can still produce copious amounts of rain.)

As mentioned in section 2.2, MCH79 found that flash floods commonly form in environments with weak to moderate vertical wind shear. Davis (2001) notes that the greatest threat for extreme rainfall occurs when low-level southerly flow is strong while winds veer with height, promoting storm motion along an east-west oriented boundary (as in MCH79's frontal and mesohigh type flash flood scenarios.) Junker et al. found similar behavior when taking the average of 85 heavy rainfall soundings (Fig. 2.9).

To summarize, Chappell (1993) offered the following four characteristics of an optimal sounding for extreme precipitation:

(1) A deep moist layer with atypically high precipitable water (PW).

(2) Moderate CAPE (1500-2000 J kg^{-1}.)

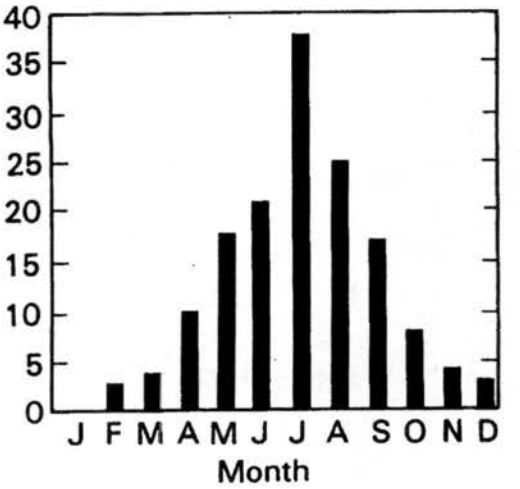

Figure 2.10: Monthly distribution of the flash flood events studied by Maddox et al. (1979).

(3) A [vertically] elongated distribution of CAPE, indicating a low, warm cloud base and a high equilibrium level.

(4) Relatively weak vertical wind shear.

2.2.2 Spatial and temporal characteristics

In addition to the atmospheric conditions associated with extreme rain events, several studies have considered the spatial and temporal characteristics of these events. MCH79 found that flash floods are possible during all seasons and are most common in the summer months (Fig. 2.10). However, this statement is highly dependent on the type of flash flood being considered. Synoptic events are distributed fairly evenly throughout the year with slight maxima in the spring and fall, while frontal and mesohigh events occur almost exclusively during the warm season. This behavior is not surprising, since the baroclinic conditions necessary for synoptic weather system (i.e., extratropical cyclone) development are most often in place in the spring and fall, while MCSs and other convective events are more prominent in summer. More recently, Brooks and Stensrud (2000) objectively analyzed hourly precipitation data and also found a July maximum for rainfall rates greater than 1 in h^{-1}. Their analysis of the seasonal distribution of this heavy rainfall shows that

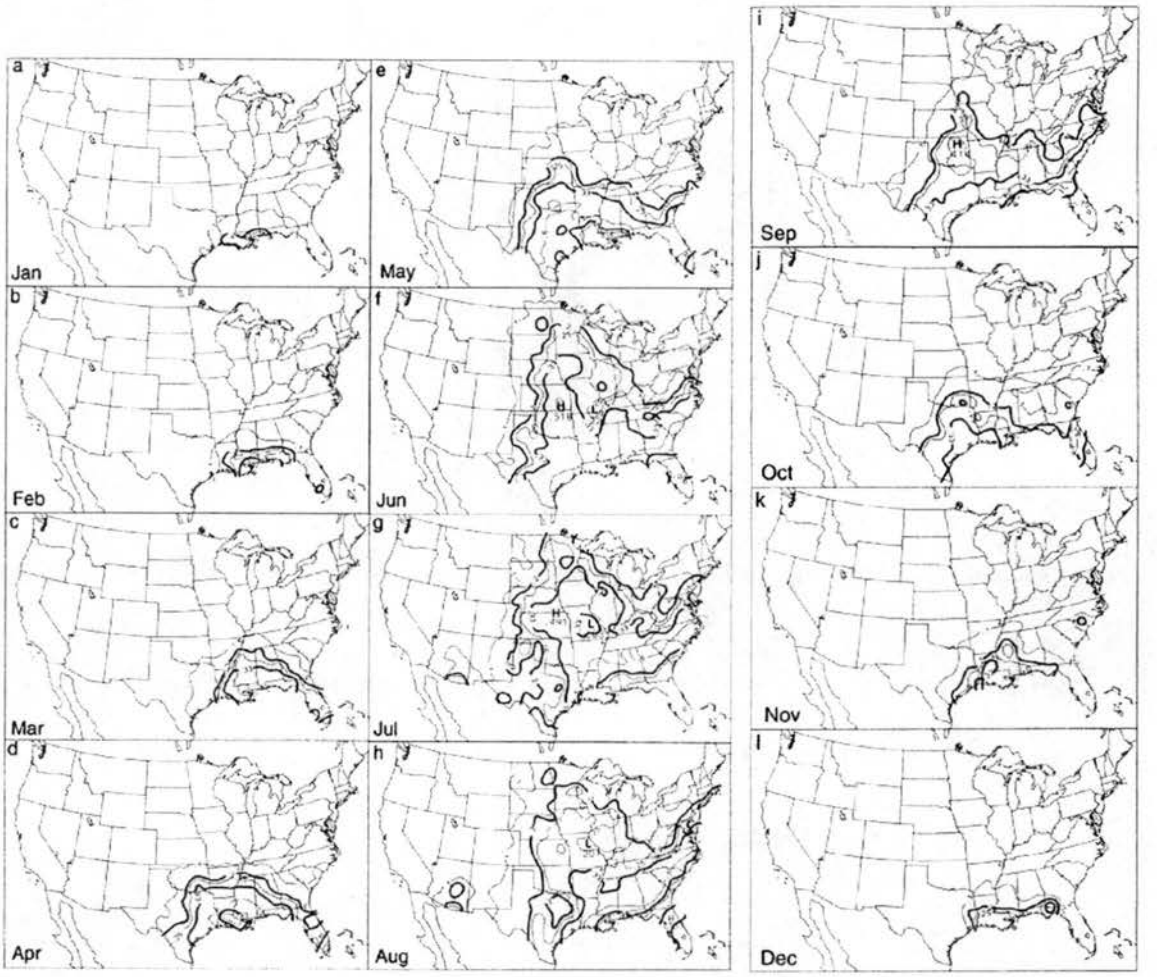

Figure 2.11: Frequency (events/year) of 1 in h^{-1} or larger rainfall totals for each month objectively analyzed to a regular grid from the hourly precipitation data stations. Contours are of 0.1, 0.2, 0.25, 0.33, 0.5, 0.66, 0.75, and 1.0 events $year^{-1}$. From Brooks and Stensrud (2000).

from October through March, rainfall of this magnitude is mainly confined to the Gulf Coast states, while from April through September, it occurs relatively frequently in all parts of the country east of the Rocky Mountains (Fig. 2.11). One of the goals of their work was to make forecasters aware of how likely heavy rainfall might be during a particular time of year at a given location, which is a goal of this research as well. An understanding of the regional distribution of extreme rainfall is one key aspect of attaining this goal, with Brooks and Stensrud's work representing an important first step. Though this study will not consider rainfall rate, *per se*, it will hopefully provide new information about where

and when extreme rain can be expected.

Also key to this discussion is the variation in extreme rainfall frequency throughout the day. Wallace (1975) examined the diurnal variation of "heavy" precipitation across the United States, and found a nocturnal maximum for rain rates greater than 2.5 mm h^{-1} in the Plains and midwest, and an afternoon or evening maximum in the east and south. Winkler et al. (1988) examined the seasonal variability of the diurnal distribution for even heavier rainfall, and obtained results similar to Wallace's: in the warm season, heavy precipitation is maximized during the overnight hours in the central part of the country, but an afternoon/evening maximum is evident across the southern and eastern states (Fig. 2.12). However, MCH79 found a strong nocturnal maximum for *all* non-western flash floods that they studied (Fig. 2.13). An explanation for this seeming discrepancy was offered by Crysler et al. (1982). They found that for the central and eastern part of the country, short-duration heavy rains (which are more common) occur most frequently in the afternoon and evening (explaining the afternoon/evening maximum observed by Wallace 1975 and Winkler et al. 1988), but longer-duration events are most often nocturnal in nature. These events, they pointed out, pose the most serious threat for flash flooding.

Radar data can provide a further avenue for attaining information about the diurnal characteristics of extreme rainfall, as it is not limited by flood reports nor by the sparsity of the rainfall observing network. Now that data from the Weather Surveillance Radars-1988 Doppler (WSR-88D) are readily available, such projects can be undertaken relatively easily. In this study, radar data will be used to observe various characteristics of extreme rainfall events, such as the time of the heaviest rain and the times of precipitation onset and dissipation, aspects not always observable at a high resolution using traditional rain gauges.

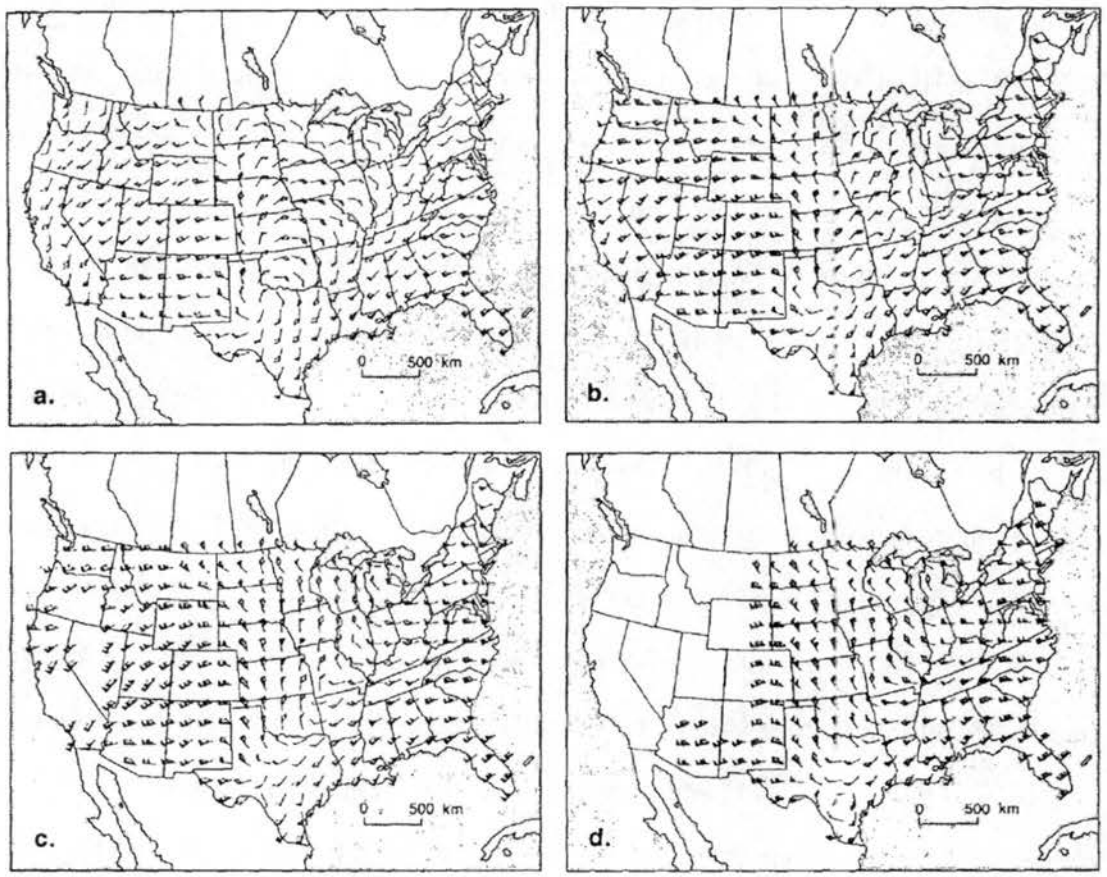

Figure 2.12: Normalized amplitude and phase of the first harmonic during summer for precipitation rates of (a) 2.5–6.2 mm h^{-1}, (b) 6.3–12.6 mm h^{-1}, (c) 12.7–25.3 mm h^{-1}, and (d) $\geq$25.4 mm h^{-1}. An arrow directed from the north represents a phase angle of midnight LST, an arrow directed from the east indicates a 0600 LST maximum, etc. The normalized amplitude is represented by the flags and barbs on the arrows with each flag indicating a value of 0.5, each full barb 0.10, and each half barb 0.05. From Winkler et al. (1988).

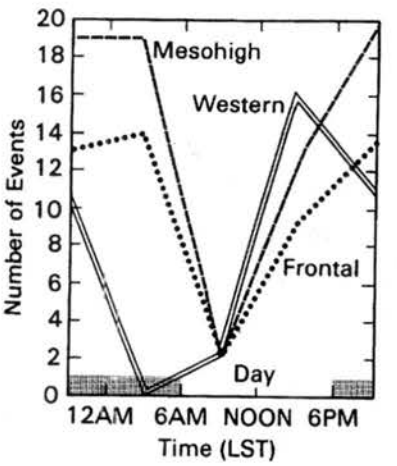

Figure 2.13: Timing of the onset of heavy rains for three types of flash flood events. The number of events that began in each 6-h interval is plotted at the midpoint of the interval. From Maddox et al. (1979)

2.3 Storm types conducive to extreme precipitation

As discussed in section 2.2, extreme rainfall at a particular point requires either a large rainfall rate or a long rainfall duration, or both. The most common situation in which this occurs is when deep convective cells (which typically produce large rainfall rates) are organized such that they move repeatedly over a given area. When the motion of the convective system is slow, the duration is increased even further.

Chappell (1986) describes the motion of a convective system as the sum of two vectors: the velocity of the individual convective cells, and the propagation velocity resulting from the formation of new cells. The cell motion is typically to the right of and slightly slower than the mean wind in the cloud layer (often calculated using the 850–300 hPa layer). The propagation velocity is defined by a variety of factors, including the location of boundaries and the outflows produced by ongoing convective cells. When these vectors are nearly equal and they oppose each other, the motion of the overall system will be minimal (Fig. 2.14). An example of such a system is shown in Fig. 2.15. In this situation, new cells form upstream of the outflow boundary left behind by mature cells (i.e., a leftward-pointing propagation vector) and move from left to right (a rightward-pointing cell motion vector) over the same

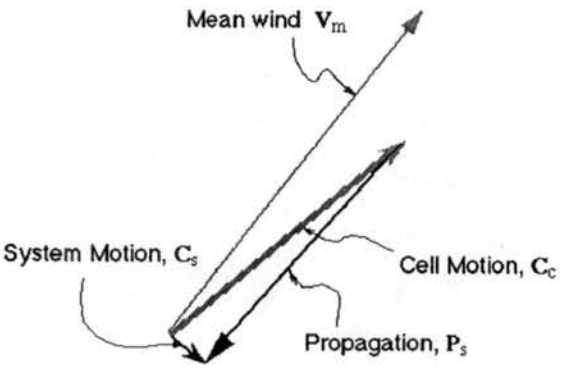

Figure 2.14: Schematic showing the near cancellation between cell motion and propagation, resulting in a quasi-stationary storm system. From Doswell et al. (1996).

area, leading to large rainfall totals. Systems such as these with propagation vectors that oppose the cell motion are often described as "backward propagating" or "backbuilding."

What types of storms, then, are most likely to behave in such a way? DBM96 note that multicell convection that is organized into squall lines and mesoscale convective systems is often responsible for producing extreme precipitation. In addition, high-precipitation supercells have been observed to produce flash floods (e.g., Moore et al. 1995, Smith et al. 2001). Others have shown that extreme precipitation can result from both strongly- and weakly-forced synoptic systems (MCH79, Heideman and Fritsch 1988, Bradley and Smith 1994), from tropical storms and hurricanes (Davis 2001), and from terrain-forced convection (Petersen et al. 1999, Pontrelli et al. 1999). It is clear that extreme rain events can be associated with a wide variety of storm types, however, there is no current information regarding which of these storm types is most commonly associated with extreme precipitation, and how much the dominant types vary spatially and temporally throughout the United States. As noted by Doswell (1991) and DBM96, categorizing convective storm types is a "task replete with pitfalls," and anticipating which types to expect is even more difficult. However, it seems that knowing more about which storm types are most likely to produce extreme rainfall would be helpful to both forecasters and to those seeking greater understanding of how quasi-stationary and extreme-rain-producing storms operate, even

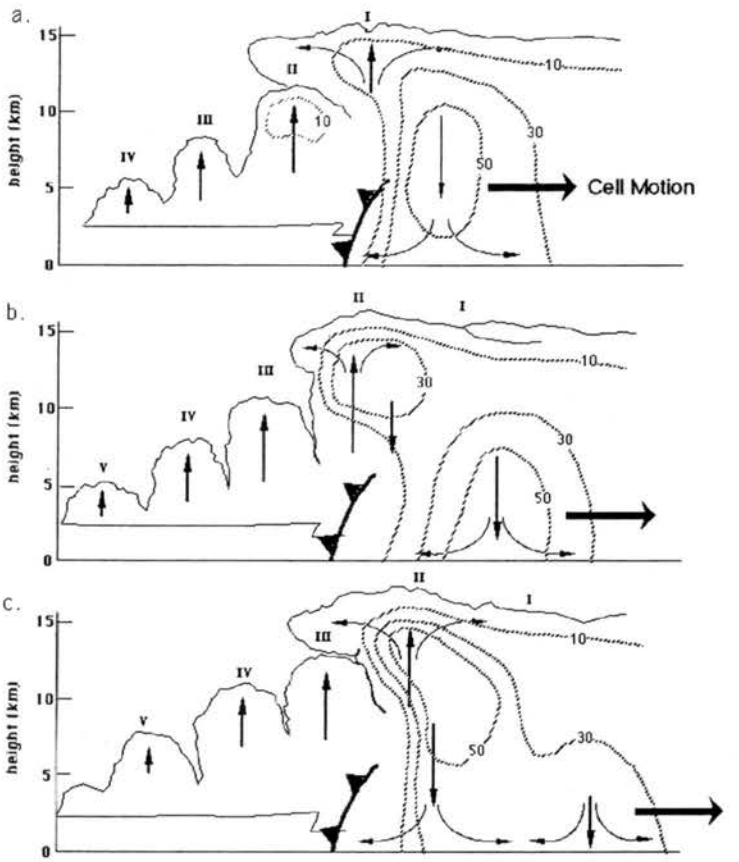

Figure 2.15: Schematic showing three stages in the evolution of a multicell thunderstorm system. Cells are labeled with Roman numerals (I, II, III, etc.); thin arrows indicate the updrafts, downdrafts, and divergence at the storm top and the surface associated with each cell; the frontal symbol indicates the low-level outflow boundary; the cell motion is indicated by the heavy arrow; and hatched lines show radar reflectivity and are labeled in dBZ. Note that the cells are moving left to right while the outflow boundary remains fixed in place. From Doswell et al. (1996)

if the classifications are imperfect. This study aims to determine how many extreme rain events are associated with each of a number of storm types, and to find out how the important storm types vary from region to region and from month to month.

2.4 Extreme rainfall associated with mesoscale convective systems

DMB96 state that "virtually all flash floods are produced by MCSs," at least in terms of characteristics that can be observed by satellite. They also speculate that a radar depiction of flash flood-producing MCSs "would probably show a linear organization in many cases." It is clear that MCSs are an important producer of extreme rainfall, though these particular assertions have not been thoroughly tested in the literature. This study will attempt to quantify *how* important MCSs are in the spectrum of extreme-rain-producing storms, where and when they typically occur, and, especially, how they are organized.

Past studies have found that MCSs can account for 30-70% of the total warm season precipitation in the central part of the United States (Fritsch et al. 1986); this statistic alone indicates that we should look to these systems for the production of *extreme* precipitation as well. Mesoscale convective complexes (MCCs, Maddox 1980), which are large MCSs that exceed a threshold cold cloud shield size, have been found to produce extreme rainfall at a rate far greater than that produced by other types of weather systems (Fritsch and Forbes 2001).

However, since MCSs are quite common in the central part of the United States, and truly extreme precipitation is rather rare, it is obvious that not all MCSs are extreme rain-producers. The size, organization, and motion characteristics of the MCS are the key factors that determine whether an MCS produces, for example, one inch or six inches of rain at a given location. Figure 2.16 illustrates the importance of these factors. If a linear MCS has motion approximately normal to the convective line, then the rainfall total at a given point is relatively small (though the squall line may cover a large area.) When the cell motion is nearly parallel to the line, convective cells with high rainfall rates can repeatedly

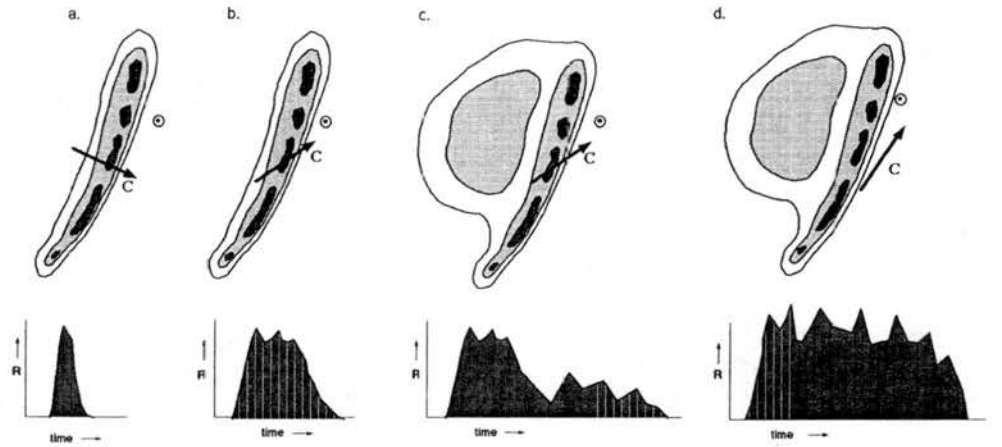

Figure 2.16: Schematic showing how different types of convective systems with different motions affect the rainfall rate (R) at a point (indicated by a circled dot) as a function of time; contours and shading indicate radar reflectivity. For case (a) a convective line is passing the point with a motion nearly normal to the line; for case (b) the line is moving past the point with a large component tangent to the line itself; for case (c) the line has a trailing region of moderate precipitation but is otherwise similar to (b), and for case (d) the motion of the line has only a small component normal to the line but is otherwise similar to (c) . Total rainfall experienced at the point is the shaded area under the R vs. time graphs. From Doswell et al. (1996)

pass over a point and result in extreme rainfall totals. (This process is often called "echo training.") Figure 2.16 also shows the effect of regions of stratiform precipitation that often accompany linear MCSs, namely that lighter rain can persist for hours after the convective line passes, resulting in larger rainfall totals and increased risk of flooding.

Houze et al. (1990) did indeed find that linear MCSs are more likely to produce flash flooding than non-linear ones in Oklahoma. Parker and Johnson (2000) identified three modes of linear MCSs that are common in the Southern Plains—those with trailing stratiform (TS) precipitation, those with leading stratiform (LS), and those with parallel stratiform (PS, Fig. 2.17). They found that LS MCSs typically move slower than the other modes, and thus may be more conducive to extreme rainfall and flash flooding. Another purpose of this study is to determine which of these or whether any other organizational modes of MCSs are most often responsible for extreme rain events.

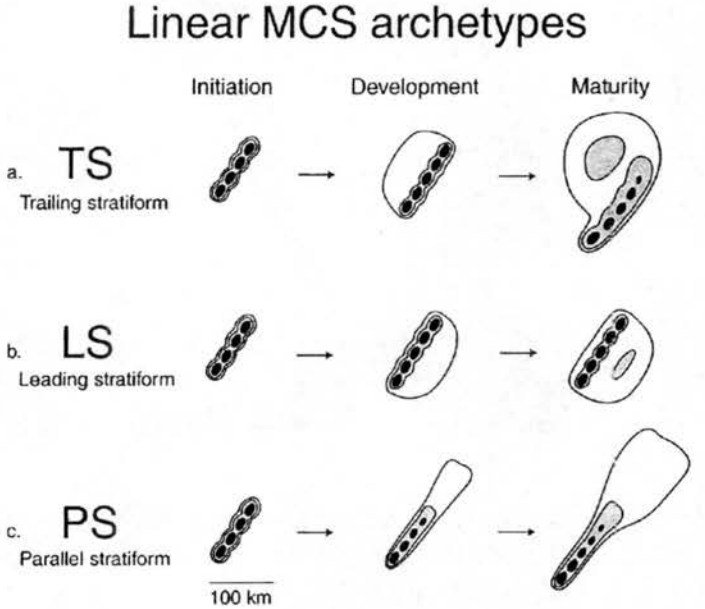

Figure 2.17: Schematic reflectivity drawing of idealized life cycles for three linear MCS archetypes: (a) trailing stratiform (TS), (b) leading stratiform (LS), and (c) parallel stratiform (PS). Approximate time intervals between phases: for TS 3-4 h; for LS 2-3 h; for PS 2-3 h. Levels of shading roughly correspond to 20, 40, and 50 dBZ. From Parker and Johnson (2000).

2.5 Forecasting concerns

One reason why flash floods continue to be a major threat to life and property in the United States is because they are extremely difficult to forecast. There are several explanations for this difficulty. Predicting the amount of rainfall that will fall from a convective storm or an MCS is a great challenge when using today's numerical weather prediction models. Extreme warm-season rainfall is almost always convective in nature, and most convective processes are not explicitly resolved by the numerical models. This leads to poor quantitative precipitation forecasting (QPF) during the summer months, when convective rainfall accounts for approximately half of the total precipitation (Heideman and Fritsch 1988, Fritsch et al. 1998). The area where the total precipitation is actually "extreme" is often very small as well, complicating the situation further. Even if improvements are made to the overall warm-season QPF, the predictability of a small-scale extreme rain

event will likely still be very small. In addition, as mentioned in chapter 1, flash floods are both a meteorological and hydrological forecast problem—predicting the amount of rainfall correctly is only the first step. (Some new advances have been made by the National Weather Service on this front, including the techniques described by Davis 2001, and an experimental flash flood guidance product that is based on soil moisture conditions for the Southern region, available at http://www.srh.noaa.gov/rfcshare/ffg_SR.php.)

So, while it may be an unreasonable goal at this time to expect the accurate prediction of a particular flash flood event, a great deal is known about the meteorological ingredients necessary for extreme rain production and the types of environments in which such storms typically form. This research will hopefully add to this knowledge by providing further information about where and when extreme-rain-producing storms most often develop, and how they are typically organized when they do. This information should be of benefit to operational forecasters so that they can recognize such patterns and know how they might appear in real-time meteorological observations.

Chapter 3

DATA AND METHODS

3.1 Selection of cases

The main challenge of creating a flash flood or extreme rain climatology is the lack of a universally accepted definition for a "flash flood" or an "extreme rain event" (Table 2.1). Researchers studying other severe convective storms have strict definitions that determine what is or is not "severe," but there is no such guideline for precipitation. This is partly because the effects of precipitation are extremely variable; the same amount of rainfall may be devastating in one area and relatively benign in another, depending on the local terrain, properties of the drainage basin, antecedent precipitation, urban development, and a number of other factors.

As discussed in chapter 1, it is very difficult (at this time) to observe both the meteorological and hydrological aspects of a large number of extreme precipitation events. Since the main motivation for this study is to learn more about the meteorological characteristics of extreme-rain-producing weather systems, meteorological data will be used, without regard to the magnitude of any flash flooding caused by the systems. Because extreme rainfall in the western United States is often isolated and dependent on local terrain effects (and is therefore highly unpredictable), this study will focus on the part of the country east of the Rocky Mountains, excluding Florida. This region also has generally better data coverage and is presumably where most MCS-related extreme rain events occur. Upon making these decisions, two further questions remain: what data will be used to select the

cases for further study, and how will an "extreme rain event" be defined?

Two sets of rain gauge data are readily available: observations from the NWS/Cooperative high-resolution 24-h network, and the hourly precipitation dataset (HPD). The benefit of the HPD for this type of study is that it can resolve the characteristics of convective rainfall on more appropriate timescales. However, since it would be advantageous to pinpoint a large number of events and neglect as few as possible, the NWS dataset will be used because it has far superior spatial resolution (Fig. 3.1). To quantify the difference in spatial resolution, the NWS network had 7923 active stations in the United States, while the HPD had 2707 in the month of May 2001. (See Brooks and Stensrud 2000 for a climatology of heavy rain events using the hourly observations.) The NWS/Cooperative rain gauge data are available from the National Climatic Data Center (NCDC) and include the daily precipitation observations as well as the latitude and longitude of each station and the observing time. Most stations report rainfall from the previous 24 h at 7 or 8 AM local time, though some report at other times. (For instance, an observation reported at 7 AM local time on 15 June includes the rainfall from 7 AM 14 June through 7 AM 15 June.)

Of the numerous extreme-rain thresholds shown in Table 2.1, not many studies have used both the 24-h rain gauge observations *and* considered a large spatial domain. Bradley and Smith (1994) defined an "extreme rainstorm" in Oklahoma as an event with a daily rainfall accumulation of 125 mm (approx. 5 in) or more at one or more gauge. As will be explained later, while 125 mm of rainfall is more momentous in some places than in others, it still represents a significant amount of precipitation for one day's time. This fixed threshold was applied to the entire region of interest over the three-year period from 1999–2001. A three-year period was chosen to partially eliminate biases from any one year, and this particular period was chosen because many data sources from these years are readily available. The date, observing time, and location of each rain gauge that reported more than 125 mm during this period was recorded. These reports were then checked against

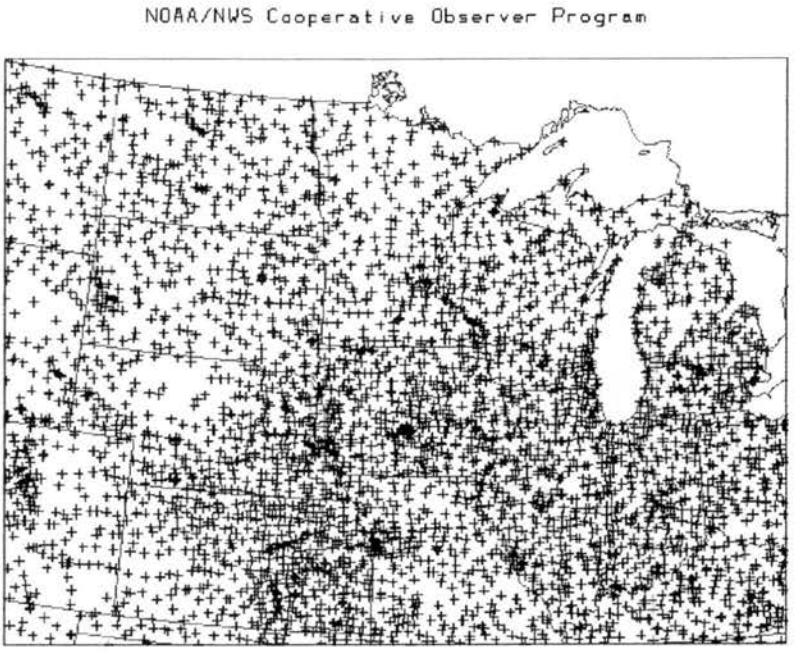

(a) NWS/Cooperative Network

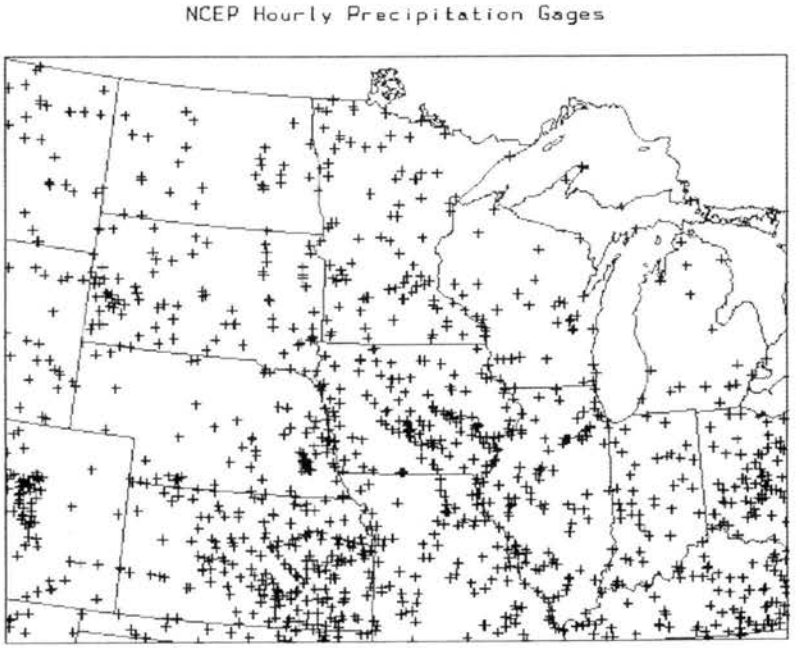

(b) Hourly Precipitation Network

Figure 3.1: Locations of the active stations in (a) the NWS/Cooperative observing network and (b) the HPD network in the north central part of the United States. Station density is similar for other regions of the country. Figures courtesy of the Joint Office for Science Support at the University Corporation for Atmospheric Research.

surface observations, flash flood reports, national mosaic radar data, and other observations to eliminate bad data (e.g., when radar did not observe precipitation at that site, or when nearby stations reported no rainfall) and consolidate the gauge observations into events. For the purpose of this study, an "event" refers to a weather system that produces one or more rainfall observations over the given threshold. This typically represents all or part of the 24-h period in which the rainfall was reported. However, a single event can include multiple 24-h periods if the same weather system is responsible for the precipitation (i.e., an extratropical cyclone that produces heavy rainfall over several states in a two or three day period). Because the rainfall observation times vary in some locations, the possibility exists that events could have been missed because they occurred across the observation time, or that nearby stations could report high rainfall totals on consecutive days that were really produced by the same storm system. When the second scenario took place, great care was taken (by referring to radar data) to determine whether the high rainfall totals were caused by the same storm or by two distinct systems.

After obtaining the results from this analysis (presented in the next chapter), it was clear that a spatially-varying definition for "extreme rain" must be used so that the sample of cases selected represents events that are truly *extreme* for their location. Furthermore, to make any generalizations about the storm structures that produce extreme rain in different parts of the country, it is necessary to have an adequate number of cases from each of these regions. Therefore, thresholds were chosen that approximately balance the number of events in each state (Fig. 3.2). These thresholds vary from 175 mm day^{-1} (at one or more gauge, as before) along the Gulf Coast to 100 mm day^{-1} in the northern Plains and some of the northeast states. The thresholds were created so that average-sized states had between 6 and 12 total events over the three-year period. This criterion provides an adequate sample size, while not including so many events that those chosen would no longer be significant. After using the techniques mentioned above and eliminating bad data, there were 193 events over the 1999-2001 period, which will be hereafter termed "extreme rain

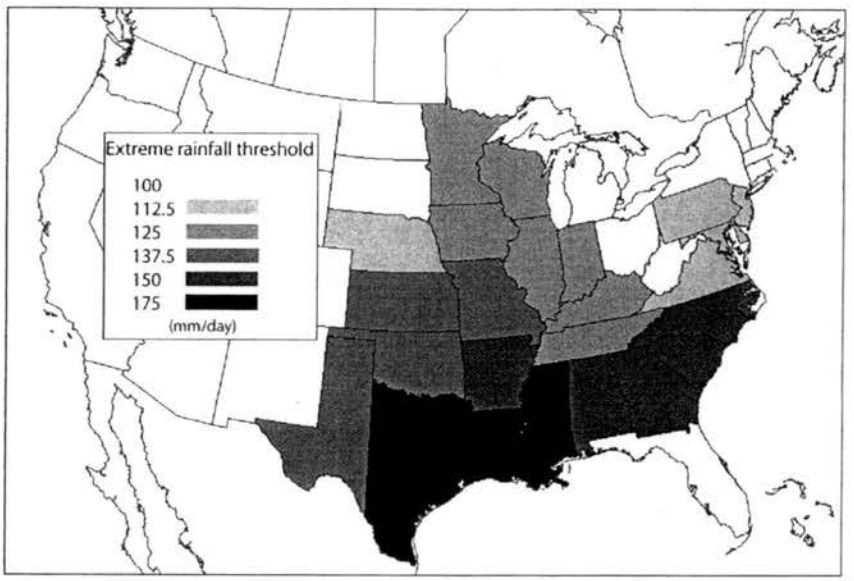

Figure 3.2: Thresholds used to define extreme rain events for this study, in mm $(24\ \mathrm{h})^{-1}$. Thresholds, though somewhat arbitrary, were selected to approximately balance the number of extreme rain events in each state. States in the Rocky Mountains and westward, as well as Florida, are not included in the area of study.

events." Of course, some significant rain events that occurred between rain gauges will be missed, but a sample of this size should show most of the types of systems that commonly produce extreme rainfall. Each event was entered into a database with the date, location, number of stations reporting rainfall amounts greater than the extreme rain threshold, and the maximum rainfall total reported. Information about each event from this database is presented in Appendix A.

3.2 National composite radar reflectivity data

Having selected a satisfactory sample of extreme rain events, radar data were used to further investigate the types of storm systems responsible for the rainfall. Each event's life cycle was observed using composite radar reflectivity data from the Global Hydrology Resource Center (GHRC) at the Global Hydrology and Climate Center, Huntsville, Alabama. Data from the WSR-88Ds are used to generate this dataset, which has pixel resolution of 2

km × 2 km and temporal resolution of 15 min. The radar composites are created by taking the maximum instantaneous reflectivity found in a vertical column above each point in the display, and classifying the observed reflectivity into one of 16 5-dBZ increments (beginning with 0-5 dBZ). While the spatial and temporal resolution of the composite data does not allow for analysis of individual convective elements, it provides sufficient information for understanding the organization and motion characteristics of extreme-rain-producing storms.

Initially, each case was observed using NEXRAD National Mosaic Reflectivity images (one hour temporal resolution, available from NCDC) to determine the approximate times at which the precipitation occurred and to determine an appropriate grid size for viewing animations of the radar composites. Then, the composite radar data for the life cycle of each extreme rain event (from initiation to dissipation) were animated and observed. Fifteen-minute time steps were used in most cases, though 30- and 60-minute resolutions were used for some longer-lived events. A number of characteristics of each event were then recorded, including the time of heavy rain onset in the area where extreme rainfall was reported, the time of peak rainfall (as inferred from the radar data), and the time when the radar echoes ended or moved out of the area. In addition, features such as quasi-stationary convection and echo training were noted, along with a subjective description of the weather system responsible for the extreme rainfall.

Each event was then classified into one of the following categories: MCS, synoptic, isolated, or tropical. MCSs were defined using the criteria of Parker and Johnson (2000) and Orlanski (1975). Convective systems (those with reflectivity greater than 40 dBZ) with areal extents greater than 100 km and with durations between 3 and 24 h were classified as MCSs. Events caused by systems with smaller areal extent than these criteria were deemed isolated, and those characterized by the large-scale ascent commonly associated with strong synoptic features (i.e., extratropical cyclones) and/or lasting longer than 24 h were classified as synoptic. Thus, pre-frontal squall lines and other convective systems that

persisted for longer than 24 h were classified as synoptic systems rather than MCSs, though mesoscale aspects (and even individual MCSs) clearly played an important role in the heavy rainfall in some systems. Events were classified as tropical if they were the direct result of a tropical cyclone or its remnants. Synoptic and MCS events were then arranged into subclassifications based on their organizational structures and system evolutions. These subclassifications will be described in greater detail in chapter 5.

3.3 Flash flood and severe weather reports

Though rain gauge observations were used as an objective way to select events for this study, it is also helpful to know whether the events selected actually caused flash floods, damage, or injury. In addition, since flash flood-producing storms in the past have been associated with other types of severe weather (e.g., Rogash and Smith 2000, Rogash and Racy 2002), the proximity of severe wind, hail, and tornadoes to extreme rainfall would also be valuable information. To this end, two online databases were surveyed to determine whether flash flooding and/or severe weather was reported in conjunction with the extreme rainfall totals. The first is the NCDC Storm Events database (http://www4.ncdc.noaa.gov/cgi-win/wwcgi.dll?wwEvent~Storms), which has written accounts of flash flooding, river flooding, severe weather, and several other weather-related phenomena. For each storm report, the database includes the location, time of day, and any resulting damage or injury. In addition, many of the reports include descriptions of the event, both from a meteorological and societal perspective. The second source is the preliminary storm reports archive from the Storm Prediction Center (SPC, http://www.spc.noaa.gov/climo/). This database provides a map of all tornadoes, severe wind, and severe hail reports on a given day, along with the time of occurrence and a brief description of each event.

For each extreme rain event, the NCDC database was used to determine if flash flooding occurred at or near the location where the extreme rainfall totals were observed. Similarly, the SPC archive was used to find the locations and times of any nearby severe

weather reports. If tornadoes were reported, the NCDC database was then checked to find their Fujita scale rating. If flash flooding, severe wind, severe hail, tornadoes, or significant tornadoes (F2 or greater) were reported in conjuction with the extreme-rain-producing storm system at approximately the same time as the heavy rainfall was occurring, a "yes" was assigned for that phenomenon for that event. These determinations were made as accurately as possible using the available datasets, and the results are presented in chapter 5. While determining details such as the time lag between heavy rainfall and severe weather, the location of severe weather in relation to particular convective features, and so forth is beyond the scope of this study, such information would surely be valuable and is a possible avenue for further research. (See Rogash and Racy 2002 for results regarding relationships between flash flooding and significant tornadoes.)

3.4 Surface, upper air, and RUC analysis data

To determine the synoptic and mesoscale atmospheric conditions in which the different types of extreme-rain-producing storms occur, surface and upper-air observations and initial-hour analyses from the Rapid Update Cycle–Version 2 (RUC–2, Benjamin et al. 1998) model were used. First, standard surface and upper-air analyses from the National Centers for Environmental Prediction (NCEP) were observed for each extreme rain event to create a "mental composite" of the conditions in which the systems formed, especially for the synoptic and MCS cases (and their subclassifications). Then, composite analysis was performed on the RUC–2 analyses to obtain a more objective idea of the conditions in place for each type of event.

In the 1999–2001 time period, hourly RUC–2 analyses with horizontal grid spacing of 40 km are available. These analyses were obtained from the Atmospheric Radiation Measurement Program (ARM) archive, and they contain a variety of atmospheric variables, including temperature, moisture, and wind at the surface and on 37 constant pressure surfaces. In addition, several other thermodynamic fields such as CAPE, surface θ_e, and

precipitable water are analyzed. Of course, the quality of these analyses is highly dependent on the quality of the data ingested, as well as the model itself and its parameterizations. However, these data provide a way to objectively observe and, where possible, make generalizations about the conditions responsible for producing extreme rainstorms.

The composite analysis was performed using a 31 $\times$ 31 grid point domain (approximately 1240 $\times$ 1240 km) centered at the grid point nearest the location where the highest rainfall total was reported. (Since the RUC–2 data are actually on a Lambert conformal projection, the grid length does vary slightly between the northern and southern parts of the United States.) Composites were created for the peak rainfall time, and for the analyses 12 hours before this time. For the sake of this discussion, let us consider the creation of a composite of surface dew point at the peak rainfall time for all "type A" MCSs. For each case, an algorithm is used to select the grid point nearest the extreme rain location. Then, the dew point values at the 15 grid points to the north, south, east, and west of the center are compiled onto the 31 $\times$ 31 point map. The values on these dew point maps for all of the type A MCSs are then added together and divided by the number of cases being considered, yielding the average dew point value for a type A MCS at each location relative to the extreme rainfall location. This process can then be repeated for other variables and for other storm types. To obtain the composite wind fields, the individual zonal and meridional components of the wind for each case were averaged.

While most important atmospheric variables are included in the RUC–2 analyses, a few important fields need to be calculated. To calculate θ_e on a constant pressure surface, the method of Bolton (1980) was used. Standard finite-difference methods were used to calculate the advection or convergence/divergence of certain variables. Advection and convergence/divergence fields were calculated for each case, and then averaged (rather than calculated from the composite values of the wind and other variables).

Chapter 4

CLIMATOLOGICAL CHARACTERISTICS OF EXTREME RAIN EVENTS

Before inspecting the radar data in greater detail, a great deal of information can be gained from simply analyzing rain gauge observations of extreme rainfall in the United States. After using the techniques and definitions described in chapter 3 to consolidate the extreme rainfall observations into events, we can observe some of the climatological characteristics of these events. In this chapter, some of these characteristics will be presented using both the fixed (125 mm day^{-1}) and the spatially varying (Fig. 3.2) thresholds.

The composite radar data are then utilized to classify each extreme rain event by storm type. This analysis reveals which weather systems are most often associated with extreme rainfall in each region and when these systems are most likely to occur.

4.1 Characteristics with a fixed threshold

Using the criteria already described, there were 218 events in the years 1999–2001 where 125 mm of rain was reported in 24 h at one or more gauge. As one might expect, rainfall of this magnitude occurs most frequently in the southern part of the country (where moisture from the Gulf of Mexico is abundant) and is less frequent to the north (Fig. 4.1). Texas and Louisiana were the most frequently affected states, with 38 and 31 events, respectively. These results can be compared to the total annual rainfall distribution in the United States, where the large-scale maximum in our area of interest is along the Gulf coast, and the minimum is in the northern Plains (Fig. 4.2). (When considering the number

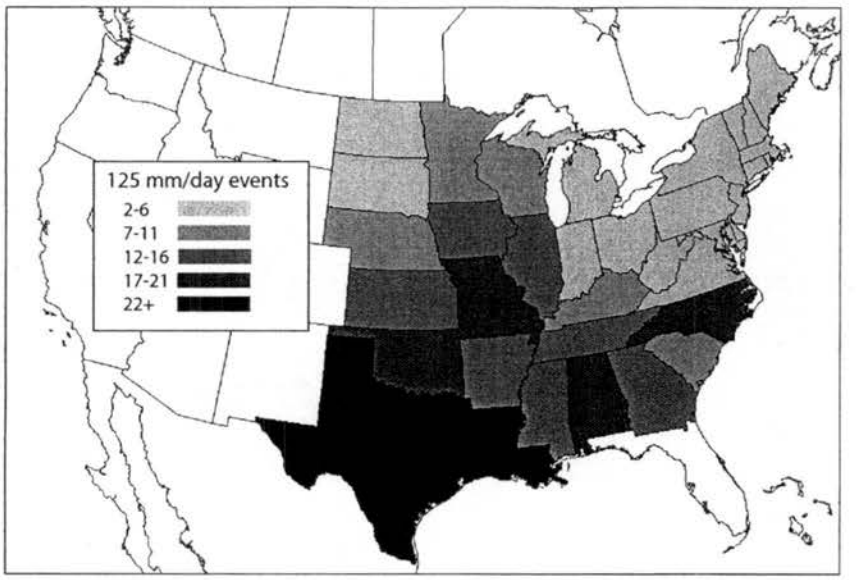

Figure 4.1: Number of 125 mm (24 h)$^{-1}$ events from 1999-2001 in each state in the study area. Florida is excluded from the analysis.

of events in each state, there are two caveats to remember. First, the number of events occurring in a given state is heavily dependent on the size of that state. Thus, the number of events per unit area in Louisiana is much higher than that in Texas. Secondly, the state-by-state totals include some overlap (i.e., a single event that caused 125 mm of rain in both Texas and Louisiana is counted in both states here).) One curiosity in the results shown in Fig. 4.1 is the sharp dropoff in 125 mm day^{-1} events from Wisconsin and Illinois to the neighboring states of Indiana, Michigan, and Ohio. Since only three years have been considered here, it is possible that the conditions were just not favorable for rainfall of this magnitude in these states during this time period. A longer record would need to be analyzed to determine whether such events are really more rare in these states than in their neighbors. [The summer of 2003 showed that Indiana and Ohio are not immune to extreme precipitation—Indianapolis received 7.2 in of rain on 1 September and these states experienced major flooding throughout the summer.]

The monthly frequency distributions of 125 mm day^{-1} events by region show that

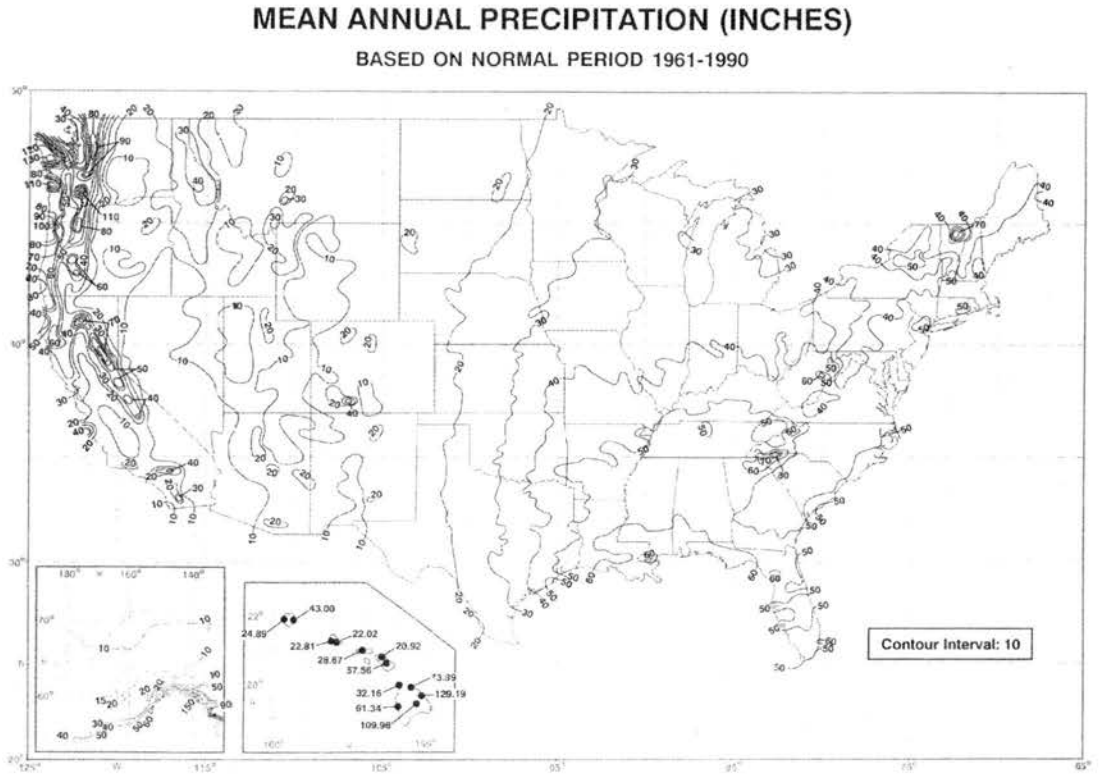

Figure 4.2: Mean annual precipitation (in) in the United States from 1961-1990. From Owenby et al. (2003).

they can occur in all seasons in the southern U. S., but are mainly confined to the warm season in the northern part of the country (Fig. 4.3). (The regions used are the same as those used in Karl and Knight (1998) and, though they do not correspond exactly to the divisions for the extreme rain thresholds, they provide logical divisions within which the characteristics of these events can be considered.) In total, such events are most common during June and July. In the south and southeast regions, there are relative minima in July and August, with relative maxima before and after. The summer minima are likely attributable to the onset of the Bermuda high and the northward migration of the jet stream during the summer. Bradley and Smith (1994), studying rainfall in Oklahoma and northern Texas, found a similar bimodal distribution in 125 mm day^{-1} events over a 43-

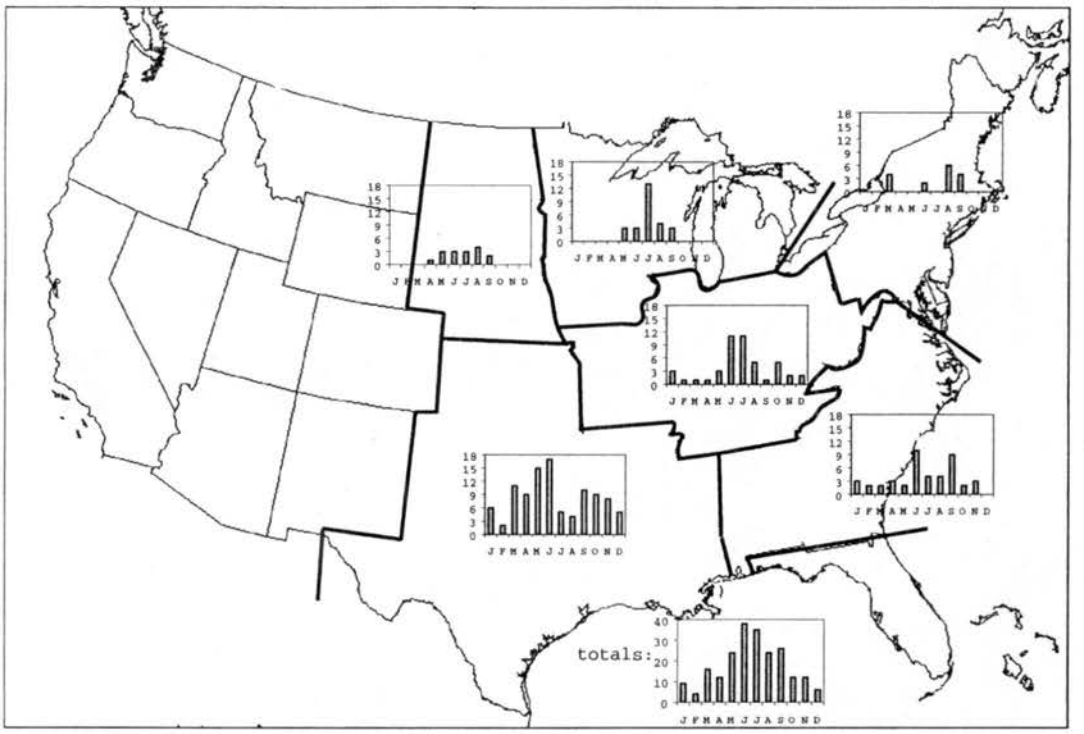

Figure 4.3: Monthly frequency distribution of 125 mm $(24\ \mathrm{h})^{-1}$ events, by region. The total distribution is shown at the bottom. Ordinates are scaled equally for the regional graphs and range from 0 to 18 events. Regions are the same as those used in Karl and Knight (1998), and will be referred to as: (clockwise from upper left) Plains, north, northeast, Ohio/Mississippi valley, southeast, and south.

year period (Fig. 4.4). In contrast, July is the peak month for 125 mm day^{-1} events in the north and Ohio/Mississippi valley regions. Rainfall of this magnitude is quite rare in the Plains and northeast regions. Nearly all such events in the Plains region occur in the warm season, while those in the northeast are most frequently observed in March, September, and October. The reasons for this behavior in the northeast will be discussed later.

This analysis shows the frequency at which 125 mm day^{-1} rainfall events occur in the U. S. and in what months they are most likely to occur in different regions. As mentioned in the previous chapter, 125 mm is a significant amount of precipitation for one day in any area, and these results provide some new information about where and when this much

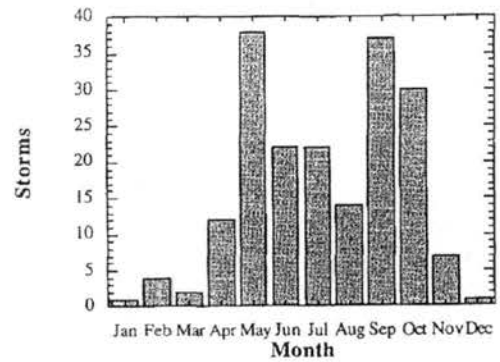

Figure 4.4: Occurrence of 125 mm (24 h)$^{-1}$ rainstorms during a 43-year period in a region including central Oklahoma, southern Kansas, and northern Texas. From Bradley and Smith (1994)

rain might be expected to fall. However, as these results show, it does not represent a truly *extreme* amount in all areas, and it happens so rarely in others that any generalizations made about the events that cause it would not be very meaningful. Therefore, the spatially varying extreme rain threshold (described in section 3.1 and shown in Fig. 3.2) is applied, which yields the cases ("extreme rain events") that will be considered in the rest of the study.

4.2 Characteristics with a spatially varying threshold

The application of this threshold provides a sample that is much more suitable for further study, since the number of events are appropriately balanced throughout the country (Fig. 4.5). A couple of minor inconsistencies are apparent: Texas, being by far the largest state in the study region, intentionally has a greater number of events than the other states, and Indiana (unintentionally) still has far fewer events than the surrounding states of Illinois and Kentucky, even though they receive comparable amounts of rainfally annually and they have the same extreme rain threshold. Despite these concerns, the cases selected offer a balanced sample that represents events that are indeed significant for their particular area.

The monthly frequency distributions (Fig. 4.6) are similar to those for the 125 mm day^{-1} events, and the consideration of more events in the Plains, north, and northeast

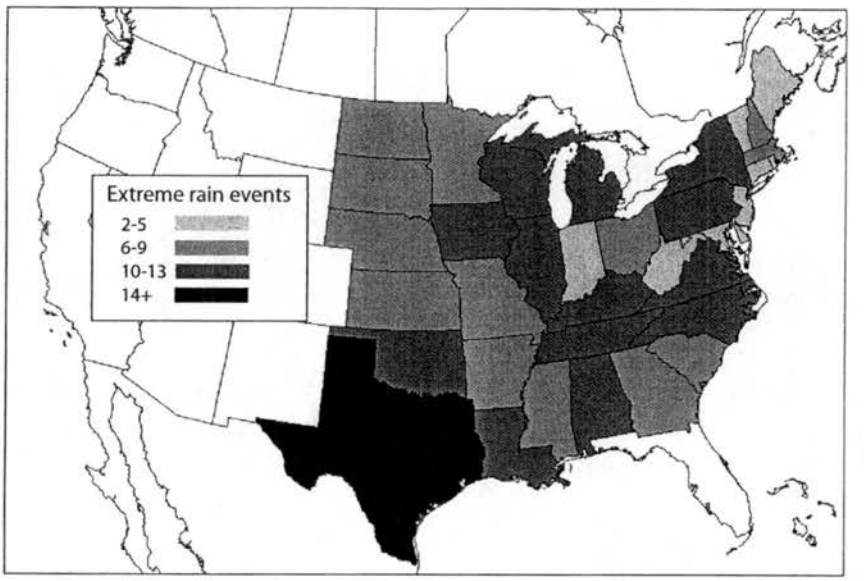

Figure 4.5: As in Fig. 4.1, except for extreme rain events as defined in the text.

regions leads to more meaningful distributions. The strong warm-season maxima in the Plains and north regions are emphasized, and a more distinct August-September maximum is apparent in the northeast.

The overall monthly frequency distribution (bottom of Fig. 4.6) very closely resembles the findings of MCH79 (Fig. 2.10). This result confirms the idea that flash floods and extreme rain events in the United States are most common in the summer months.

4.3 Characteristics obtained from radar analysis

Since the monthly frequency distributions of extreme rain events vary greatly throughout the U. S., it is likely that the types of weather systems responsible for these events also vary both seasonally and from region to region. These characteristics have not been quantified in the literature, however. With this in mind, national composite radar data were used to classify each event as synoptic, MCS, isolated, or tropical (as explained in chapter 3). This analysis shows that over half of all extreme rain events considered were associated with MCSs, and just over one quarter were associated with synoptic weather

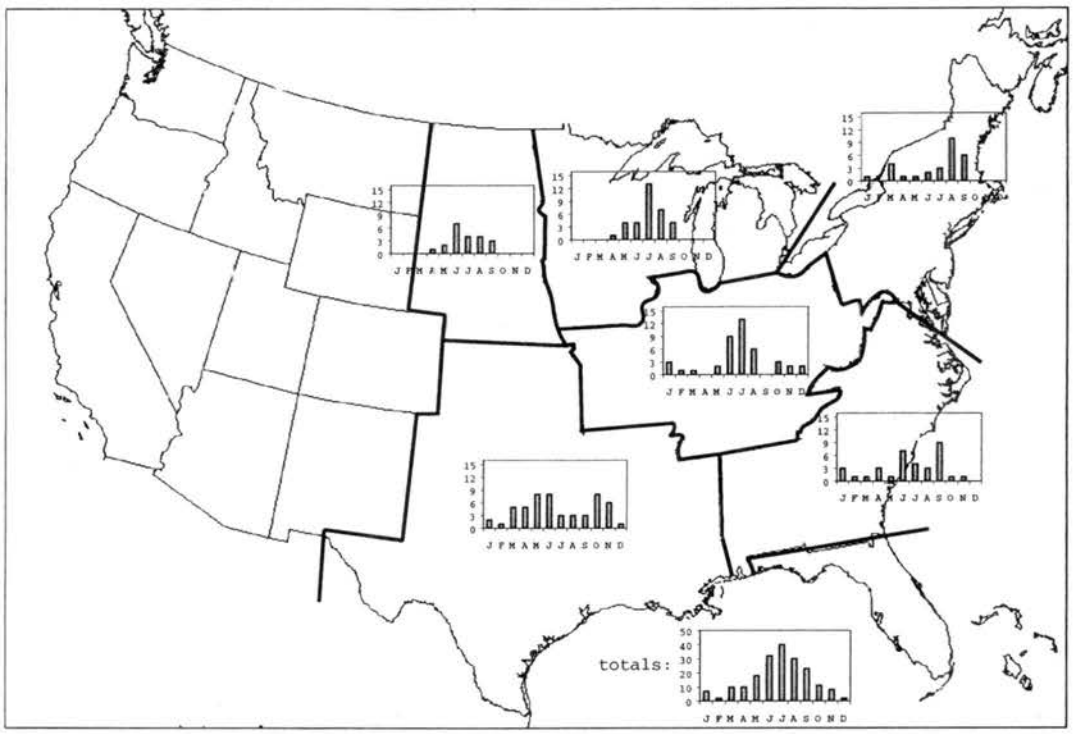

Figure 4.6: As in Fig. 4.3, except for extreme rain events as defined in the text. Ordinates range from 0 to 15 events on the regional graphs.

systems (Table 4.1).

These results confirm the speculation of DBM96 and others that most extreme rain events and flash floods are caused by MCSs. MCSs were the most common extreme rain

Table 4.1: Weather systems associated with extreme rain events, by region. Numbers in parentheses represent the percentage of events (rounded to the nearest whole percent) a given region that are caused by the respective storm type. The sum of the regional values for each storm type does not necessarily equal the total in the right–hand column, because events spanning more than one region are counted in both regions but only once in the overall total.

System	Plains	North	OH/MS	NE	South	SE	**Total**
MCS	16 (76%)	29 (88)	25 (60)	8 (29)	29 (55)	14 (41)	114 (59.1)
Synoptic	3 (14)	4 (12)	14 (33)	12 (43)	18 (34)	9 (27)	52 (26.9)
Isolated	2 (10)	0	3 (7)	6 (21)	4 (8)	2 (6)	17 (8.8)
Tropical	0	0	0	2 (7)	2 (4)	9 (27)	10 (5.2)
Total	21	33	42	28	53	34	193

producers in every region except the northeast, where synoptic systems caused the most extreme rain events. (Laing and Fritsch 1997 showed that MCCs are very rare in the northeast U. S., indicating that organized but smaller MCSs are probably rare as well.) In the Plains and north regions, MCSs accounted for a large majority of the events, while the Ohio/Mississippi valley and south regions had percentages of MCSs and synoptic events that were similar to the overall percentages. There were more tropical cyclone-related events in the southeast than in any other region. While the overall percentage of tropical events was relatively low, there were two events that led to the most widespread and destructive flooding of the entire population: Hurricane Floyd (1999) along the east coast, and Tropical Storm Allison (2001) in the Gulf Coast states. So, while there may be relatively few extreme rain events associated with tropical cyclones, the potential for damage and injury is much greater when they do occur. (Presumably, the likelihood that a given tropical cyclone will produce extreme rain is much higher than that for MCSs or synoptic systems as well.)

The monthly frequency distribution of extreme rain events, separated by storm type, shows that most of the events occurring in the summer months are caused by MCSs, while nearly all of the cool-season events are associated with synoptic systems (Fig. 4.7). This result is not especially surprising, considering that the strongly baroclinic conditions that are prevalent in the cool season are supportive of strong synoptic systems, while MCSs typically occur in the weaker forcing and greater moisture of the warm season in the United States. However, it expands upon Fritsch et al.'s (1986) finding that 30-70% of the total warm season precipitation in the midwest results from MCSs by showing that over 70% of *extreme* warm season (April–September) precipitation events in the *entire country* result from MCSs. While this does not speak to the proportion of the total *amount* of precipitation that results from extreme-rain-producing MCSs, it further emphasizes the important role that MCSs play in determining the precipitation characteristics of the United States.

It was shown above that nearly all extreme rain events in the Plains and north regions occur during the warm season. In addition, nearly all of them are associated with MCSs.

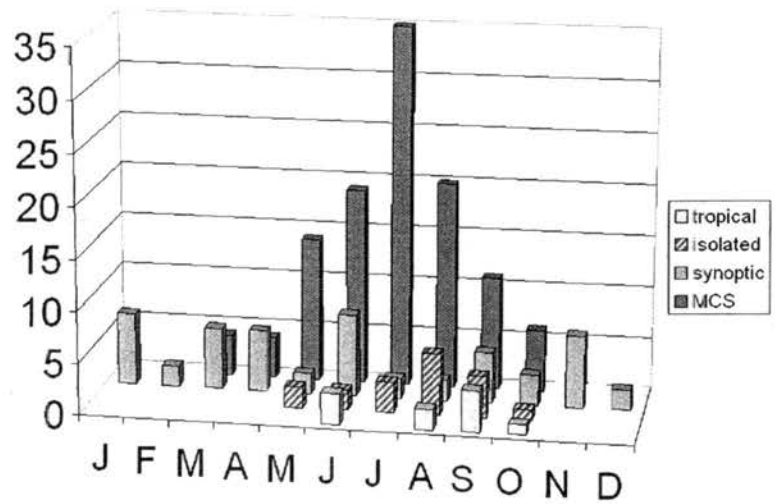

Figure 4.7: Monthly frequency distribution of all extreme rain events, separated by storm type.

As such, the monthly frequency distributions for these regions (Figs. 4.8 and 4.9) show an expected result: MCS-caused events that occur between May and September are the dominant extreme-rain-producing phenomena in these locations. Each of these regions did receive a few synoptic events (mainly in the spring and early summer), and the Plains region received two isolated events. At locations this far north, temperatures are typically too cold and the necessary moisture is unavailable for extreme precipitation to occur outside of the warm season. While extratropical cyclones certainly affect these regions during the winter, they usually bring snow instead of rain.

Slightly farther south and east in the Ohio/Mississippi valley region, synoptic systems play a greater role. While MCSs produce the majority of the extreme rain events and are maximized in July here as well, cool-season synoptic events are also important (Fig. 4.10). Because the temperatures and dew points in this region, on average, are higher than those farther north, some extratropical cyclones that traverse this region during the autumn and winter bring long-lived convective systems rather than heavy snow.

In the northeastern United States, extreme rainfall appears to occur on a different annual cycle (Fig. 4.11). The two relative maxima in the northeast occur in March and

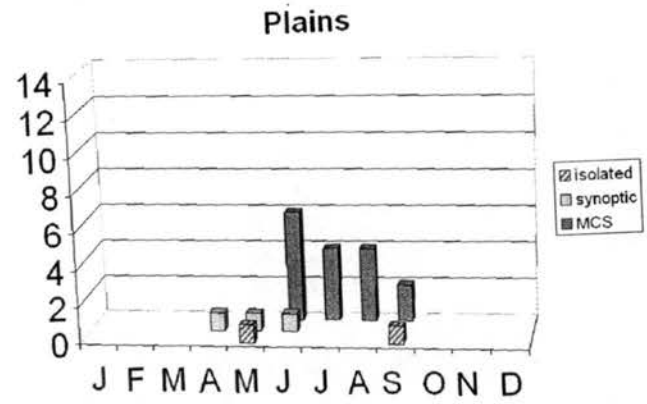

Figure 4.8: As in Fig. 4.7, except for the Plains region.

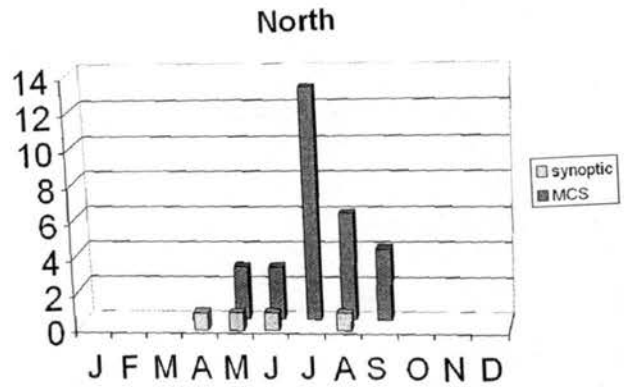

Figure 4.9: As in Fig. 4.7, except for the north region.

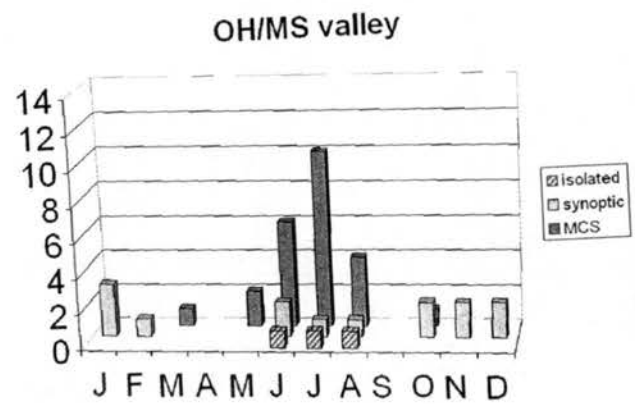

Figure 4.10: As in Fig. 4.7, except for the Ohio/Mississippi valley region.

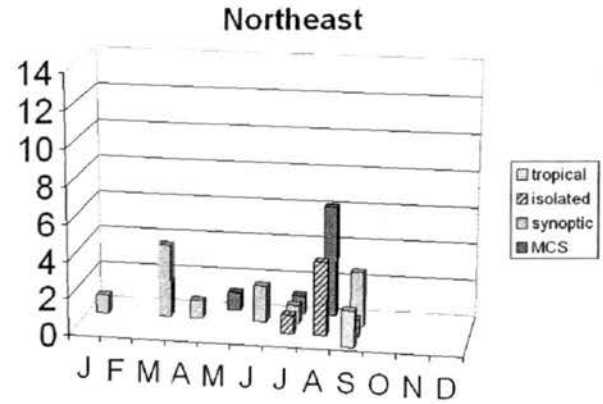

Figure 4.11: As in Fig. 4.7, except for the northeast region.

in August and September. All of the March events are associated with synoptic systems, while all four storm types play a role in August and September. The winter and spring extreme rainfall usually occurs to the north and west of an extratropical cyclone (often a "nor'easter") and persists for more than 24 h. It is the long duration of the rainfall (rather than a high rain rate) that leads to extreme totals in these events. August had the maximum for both MCS-related and isolated extreme rain events in the northeast. Only one month later, however, the largest contribution was from synoptic and tropical systems. In total, the distributions in the northeast are quite different from all of the other regions, especially because MCSs are not the most common extreme rain-producers and because the months of maximum activity vary greatly from the most active months overall.

The monthly frequency distribution in the southeast region (Fig. 4.12) is unique because it is strongly modulated by tropical cyclone activity, though MCSs do produce more extreme rain events than the other storm types. June and September are the most active months, though these were the months when several tropical systems affected this region from 1999–2001. (Since tropical cyclone activity is extremely variable from year to year, it is possible that the results found here would be completely different if another three-year period were chosen for study. Thus, generalizations made about the monthly distribution in the southeast region may not be as robust as those made about other

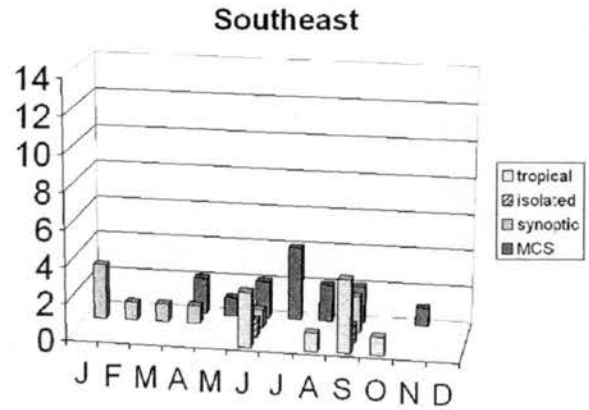

Figure 4.12: As in Fig. 4.7, except for the southeast region.

regions.) MCS events occurred from April through November, with a maximum (4 events) in July. (Geerts 1998 also found that MCSs occur most often in July in the southeast.) Synoptic systems in the spring and winter also produced several of the events in this region.

Finally, in the south region, extreme rain events occur most often in the late spring and in the autumn. Most of the springtime events result from MCSs, while both MCSs and synoptic systems play an important role in the fall (Fig. 4.13). Extreme rain events can occur in all months of the year in the south, as evidenced by the wintertime synoptic events. There is a relative minimum in extreme rainfall in July, August, and September (corresponding to a relative minimum in MCS activity), though, interestingly, there was a secondary *maximum* in September using the fixed (125 mm day^{-1}) threshold (Fig. 4.3). It is also interesting to note that the "season" for MCS-related extreme rain events is much longer in the south than in the regions to the north; they occurred from March through October.

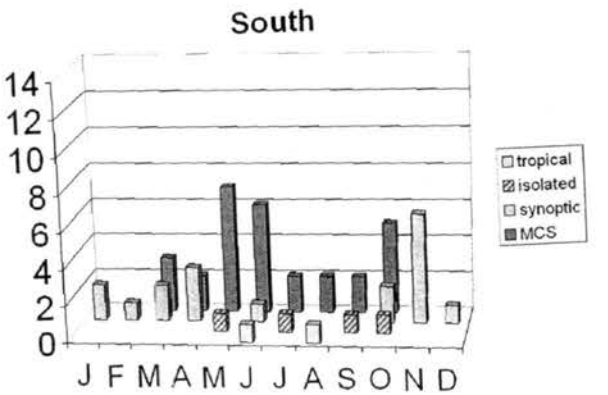

Figure 4.13: As in Fig. 4.7, except for the south region.

Chapter 5

EXTREME-RAIN-PRODUCING SYNOPTIC AND MCS TYPES

5.1 Extreme-rain-producing synoptic systems

While a thorough investigation of the precipitation features of extratropical cyclones and other synoptic systems that produce extreme precipitation is beyond the scope of this study, a description of some of the basic structures of these systems (as observed by radar) is warranted. Of the 52 extreme rain events classified as "synoptic" (see Table 4.1), 39 (75%) were caused by the repeated passage of convective storms and convective systems. The convection in these systems was typically widespread and often resulted in extreme rainfall totals in several states. The remaining 13 events were characterized not by widespread convection but by long-duration stratiform (i.e., radar echoes of less than 40–45 dBZ) rain. Embedded convective rainfall sometimes contributed to the extreme rainfall totals in these events, but the persistent stratiform precipitation was the key factor.

Most of the convective synoptic events occurred in the warm sector of an extratropical cyclone ahead of a synoptic-scale cold front, while the non-convective events typically occurred in the cool sector, often to the north and west of the low pressure center. Examples of convective synoptic events occurred on 24-25 September 2001 and 10-11 October 2001 (Figs. 5.1 and 5.2). In each case, an area of convection formed on the warm side of a synoptic-scale front, resulting in widespread extreme rainfall totals. Contrasting these two examples is the non-convective synoptic event of 6-7 June 2000, where a large area of mainly stratiform precipitation persisted for many hours to the northwest of an offshore

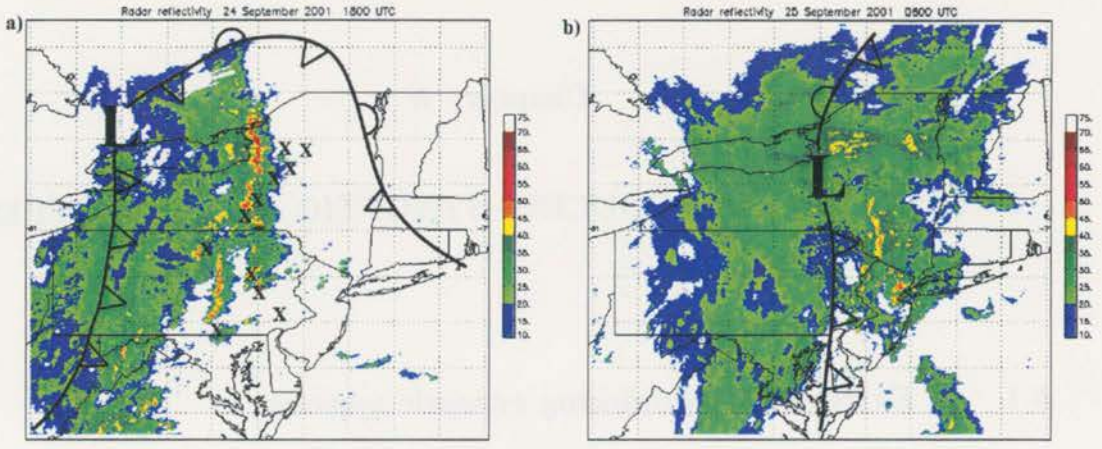

Figure 5.1: Composite radar reflectivity (dBZ) from the convective synoptic extreme rain event at (a) 1800 UTC 24 September 2001 and (b) 0600 UTC 25 September 2001. Reflectivity scale is shown at right. Locations of low pressure centers and fronts were taken from NCEP surface analyses. Stations reporting extreme rainfall totals are denoted with an "X" in (a).

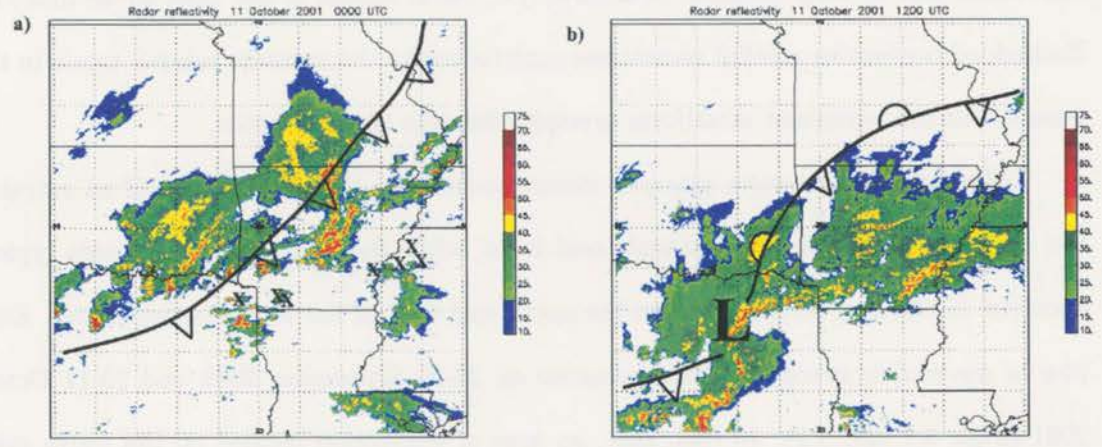

Figure 5.2: As in Fig. 5.1, except for (a) 0000 UTC and (b) 1200 UTC 11 October 2001.

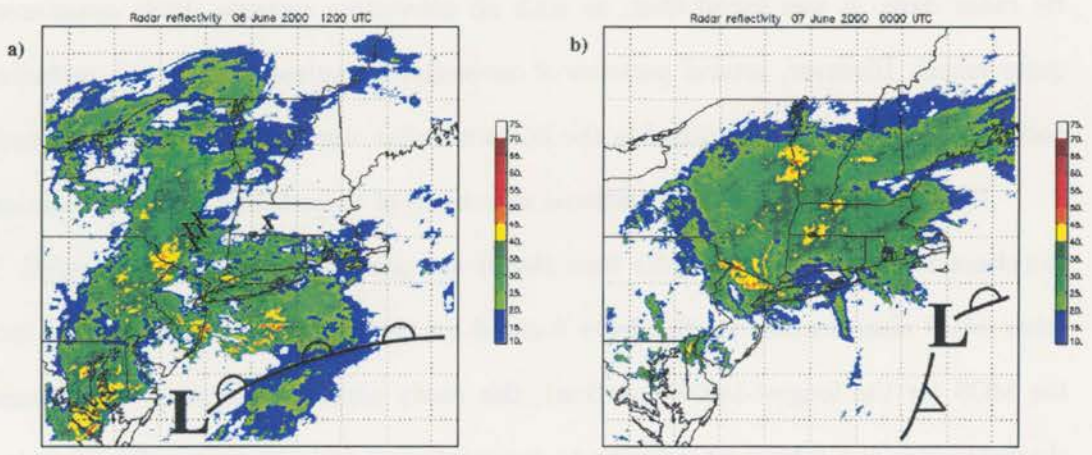

Figure 5.3: As in Fig. 5.1, except for non-convective synoptic event at (a) 1200 UTC 6 June 2000 and (b) 0000 UTC 7 June 2000. While some areas of higher reflectivity are evident in this event, many of them never impacted the area where extreme rainfall was reported, and others are likely associated with the radar "bright band" that often occurs near the melting level of stratiform precipitation.

cyclone (Fig. 5.3). While there are some areas of higher reflectivity in this event as well, many of them never impacted the area where extreme rainfall was reported, and others are likely associated with the radar "bright band" that often occurs near the melting level of stratiform precipitation (e.g., Byers and Coons 1947).

5.2 Extreme-rain-producing MCSs

As discussed in chapters 2 and 4, one of the main purposes of this study is to determine how many extreme rain events are caused by MCSs and what types of MCSs are most often responsible for producing extreme rainfall. The results presented in chapter 4 showed that 59.1% of extreme rain events in the United States in 1999–2001 resulted from MCSs; a percentage that is even higher in the north central part of the country. Since these results verify that MCSs are the predominant extreme-rain-producing weather systems in the country, and since relatively little is known about the organization of MCSs that produce extreme precipitation, much of the remainder of this study will be devoted to their characteristics.

After observing all of the extreme-rain-producing MCSs using the national compos-

ite radar data, it was found that, as with all convective systems, their structures were quite varied. However, several patterns of convective organization emerged, including two patterns not previously identified in the literature that were observed most frequently.

When classifying the organizational structures of these MCSs, the main concern was the character of the system *at the time that it was producing the extreme rainfall.* While other MCS classification studies have focused on the dominant organizational mode of the MCS (or the longest-lasting portion), this study aims to determine the organization characteristics and attendant synoptic-to-mesoscale flow features that make a certain MCS capable of producing abnormally high amounts of rain. If a system had a given structure for 2 or 3 hours during which the extreme rainfall occurred, then persisted for 8 more hours with a different organization (without extreme rain production), its structure would be classified as the former. Additionally, the evolution of the system (as seen from animating the radar images) is key to classifying and understanding these systems. As discussed in section 2.4 and illustrated in Fig. 2.16, it is not only the organization but also the motion of the system that determines whether a large amount of rain will fall at a given location.

5.2.1 Description of MCS types

Before describing the two most common patterns, some description can be made of the extreme-rain-producing MCSs that fit previously published MCS classification schemes. Some of the extreme rain events were caused by linear MCSs with the structures identified by Parker and Johnson (2000, Fig. 2.17), namely those with trailing stratiform (TS), leading stratiform (LS), and parallel stratiform (PS). A few cases were the result of multiple distinct systems (usually two) in the same 24-h period, where neither MCS alone would have produced enough rainfall to achieve the extreme rainfall threshold, but the combination of them did. A few others occurred in coastal areas and were forced by the sea-breeze front. Several were associated with a convective system that met the definition of an MCS but did not conform to other MCS classifications in the literature. These systems were typ-

ically not organized into convective lines or large clusters, and were deemed "disorganized MCSs," though this is not a completely accurate name—a certain degree of organization exists in all such systems. In these MCSs, the "echo training" or other behavior leading to the extreme rainfall often appeared to be fortuitous rather than well-organized. (The numerical distributions of these classifications will be provided below.)

The two most frequently observed patterns, however, do not exactly fit any of the accepted MCS archetypes appearing in the literature, though the behavior that they display brings together all of the ingredients necessary for extreme rainfall and flash flooding described in chapter 2. They are both organized and move in such a way that heavy convective rainfall passes over a given area for an extended period of time. The patterns have been classified and named in a manner consistent with the archetypes for linear MCSs presented by Parker and Johnson (2000) to minimize confusion over acronyms and abbreviations, and so that they can be compared and contrasted with systems fitting those archetypes.

The first, which will be termed "training line, adjoining stratiform", and abbreviated "TL/AS" or simply "AS", is a linear MCS with cell motion approximately parallel to the convective line. As the cells move in a line-parallel direction, there is very little motion in the line-perpendicular direction, which distinguishes them from the TS and LS archetypes. This combination of motion characteristics leads to prolonged heavy convective rainfall at locations along the line of convective cells (i.e., a training line). The convective clusters within the line are often elongated at an angle to the line itself, a characteristic that was also observed in MCSs by Houze et al. (1990) and Pettet and Johnson (2003) but has not been thoroughly explained.

As these systems develop, an area of stratiform precipitation forms adjacent to the convective line and moves in approximately the same direction as the line. TL/AS MCSs almost always form on the cool side of a slow-moving boundary, such as a warm front, stationary front, or remnant outflow boundary, and the stratiform precipitation forms further toward the cool side of this boundary. (The synoptic and mesoscale environments of these

MCSs will be discussed in greater detail in chapter 6.) TL/AS systems are often oriented approximately east-to-west, though their orientation can vary along with the orientation of the boundary.

The second-most-common extreme-rain-producing MCS pattern is a modified version of the PS archetype, and will be called "backbuilding, with parallel stratiform" and abbreviated "BPS." BPS systems are characterized by a line or cluster of quasi-stationary or backbuilding convection with a region of stratiform precipitation downstream and approximately parallel to the cell motion vector. In this pattern, convective cells repeatedly form upstream of their predecessors and train over a particular area, leading to large local rainfall totals. Decaying cells move downstream and are replaced by cells reaching their mature stage, behavior which sometimes appears in radar data as an unmoving area of high reflectivity. These systems sometimes form after the passage of a previously existing area of precipitation, and then leave outflow boundaries behind for further development upstream, such as is described by DBM96 and in the "mesohigh" type flash flood of MCH79.

Some of the MCS events classified as BPS in this study would fit the PS classification of Parker and Johnson (2000). However, there are two important features that distinguish the majority of BPS systems from the PS archetype. First, not all MCSs classified herein as BPS were "linear" in organization. Some only exhibited a relatively small area of backbuilding or quasistationary convection, though the region of parallel stratiform precipitation downstream was still present. Second, a few extreme-rain-producing systems that were indeed linear and had parallel stratiform precipitation were characterized by significant forward propagation, rather than backbuilding. Parker and Johnson found that the mean speed of the PS systems they observed was 11.4 m^{-1}. In contrast, many of the convective clusters and lines in the extreme-rain-producing systems observed here were nearly quasistationary or moved very slowly. Parker and Johnson (and Parker 1999) mentioned that some PS MCSs display significant backbuilding, while others do not. Such MCSs in which the line moved forward with little backbuilding were classified here as PS. Since these

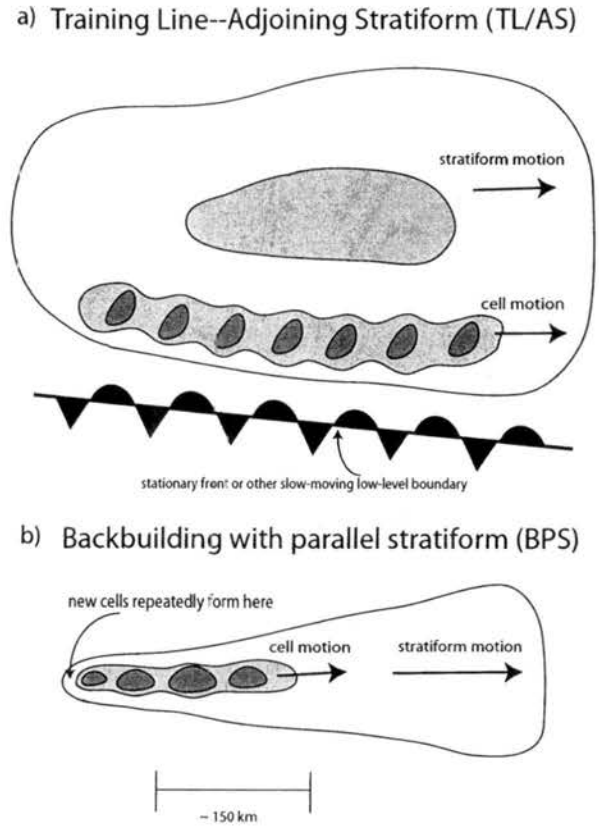

Figure 5.4: Schematic diagram of the radar-observed features of the (a) TL/AS and (b) BPS patterns of extreme-rain-producing MCSs. Contours (and shading) represent approximate reflectivity values of 20, 40, and 50 dBZ. The length scale at the bottom is approximate and can vary substantially, especially for BPS systems, depending on the number of mature convective cells present at a given time.

were relatively few, and since the processes governing backbuilding convection should be the same whether or not the convection is organized into a line, a new classification was created. Therefore, all MCSs in which significant backbuilding took place and in which there was a region of approximately parallel stratiform precipitation downstream while the system was producing extreme rainfall were classified as BPS.

A summary of the radar-observed characteristics of the TL/AS and BPS MCS patterns is shown in Fig. 5.4. This conceptual diagram shows how both systems are organized so that convective cells can pass over a given point repeatedly for an extended period, yielding large values of both rainfall rate and rainfall duration, and therefore extreme rainfall totals. BPS systems also appear to correspond very well to the schematic introduced by

Doswell et al. (1996), shown in Fig. 2.15. In this type of system, new cells form upstream of the nearly stationary outflow boundary left behind by mature cells and move from left to right (in the sense of the diagram) over the same area, leading to large rainfall totals.

Of course, not all of the MCSs classified as "TL/AS" or "BPS" (or as any other storm type, for that matter) correspond perfectly to the schematic shown in Fig. 5.4 or to the descriptions given above. When classifying leading-line, trailing-stratiform MCSs, Houze et al. (1990) noted whether each system was strongly, moderately, weakly, or not classifiable into this archetype. While these particular distinctions have not been made in the classification of extreme-rain-producing MCSs in this study, the reason for making such a distinction has not been ignored. In this sample as well, there were MCSs that fit exactly the TL/AS and BPS classifications (such as those that will be shown in Figs. 5.5–5.8), and those that were more difficult to classify. As mentioned above, the key factor in making classification decisions was the structure of the system at the time when the heavy rain was occurring. If the organizational structure of an MCS at and around this time did not closely resemble the TL/AS, BPS, or any of the other classifications, it was put into the "disorganized MCS" category.

Examples of portions of the life cycles of two TL/AS systems in different parts of the country and in different seasons are shown in Figs. 5.5 and 5.6. In each case, an area of convection began to form that eventually organized into a quasi-linear system with a region of stratiform precipitation moving in approximately the same direction as the convective cells. The stations reporting extreme rainfall totals were along the convective line and were therefore in an area conducive to echo training, consistent with the discussion in section 2.4. The 12–13 June 2001 system produced one report of extreme rainfall along the Minnesota/Iowa border and several reports of flash flooding in that area. The 22–23 October 2000 MCS produced over 225 mm (approx. 9 in) of rain in some locations and resulted in record flooding in west-central Oklahoma. It is difficult to distinguish radar snapshots of these two systems from those that might be observed with TS MCSs, which

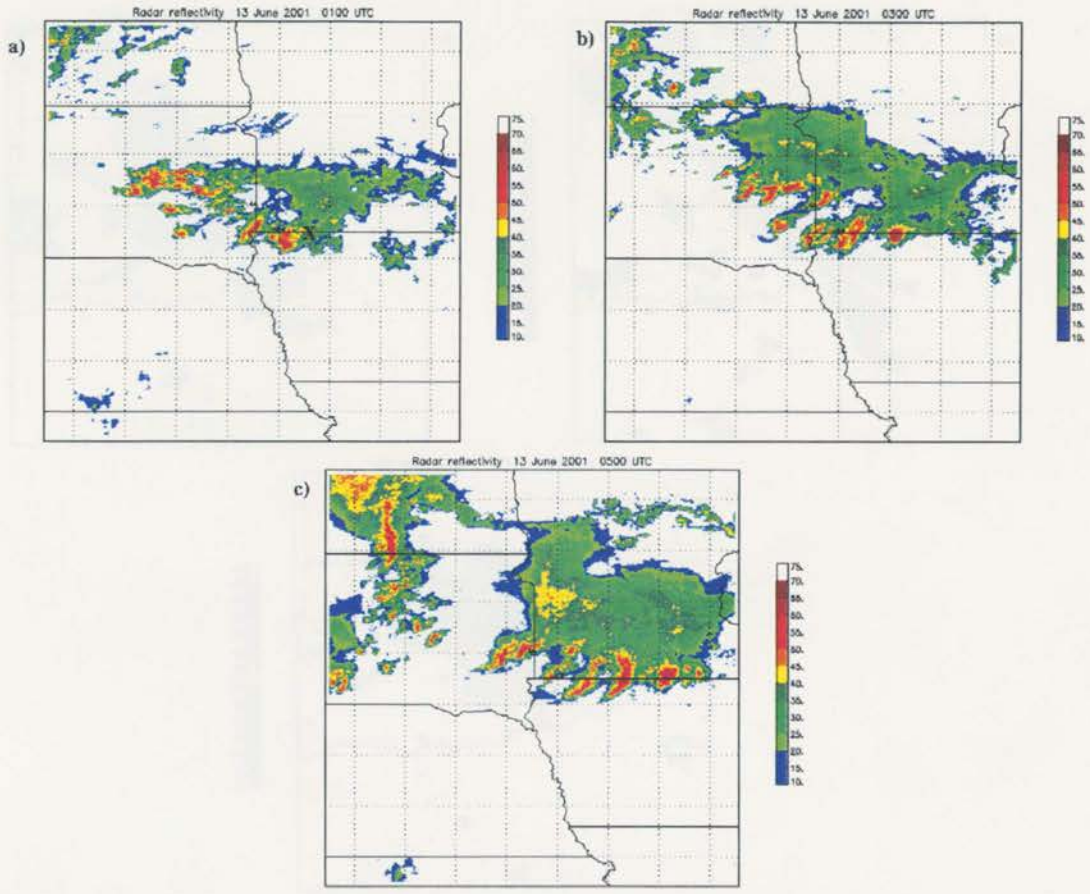

Figure 5.5: Composite radar reflectivity (dBZ) from TL/AS MCS extreme rain event at (a) 0100 UTC, (b) 0300 UTC, and (c) 0500 UTC 13 June 2001. Reflectivity scale is shown at right. Stations reporting extreme rainfall totals are denoted with an "X" in (a).

further emphasizes the importance of animating the radar data. Actually, both of these MCSs did evolve into TS systems after producing the extreme precipitation as TL/AS MCSs, a behavior that was observed in several of the TL/AS cases.

Because they may only have TL/AS characteristics for a small fraction of their lifetime before evolving into a more recognizable structure, these MCSs may have eluded the attention of previous MCS-classification studies. For instance, Parker and Johnson (2000) classified convective systems based on the radar-observed structure that existed for the largest portion of the system's life cycle. In addition, TL/AS MCSs do not typically occur in the warm sector, so they may have been excluded from other MCS studies that focused on warm-sector systems.

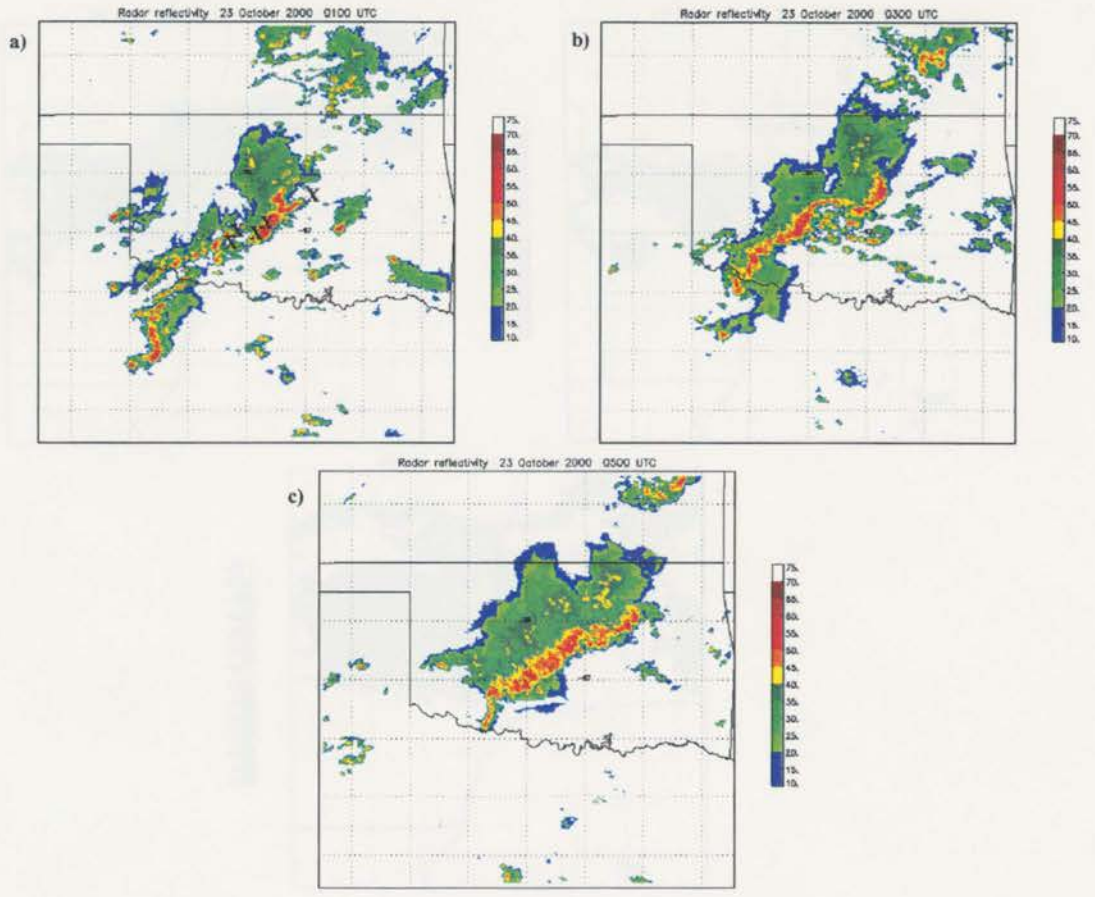

Figure 5.6: As in Fig. 5.5, except for (a) 0100 UTC, (b) 0300 UTC, and (c) 0500 UTC 23 October 2000. Cell motion within the line is from southwest to northeast.

Two BPS MCSs are shown in Figs. 5.7 and 5.8. In the 12–13 June 2000 case (incidentally, exactly one year earlier than the case shown in Fig. 5.5), a line of convection formed that backbuilt and resulted in echo training in northern North Dakota. The 19–20 June 2001 BPS event formed upstream of a previous convective system. At 1630 UTC (Fig. 5.8a), a dissipating area of rainfall was passing eastward through northeastern Kansas. By 1830 UTC (Fig. 5.8b), a cluster of intense convection had developed behind the earlier convection that had weakened. New cells continued to form upstream and move eastward, resulting in an area of nearly stationary convection for several hours. One station reported 209 mm (8.25 in) of rain from this system, and there were unofficial reports of over 250 mm, though only one station officially reported a total above the extreme rainfall thresh-

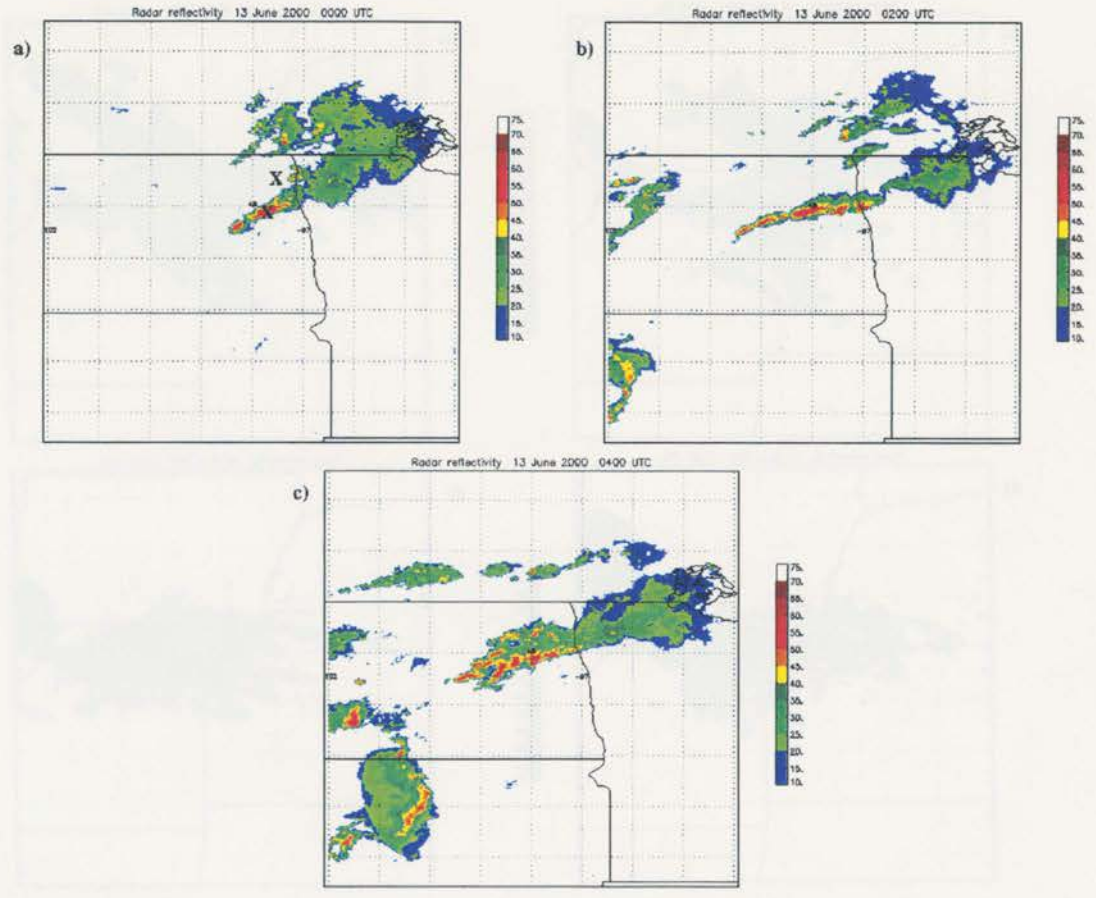

Figure 5.7: As in Fig. 5.5, except for BPS MCS extreme rain event at (a) 0000 UTC, (b) 0200 UTC, and (c) 0400 UTC 13 June 2000. Note how new convective cells and convective clusters form upstream of the previous convection at 0200 and 0400 UTC.

old. Another example of an extreme-rain-producing BPS MCS is the system described by Chappell (1986, his Fig. 13.11).

5.2.2 Climatological characteristics

Now that the subclassifications of extreme-rain-producing synoptic systems and MCSs have been defined, an analysis of where, when, and how often they occur can be presented. The approximate location and storm type of each extreme rain event from 1999–2001 is shown in Fig. 5.9. These figures allow for comparison between years within the sample and show where synoptic events dominate over MCS-related events and vice versa. In 1999, a large number of events were concentrated in a few states, with a large number

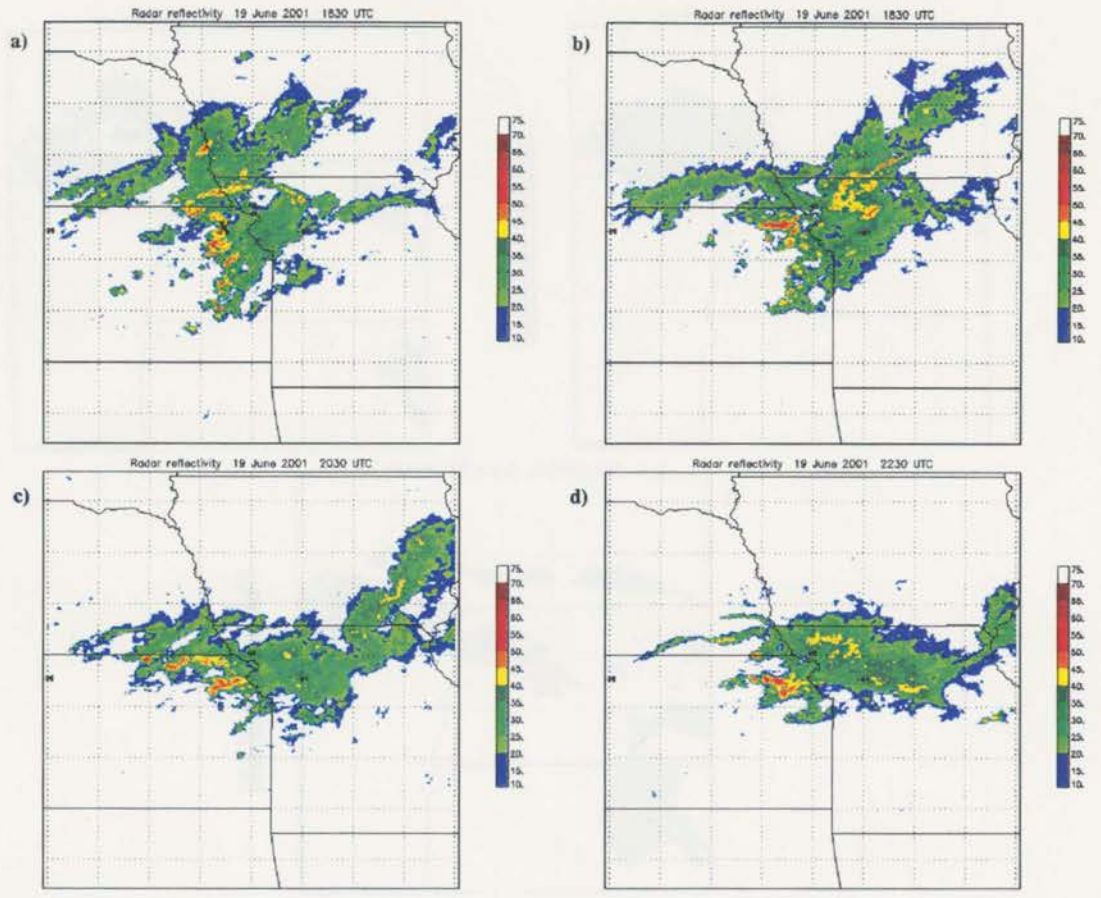

Figure 5.8: As in Fig. 5.5, except for BPS MCS extreme rain event at (a) 1630 UTC, (b) 1830 UTC, (c) 2030 UTC, and (d) 2230 UTC 19 June 2001. Note the area of quasi-stationary convection in northeastern Kansas from 1830–2230 UTC.

of MCS cases in South Dakota, Nebraska, Kansas, Iowa, and Illinois. Several tropical systems affected the east coast and caused major flooding there, including Hurricanes Dennis, Floyd, and Irene. In 2000, the extreme rain events were relatively balanced throughout the country, while in 2001, several large synoptic systems in the south and southeast produced widespread extreme rainfall. A number of synoptic systems also affected the northeast in 2001, with relatively few events in the upper Midwest.

The number of events grouped into each of the synoptic and MCS subclassifications is given in Table 5.1. As discussed in section 5.1, synoptic events that are dominated by convective storms produce extreme precipitation totals more often than those where non-convective processes are responsible for most of the rainfall. The TL/AS and BPS

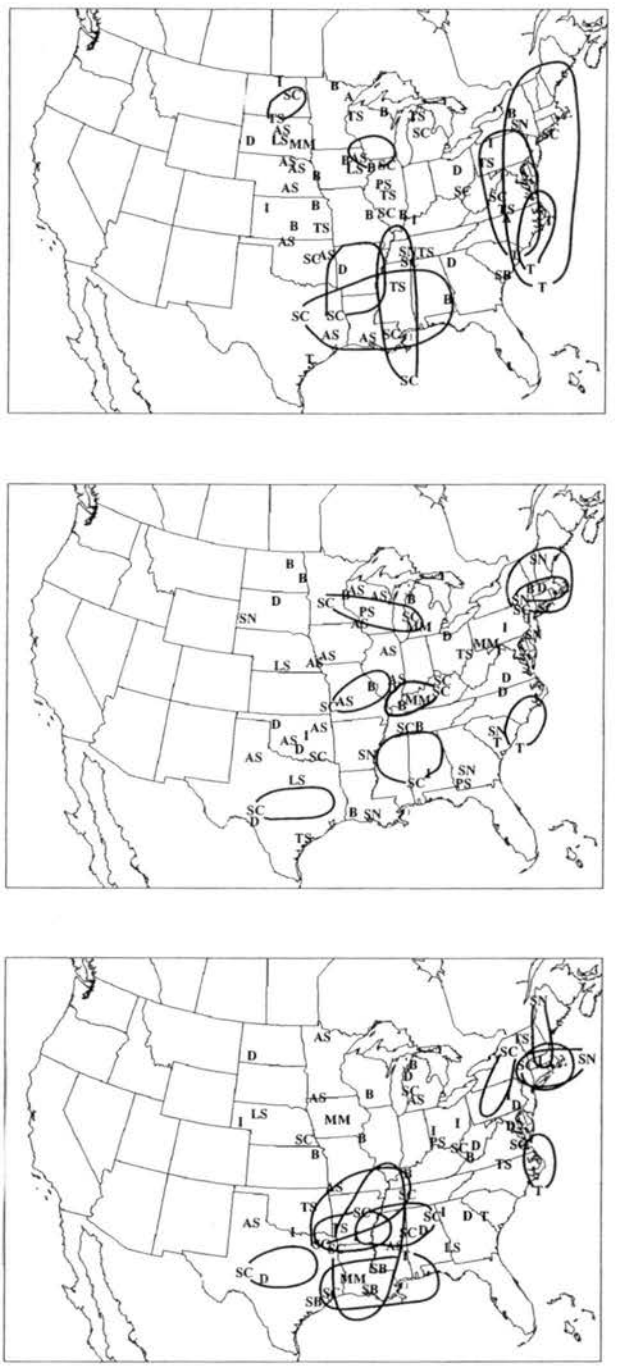

Figure 5.9: Approximate locations and storm types of all extreme rain events in (a) 1999, (b) 2000, and (c) 2001. Lettering system is as follows: B=BPS, MM=multiple MCS, D=disorganized MCS, SB=sea-breeze front MCS, SC=synoptic/convective, SN=synoptic/non-convective, I=isolated, T=tropical. AS, TS, LS, and PS systems are lettered accordingly. Cases where widespread extreme rainfall was reported are outlined.

Table 5.1: Number of extreme rain events associated with the subclassifications of synoptic systems and MCSs.

Synoptic systems	Events	Percentage of synoptic	Percentage of all events
Convective	39	75.0%	20.2%
Non-Convective	13	25.0%	6.7%
Total	52	100%	26.9%
MCSs	Events	Percentage of MCSs	Percentage of all events
TL/AS	29	25.4%	15.0%
BPS	26	22.8%	13.5%
TS	17	14.9%	8.8%
LS	6	5.3%	3.1%
PS	4	3.5%	2.1%
Mult. MCS	7	6.1%	3.6%
Disorganized	21	18.4%	10.9%
Sea-breeze	4	3.5%	2.1%
Total	114	100%	59.1%

patterns are the most common MCS types. Though "disorganized" MCSs are the next most frequently observed type, they exhibited any number of convective structures and will therefore not be explored in detail in this study. There were 17 cases associated with TS systems, which usually had anomalous motion characteristics (rather than the more common line-perpendicular motion) that allowed them to produce extreme rainfall totals. For instance, some moved very slowly and others had bowed segments that allowed for periods where cell motion was parallel to the convective line.

The distribution of MCS types in the Plains and Ohio/Mississippi Valley regions resembles the overall distribution closely, while the distributions are quite different in the other regions (Table 5.2). In the north region, TL/AS and BPS systems were associated with a greater proportion of the MCS events than in the overall sample, with relatively few disorganized MCSs. In contrast, the southeast region had relatively few TL/AS and BPS systems, and disorganized MCSs played a large role. Disorganized MCSs were also the most common MCS type in the northeast region. These contrasts likely come about because the boundaries and mesoscale forcings required for organized MCSs are fairly common in the central U. S., while the atmospheric conditions leading to organized MCSs are less

Table 5.2: Distribution of extreme-rain-producing MCS types by region. Numbers in parentheses represent the percentage of MCS events in that region associated with the respective storm type. For example, the entry in the upper left indicates that TL/AS systems accounted for 31.3% of Plains MCS cases.

System	Plains	North	OH/MS	NE	South	SE	**Total**
TL/AS	5 (31.3%)	10 (34.5)	6 (24.0)	0 (0)	10 (34.5)	1 (7.1)	29 (25.4)
BPS	3 (18.8)	11 (37.9)	8 (32.0)	2 (25.0)	4 (13.8)	1 (7.1)	26 (22.8)
TS	1 (6.3)	3 (10.3)	4 (16.0)	2 (25.0)	5 (17.2)	2 (14.3)	17 (14.9)
LS	3 (18.8)	1 (3.4)	0 (0)	0 (0)	1 (3.4)	1 (7.1)	6 (5.3)
PS	0 (0)	1 (3.4)	2 (8.0)	0 (0)	0 (0)	1 (7.1)	4 (3.5)
Mult.	1 (6.3)	2 (6.9)	1 (4.0)	1 (12.5)	1 (3.4)	1 (7.1)	7 (6.1)
Disorg.	3 (14.3)	1 (3.4)	4 (16.0)	3 (37.5)	5 (17.2)	6 (42.9)	21 (18.4)
Sea-brz	0 (0)	0 (0)	0 (0)	0 (0)	3 (10.3)	1 (7.1)	4 (3.5)
Total	16	29	25	8	29	14	114

commonly in place in the eastern part of the country (e.g., Laing and Fritsch 1997). For reasons that are not as clear, the south had more than twice as many TL/AS systems as BPS systems in the period of study.

The monthly frequency distribution of the individual MCS subclassifications (Table 5.3) does not stray very significantly from the overall distribution for MCSs that was previously presented in Fig. 4.7. TL/AS systems were more common in the spring summer months of March and April than were the other types, with few events occurring in August or later. The monthly distribution of BPS events is similar to that of the overall distribution for MCSs, while there was a strong maximum of disorganized MCSs in July

Table 5.3: Monthly frequency distribution of the MCS subclassifications. No MCS-related extreme rain events were observed in January, February, November, or December, so these months have been omitted from the table.

Month	TL/AS	BPS	TS	LS	PS	Mult.	Disorg.	Sea-brz	Total
March	3	1	0	0	0	0	0	0	4
Apr.	2	0	0	0	1	0	1	0	4
May	5	4	4	0	0	0	0	1	14
Jun.	6	4	5	1	0	0	2	1	19
Jul.	8	9	5	3	1	0	8	1	35
Aug.	2	6	2	1	1	2	6	1	21
Sep.	1	2	1	1	1	4	1	0	11
Oct.	2	0	0	0	0	1	3	0	6

and August with few in May and June.

While determining the regional characteristics and the monthly frequency distributions of extreme rain events (and extreme-rain-producing MCSs in particular) is certainly important to understanding more about these systems, one equally important aspect that has been neglected to this point is their diurnal distribution. To understand the driving forces behind the convection and to ascertain its predictability, knowing the time of day at which it is most likely to occur is crucial. The results of previous work regarding the diurnal characteristics of convection in general and of extreme rainfall in particular were discussed in section 2.2.2, and the results to be presented here should provide further insights into the diurnal cycle of precipitation. As briefly mentioned in section 3.2, three times in the life cycle of each extreme rain event will be discussed. The *onset time* used here is the hour of *heavy* rain onset as determined using the radar data (the time of the first echo $\geq$ 45 dBZ at the extreme rainfall location for most systems), the *peak time* is the hour when the heaviest rain was falling at the station(s) where extreme rain was reported (again, inferred from the radar data), and the *end time* is the hour when *all* radar echoes have dissipated or moved out of the area. Synoptic, tropical, and multiple MCS cases have been eliminated from the diurnal distributions because their long durations make pinpointing onset and peak rainfall times difficult (and possibly not even meaningful.) This leaves all other MCS cases and isolated events. Since there are relatively few isolated events and since they may be expected to have different diurnal characteristics from the MCS-related cases, the discussion of the diurnal distributions will focus on extreme-rain-producing MCSs. The diurnal characteristics will be presented in an overall sense, and then both by region and by storm type, since each of these perspectives may be helpful in its own way.

In general agreement with past studies regarding extreme rainfall and flash floods (cf. Fig. 2.13), extreme rain events in this sample most often developed in the late afternoon and evening, peaked after dark, and dissipated or moved out of the area in the early morning hours (Fig. 5.10). The onset time for the "average" extreme rain event was between 1700

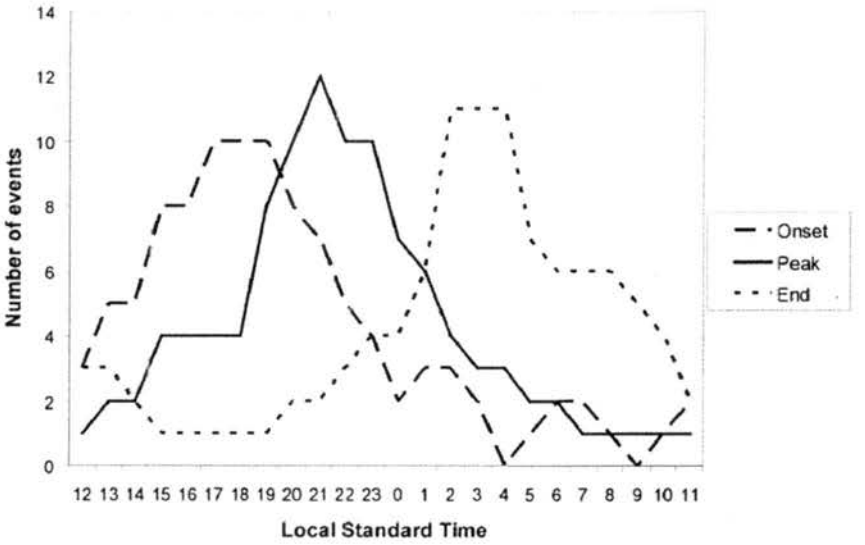

Figure 5.10: Diurnal frequency distribution for heavy rain onset, peak rainfall, and rainfall end for MCS-related extreme rain events. Number of events is smoothed with a 3-h running mean.

and 1900 LST, with a peak around 2100 LST and an end time between 200 and 400 LST. This confirms previous findings that most flash flood events are nocturnal; while the peak rainfall time of 2100 LST may not be long after sunset during the summer, the flooding generally occurs up to 6 h after the causative rainfall—well after dark. While events did begin at all times of the day, relatively few developed between 300 and 1200 LST, with an associated minimum in rainfall peaks between 600 and 1300 LST. As a whole, these findings agree with a conceptual model where convective storms form as a result of daytime heating, increase in coverage and intensity (and take on the structures that allow them to produce large local rainfall totals) as the low-level jet intensifies after dark, and either dissipate or move with greater speed in the early morning hours. Such processes have been described in part by Wallace (1975), MCH79, and others, and will receive more detailed consideration in chapter 6. It should be noted that the end time presented in these results does not necessarily indicate the complete dissipation of the convective system, only that precipitation has ended at the location where extreme rainfall was reported. The MCSs

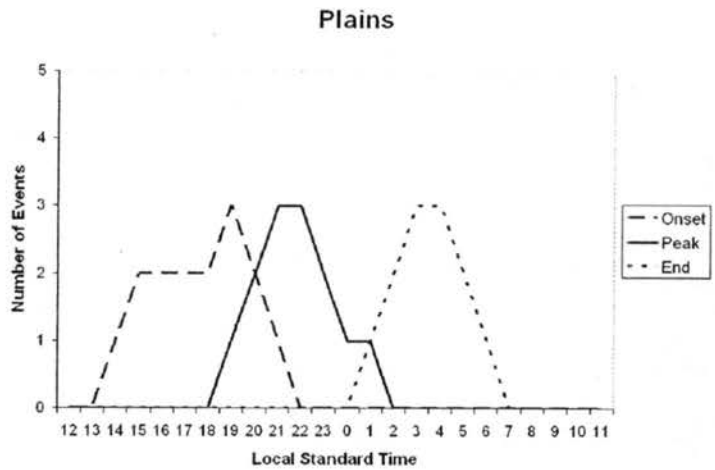

Figure 5.11: As in Fig. 5.10, except for the Plains region. Number of events is smoothed with a 3-h running mean.

responsible for extreme rainfall totals often persisted for several additional hours after propagating away from where they initially produced the heavy rains.

The diurnal frequency distributions in the Plains and north regions are very similar to the overall distribution, with heavy rain beginning in the late afternoon/evening, peaking in the nighttime hours, and ending in the early morning (Figs. 5.11 and 5.12). The peak rainfall time for MCS-related extreme rain events in the north region (2300-0000 LST) was typically a bit later than in the Plains (and the overall distribution). These results agree well with the strong nocturnal maximum for heavy precipitation in the north central U. S. found by Wallace (1975) and Winkler et al. (1988, Fig. 2.12). They are also consistent with the recent findings of Carbone et al. (2002), who found that long-lived precipitation "episodes" regularly form near the Rocky Mountains in the afternoon and evening and propagate eastward through the night. It is likely that many of the extreme-rain-producing MCSs discussed here in the Plains and north regions were part of such episodes.

In the Ohio/Mississippi valley region (Fig. 5.13), the most common onset, peak, and end times were similar to those in the sample as a whole, but the distributions of these times are wider than in the Plains and north regions. This indicates that extreme-rain-

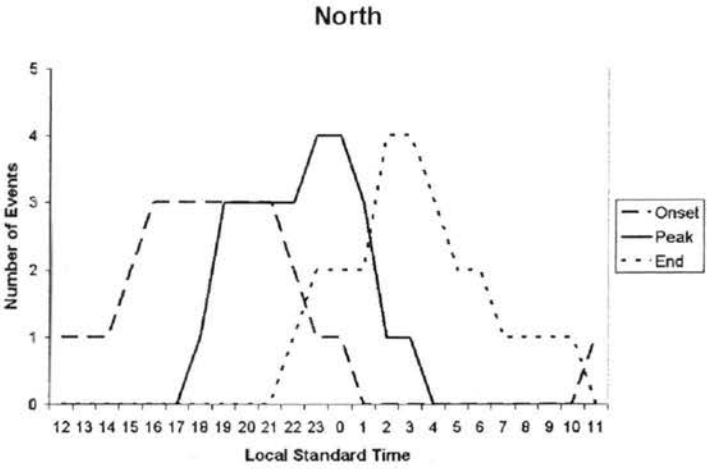

Figure 5.12: As in Fig. 5.10, except for the north region.

producing convection in the Ohio/Mississippi valley may occur at a wider variety of times than in the regions farther north and west. The south region (Fig. 5.14), along with a similarly wide diurnal distribution, had a composite peak time at 2100 UTC but both an earlier onset time and a later end time, suggesting that extreme rain events in the south have, on average, a longer duration than those in other regions. Indeed, southern events did last longer than those in any other region, which will be discussed below. This may result in part from the higher extreme rain threshold in the south, which means that southern events have inherently higher rainfall totals.

In contrast to the regions already discussed, MCS-related extreme rain events in the northeast region occurred most often in the afternoon and evening and dissipated or moved away shortly after dark (Fig. 5.15). This is consistent with the strong afternoon/evening maximum for heavy warm-season precipitation in the northeast found by Winkler et al. (1988). (Recall, however, that synoptic systems were the most common extreme rain-producers in the northeast.) The southeast region had no distinct diurnal cycle for MCS-related extreme rain events (Fig. 5.16), though Winkler et al. (1988) found that there is a strong afternoon maximum in thunderstorms and precipitation as a whole. Geerts (1998) found a comparable result for all MCSs in the southeast: "the phase of this diurnal cycle

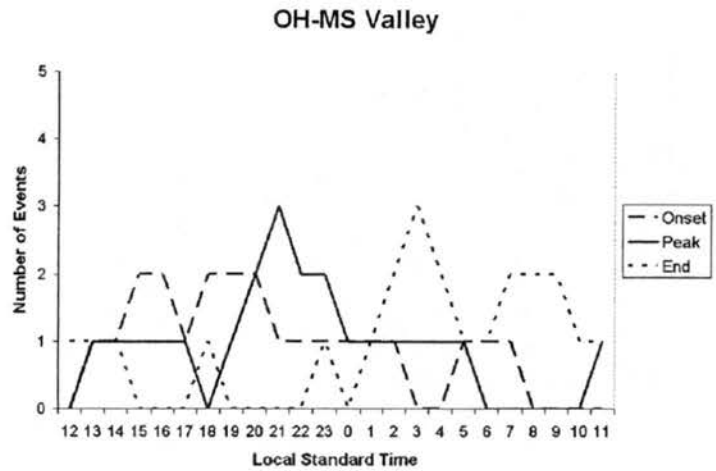

Figure 5.13: As in Fig. 5.10, except for the Ohio/Mississippi valley region.

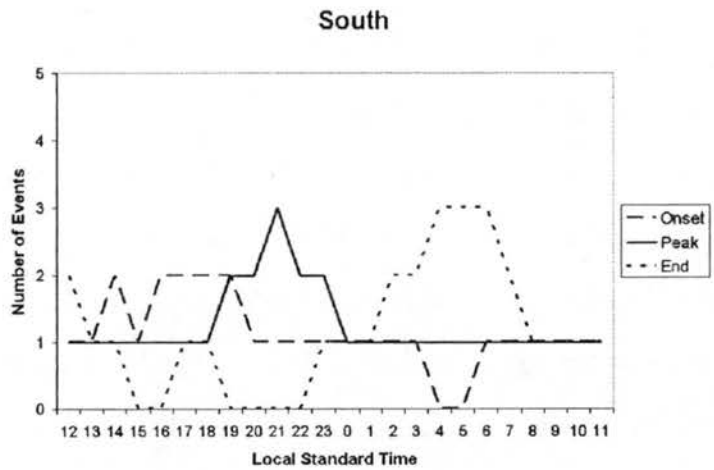

Figure 5.14: As in Fig. 5.10, except for the south region.

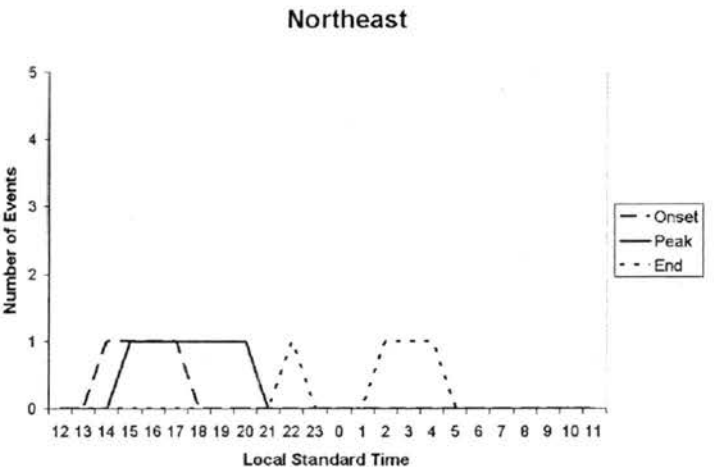

Figure 5.15: As in Fig. 5.10, except for the northeast region.

[of MCSs] is similar to that of thunderstorms ... but the amplitude is surprisingly small."

When considering the diurnal frequency distribution of extreme-rain-producing MCSs by storm type, it appears that TS and disorganized systems are more modulated by the diurnal cycle than TL/AS and BPS MCSs are. TL/AS (Fig. 5.17) and BPS (Fig. 5.18) systems had very wide distributions in onset, peak, and end times, with some BPS systems peaking at nearly every hour of the day. In contrast, TS systems (Fig. 5.19) seem to have a strong diurnal cycle, corresponding closely to the overall distribution shown in Fig. 5.10, with heavy rain onset between 1700–2000 LST, peak rainfall between 2000–2300 LST, rainfall end between 200–300 LST, and very narrow distributions of all three. These results are similar to the 2200 LST mean centerpoint for TS MCSs found by Parker and Johnson (2000). Due to the small sample of LS and PS MCSs, their diurnal distributions are not shown here. Disorganized MCSs also appear to have a relatively strong diurnal cycle, though they occurred slightly earlier than the average, with onset between 1700-1800, peak between 1900-2000, and end around 200 LST (Fig. 5.20).

The diurnal frequency distributions of extreme rain events suggest that some storm types (interestingly, the disorganized MCSs and the very organized TS systems) and the convective systems in some regions (mainly in the northern part of the country) operate on

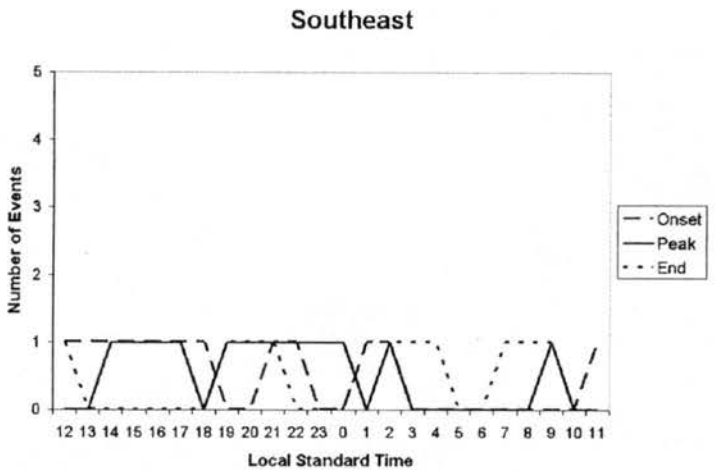

Figure 5.16: As in Fig. 5.10, except for the southeast region.

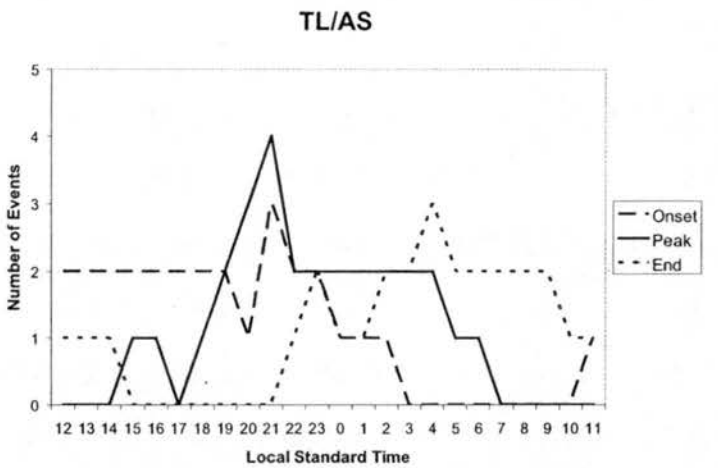

Figure 5.17: Diurnal frequency distribution of heavy rain onset, peak rainfall, and rainfall end for TL/AS MCS extreme rain events. Number of events is smoothed with a 3-h running mean. Systems most commonly had onset at 1700–1900 LST, peak at 2100 LST, and end time at 200–400 LST.

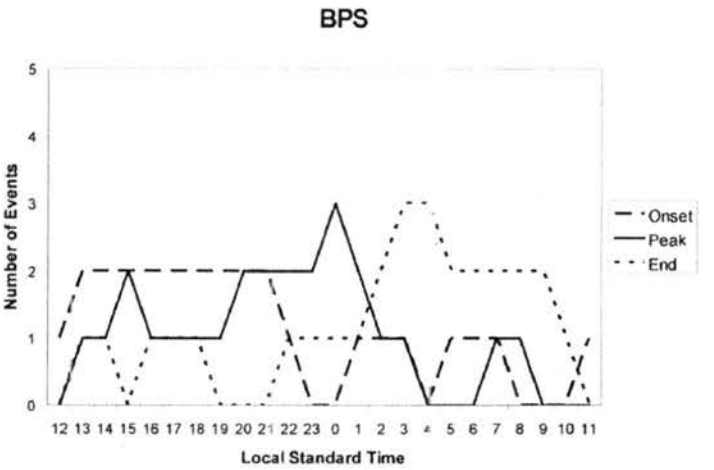

Figure 5.18: As in Fig. 5.17, except for BPS MCS events.

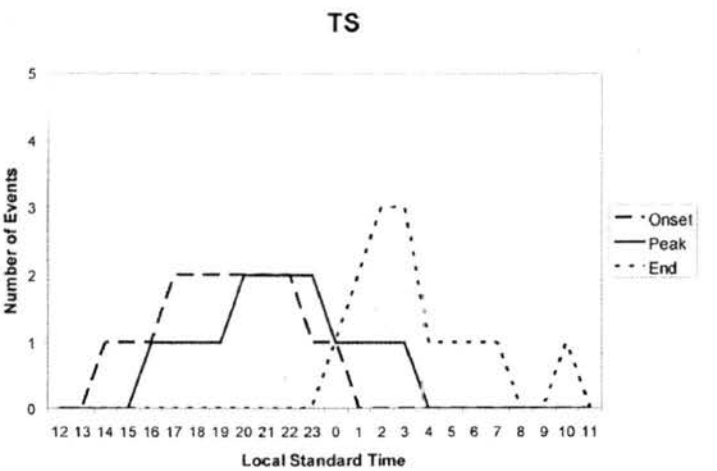

Figure 5.19: As in Fig. 5.17, except for TS MCS events.

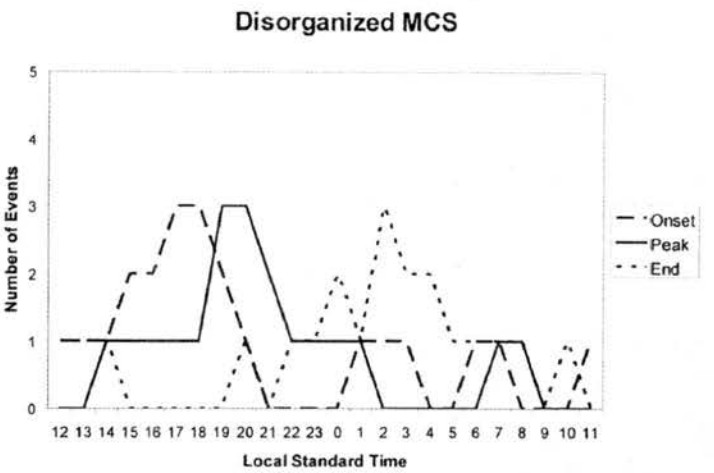

Figure 5.20: As in Fig. 5.17, except for disorganized MCS events.

a fairly consistent diurnal cycle, while other types and other regions have less predictable diurnal characteristics. These results imply that in the northern U. S., where there is also a strong seasonal cycle for extreme rainfall, that the ingredients for extreme precipitation only come into place at very specific times of year and times of day. Or, in other words, a relatively rare set of circumstances, which only occurs in certain months and at certain times, is needed for extreme rainfall to occur in the northern part of the country, while a wider variety of conditions (less dependent on the diurnal and seasonal cycles) may support such events in other regions. The same may apparently be said for a few of the storm types.

Presenting the average onset, peak, and end times of the MCS events leaves one key component missing from the discussion—the actual duration of the events. Just because the peaks in the above graphs fall at a certain time of day does not mean they indicate the duration of an average extreme-rain-producing MCS. The average duration of the MCS-related extreme rain events, by storm type and region, are shown in Table 5.4. The duration, for these purposes, is simply the time between the onset and end times (as defined above). This does not necessarily mean that heavy rain was falling for the entire duration, as there may have been periods within the duration when light rain or no rain at all was falling. The average duration for all MCS cases in the sample was 10.4 h, with TS cases

Table 5.4: Average duration (h) of MCS-related extreme rain events, by storm type and region. The duration is simply the amount of time between the event's onset and end times, as defined in the text. Therefore, these values do not necessarily represent the amount of time that heavy rain was falling, only the period between when the heavy rain started and all rain ended.

System	Plains	North	OH/MS	NE	South	SE	**Total**
TL/AS	9.0 h	11.0	11.0	N/A	12.8	6.0	10.8
BPS	11.3	9.9	10.0	6.5	13.3	19.0	10.7
TS	6.0	6.3	8.5	11.0	9.6	5.5	8.2
Disorg.	9.0	7.0	12.8	7.7	14.6	10.8	11.4
Total	9.3	9.8	10.5	8.3	12.6	10.1	10.4

typically having a shorter duration and disorganized MCSs having a longer duration than the average. These results do not necessarily imply that TS MCSs are shorter lived; Parker and Johnson (2000) showed that TS MCSs typically propagate significantly faster than other linear MCSs. Therefore, extreme-rain-producing TS systems may tend to move out of the area where the extreme rainfall occurred faster than the other MCS types, yielding a shorter duration as it is measured here. Disorganized MCSs were often more intermittent in nature, with long periods of time between the passages of convective cells. Therefore, in these events, a longer period of time is required to produce extreme rainfall at a given point. The average duration in the south was longer than in any of the other regions, which, as alluded to previously, may be explained in part by its higher extreme rain thresholds.

5.2.3 Rainfall characteristics

Another useful set of statistics is the rainfall characteristics of the various classifications of extreme rain events. While every event selected for this study has met a certain threshold to insure that it is indeed "extreme" for its area, there is still a question of which events tend to cause the most rainfall and have the most potential to cause serious damage. Two pieces of information obtained from the rain gauge data can give insight into this question: the maximum rainfall total reported during an event, and the number of stations reporting extreme rainfall totals. Certainly, these values are highly dependent on

Table 5.5: Average maximum 24-h rainfall total by region and storm type for several types of extreme rain events. For example, the upper left entry indicates that the maximum reported rainfall averaged over all Plains TL/AS events is 141.38 mm. The top entry in the "total" column, for instance, shows that the average maximum reported rainfall for all TL/AS events is 159.37 mm.

System	Plains	North	OH/MS	NE	South	SE	**Total**
TL/AS	141.4 mm	143.3	149.4	N/A	191.0	162.1	159.4
BPS	168.0	158.1	175.0	118.0	169.5	166.4	164.2
TS	128.0	137.9	153.9	123.6	189.0	139.7	154.7
Disorg.	119.1	102.1	123.1	143.2	163.0	151.0	141.3
Isolated	133.7	N/A	117.7	124.0	184.9	161.5	142.8
Synoptic	129.0	108.7	154.4	133.3	206.4	161.1	162.2
Tropical	N/A	N/A	N/A	234.3	451.9	264.3	278.5

the density of the rain gauge network in the vicinity of the event—an event occurring in a station-dense area will have more extreme rain reports than the exact same event in a station-sparse area—but the objective statistics to be shown here agree generally with my own subjective ideas about which events were the most severe.

Of the MCS-related extreme rain events, BPS systems tended to produce higher maximum 24-h rainfall totals than the other MCS types (Table 5.5, far right column), with an average maximum report of just over 164 mm (6.47 in). BPS MCSs also averaged more extreme rainfall reports than the other MCS types, with 2.73 reports per event (Table 5.6, far right column). The reason that BPS systems, on average, are capable of producing higher rainfall totals is that they appear to have no inherent temporal limit on their back-building and echo training effects. One can imagine the behavior shown in Fig. 2.15 lasting for many hours, as long as the moisture source for the convection is not removed. In contrast, forward-propagating linear MCSs usually have a convective line with certain motion characteristics, which can also result in extreme rainfall but only for the duration that the length of the line allows. (However, these statistics do not give any information about the overall rainfall coverage, which may be greater in the forward-propagating linear MCSs even though the extreme rainfall coverage is less.)

For purposes of comparison, the rainfall statistics for isolated, synoptic, and tropical

Table 5.6: As in Table 5.5, except for average number of stations (per event) reporting extreme rainfall.

System	Plains	North	OH/MS	NE	South	SE	**Total**
TL/AS	2.4	2.7	1.6	N/A	2.4	1	2.63
BPS	4.7	2.8	2.3	1	1.3	1	2.73
TS	8	3	2.3	1	1.8	1	2.29
Disorg.	2	1	1.5	1.7	1.2	1.5	1.57
Isolated	1.5	N/A	1	1.2	1	1.5	1.18
Synoptic	1.3	1.2	2.7	6.9	3.8	1.3	3.74
Tropical	N/A	N/A	N/A	99.5	40	9.7	36.60

systems have been included in Tables 5.5 and 5.6. By definition, isolated events rarely had more than one or two extreme rain reports, while synoptic systems averaged more extreme reports than any of the MCS types. Tropical cyclone-related extreme rain events were relatively rare but were by far the most devastating. Tropical Storm Allison (2001) and Hurricane Floyd (1999) both had 24-h rainfall totals that far exceeded any of the other events in the sample. This is apparent in the rainfall statistics, where the average maximum rainfall report for tropical events is nearly twice that of the other types, and the average number of reports is nearly 10 times that of the other types.

Information about the storm types that caused the highest rainfall totals and the most extreme rain reports in each region are also shown in Tables 5.5 and 5.6. The important data in these two tables are in the columns; intercomparing between regions is not helpful because the spatially-varying threshold makes the average maximum rainfall in the south inherently higher than that in the north. BPS systems produced the highest rainfall totals (of the MCS types) in all but the northeast and south regions. In the northeast, however, the sample of MCS cases was so small that these results are likely insignificant. In the south, both TL/AS and TS systems produced higher rainfall totals than the BPS MCSs. The reason for this is not entirely clear.

5.3 Flash flooding and severe weather associated with extreme rain events

5.3.1 Flash flooding

The main reason that rain gauge observations, as opposed to flash flood reports, were chosen as the criteria for selecting cases for this study is that flash flood reports are dependent on so many factors other than rainfall itself. First, using flash flooding adds the hydrological component to the problem, which adds a great deal of further complexity. Second, if flash flooding occurs, whether or not it actually gets reported depends on where it occurs and whether anyone was there to observe it. The rainfall observations are not perfect either, and the observing network has large gaps, but they provide a much more objective (and meteorological) approach to selecting cases.

With this in mind, one way to determine whether the thresholds developed for selecting extreme rain events are appropriate is to see if the cases selected were actually associated with flash flooding. If the "extreme rain events" were not responsible for flash flooding, then studying them would not get us any closer to solving the "flash flood problem." Since only 24-h rainfall is being used here, and since rain rate also plays a role, it is possible that many of the events meeting the extreme rain criteria could be longer-duration events that produce copious amounts of rainfall but occur over long enough periods of time that they do not cause flooding. Fortunately, as is shown below, almost all of the cases used in this study did cause flash flooding. Even more importantly, this is especially true of the two most common MCS radar patterns presented in the previous section.

One hundred percent of the TL/AS MCS extreme rain events considered in this study were associated with flash flood reports, as were 24 of the 26 BPS MCS events (Table 5.7). In total, 90.4% of MCS cases had corresponding flash flood reports. The two MCS types with less than this percentage were the disorganized MCSs and the events with multiple MCSs. This result is not totally unexpected in the case of multiple MCS events since, by definition, there is a time in between the convective systems where rainwater can run off or

Table 5.7: Number and percentage of extreme rain event types associated with flash flooding.

System	Number with FF reports	Total number	Percentage
TL/AS	29	29	100.0%
BPS	24	26	92.3%
TS	14	17	82.4%
LS	6	6	100.0%
PS	4	4	100.0%
Mult. MCS	5	7	71.4%
Sea-breeze	4	4	100.0%
Disorg. MCS	17	21	81.0%
All MCS	103	114	90.4%
Synop–conv.	37	39	94.9%
Synop–non-conv.	7	13	53.8%
All Synoptic	44	52	84.6%
Isolated	13	17	76.5%
Tropical	10	10	100.0%
All events	**170**	**193**	**88.1%**

evaporate, thus reducing the flash flood threat. For disorganized MCSs, the training that occurs is often spread out over longer periods of time than in the more organized systems, which also allows time for the ground to recover.

The distinction between convective and non-convective synoptic systems greatly affects the flash flood potential. Almost all of the convective events caused flash floods, while only 54% of the non-convective events did. The high rain rates of the convective storms are much more conducive to local flooding than the long-duration stratiform rain of the non-convective systems, even though their 24-h totals may be the same. While some of the isolated extreme rain events had very high local rainfall totals, only 76.5% of them were associated with flash flooding. Since they cover such a small area, there is a good chance that the systems without flood reports actually did cause flooding, but it went undetected. Their small size also decreases the chance that the rain would fall on a flood-prone area.

Table 5.8: As in Table 5.7, except for severe hail, winds, tornadoes, and significant tornadoes.

	Svr hail		Svr wind		Tornadoes		SigTor	
System	#	%	#	%	#	%	#	%
TL/AS	21	72.4%	19	65.5%	9	31.0%	0	0%
BPS	13	50.0%	17	65.4%	5	19.2%	0	0%
TS	9	52.9%	13	76.5%	4	23.5%	1	5.9%
LS	4	66.7%	3	50.0%	1	16.7%	0	0%
PS	3	75.0%	4	100%	2	50.0%	0	0%
Mult. MCS	2	28.6%	5	71.4%	0	0%	0	0%
Sea-breeze	1	25.0%	2	50.0%	0	0%	0	0%
Disorg. MCS	6	28.6%	7	33.3%	2	9.5%	0	0%
All MCS	59	51.8%	70	61.4%	23	20.2%	1	0.9%
Synop–conv.	19	48.7%	24	63.2%	16	42.1%	8	21.1%
Synop–non-conv.	0	0%	0	0%	0	0%	0	0%
All Synoptic	19	36.5%	24	46.2%	16	30.8%	8	15.4%
Isolated	6	35.3%	8	47.1%	0	0%	0	0%
Tropical	3	30.0%	4	40.0%	6	60.0%	0	0%
All events	**87**	**45.1%**	**106**	**54.9%**	**45**	**23.3%**	**9**	**4.7%**

5.3.2 Severe weather

While severe weather is not as intimately related to the events studied in this project as flash flooding is, operational forecasters have to issue warnings for both while the events are occurring. A full treatment of how and why each of these types of systems produce severe weather is beyond the scope of this study, but some basic information about how often each storm type produces hail, severe winds, and tornadoes may yield some information about the convective processes that are at work in each of them.

In total, over half of the extreme rain events also produced at least one severe wind report (58 mph or greater, as defined by the NWS), just under half produced severe hail (0.75 in or greater), almost one quarter spawned a tornado, and less than 5% produced a significant (rated F2 or higher on the Fujita scale) tornado (Table 5.8). The fact that so many extreme-rain-producing systems also caused severe winds seems to be somewhat of a contradiction, since severe windstorms typically require a dry layer aloft, but heavy rain events need a deep moist layer. However, since organized MCSs and synoptic systems

are responsible for so many of these events, it is possible that they attain a state whereby they can produce both extreme rainfall and strong straight-line winds, such as the wet microbursts described by Atkins and Wakimoto (1991) and others. This topic is suggested for future investigation. Tornadoes (and significant tornadoes) have been previously documented in conjunction with flash flood events (e.g., Rogash and Racy 2002), and a number of events of this type are found in this sample. Nearly all of the significant tornadoes were spawned by strongly-forced synoptic systems, consistent with the strong vertical shear necessary for significant tornadogenesis. Additionally, over 30% of TL/AS MCSs spawned tornadoes, though none was significant. While the national composite radar data do not have velocity information or the resolution necessary to indicate storm rotation, many of the developing convective elements in TL/AS systems took on the reflectivity signature of supercell thunderstorms before evolving into a line. This may explain the relatively high percentage of TL/AS MCSs that also produced severe weather and tornadoes.

Chapter 6

SYNOPTIC AND MESOSCALE CONDITIONS ASSOCIATED WITH EXTREME-RAIN-PRODUCING MESOSCALE CONVECTIVE SYSTEMS

One way to better understand the processes at work in the extreme-rain-producing MCS patterns introduced in chapter 5 is to observe the prevailing atmospheric conditions at the time these systems are occurring. Several methods have been used in the past to make conclusions about the conditions that are present during certain weather events, such as proximity soundings, composite analysis, and analysis of surface and upper-air weather maps to create "mental composites" of the state of the atmosphere. Here, composite analysis of hourly RUC–2 model analyses will be used to demonstrate the conditions attending TL/AS and BPS extreme rain events. The RUC–2 data were chosen for several reasons. First, the data are available at each hour, so an analysis time can be chosen that is very near when the event was actually occurring. Second, the hourly analyses should be similar to the data an operational forecaster might obtain in real time when diagnosing and forecasting the potential for heavy rainfall. Finally, the resolution (approx. 40-km horizontal grid spacing) is sufficient for analyzing both the synoptic-scale and some mesoscale features. The details of the composite analysis method were given in section 3.4.

Certainly, some aspects of the composite maps presented in this chapter should be approached with caution. The RUC–2 analyses, as with any model output, are only as good as the data ingested by the model. In addition, every model has its own inherent biases. Some of the derived fields presented here were included with the analysis product, while

others were calculated from the fields provided. Since the conditions have been averaged over many cases, the fields will often be smoother than those observed for any one case by itself. Therefore, in many cases, the exact value of a variable in the composite (e.g., CAPE, advection, convergence) is not as important as the location of relative maxima and minima in that field. Fields shown that are described as "surface" fields use the model's representation of the surface, which for temperature and moisture is 2 m above ground level (AGL) and for winds is 10 m AGL. Finally, while the RUC–2 grid point closest to the point with the highest rainfall total was chosen as the center of the grid for each case, the two were not always exactly coincident. Also, there were locations between rain gauges that could have received more rainfall than any of the gauges reported. Therefore, a square has been placed at the center of the following figures to allow for these uncertainties in where the most rain actually fell.

While composite fields were created for a number of atmospheric variables, only those that are especially helpful toward understanding the environments of extreme-rain-producing MCSs will be presented in the following, both at the peak rainfall time and at 12 h before this time. Since the environments in which the more established MCS types (i.e., TS, LS, PS, etc.) are fairly well known, the discussion to follow will focus on the two most common extreme-rain-producing MCS types presented in chapter 5, TL/AS and BPS.

6.1 TL/AS MCSs

6.1.1 Composite analysis

At the surface, the composite maps for the 29 TL/AS MCSs show southerly winds to the south of the extreme rainfall location, with a shift to weak winds from the east and southeast to the north of this point (Figs. 6.1 and 6.2). During the 12 h period prior to the extreme rainfall, an area of low pressure moves in from the west, causing pressures to fall slightly near the centerpoint. In the composite virtual potential temperature (θ_v) field, which is proportional to the density of the air, there is a weak northeast-to-southwest

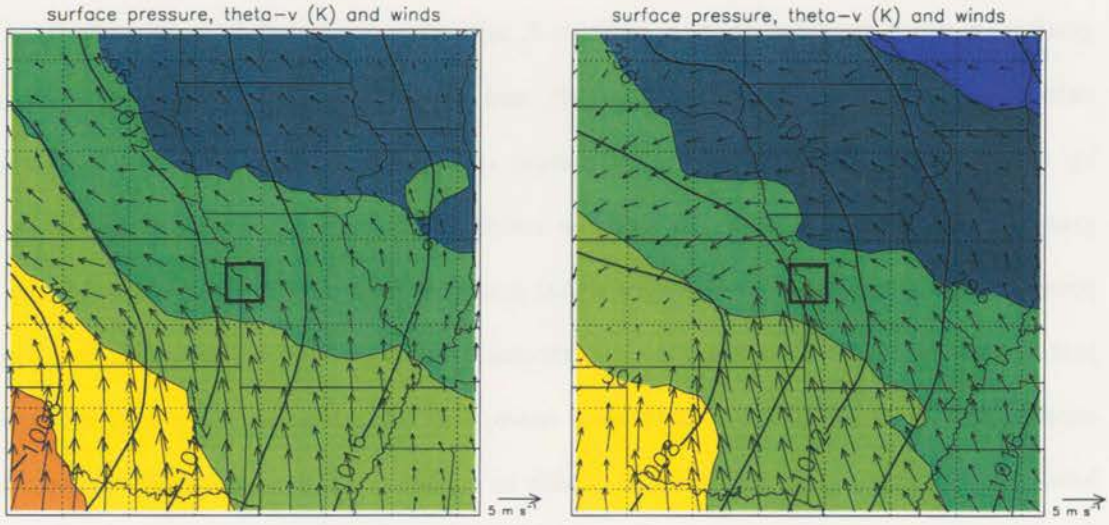

(a) 12 h before peak rainfall

(b) Peak rainfall time

Figure 6.1: Composite of surface virtual potential temperature (K, color contours), winds, and mean sea level pressure (hPa, thick black contours) for TL/AS MCS extreme rain events. Times shown are (a) 12 h before the peak rainfall and (b) the peak rainfall time. Maximum wind vector is shown in the lower right. Composite is projected onto a map of the central United States, centered near Kansas City, Missouri. The square at the center of the figure indicates the approximate location of the highest rainfall report.

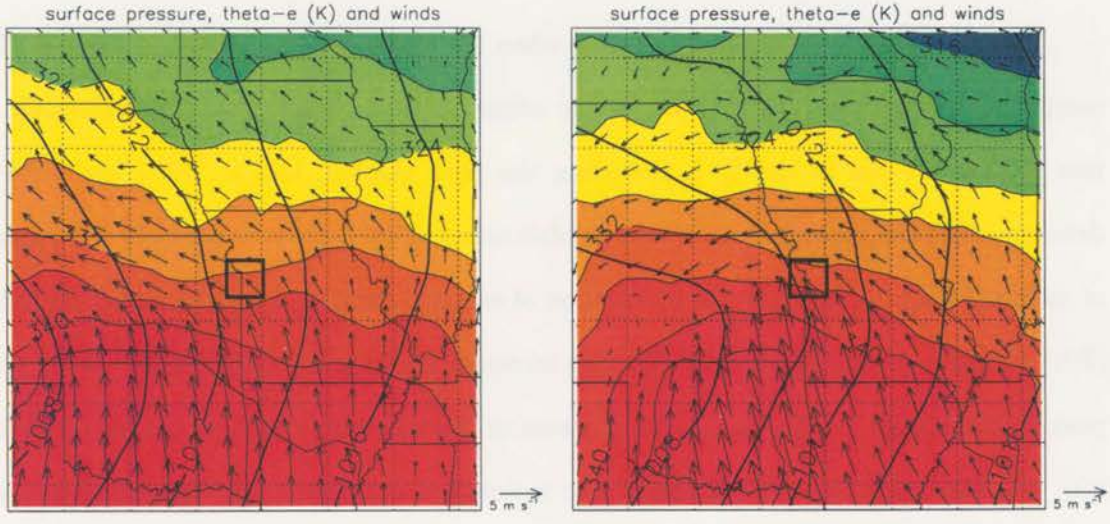

(a) 12 h before peak rainfall

(b) Peak rainfall time

Figure 6.2: As in Fig. 6.1, except for surface equivalent potential temperature (K), winds, and mean sea level pressure.

gradient that tightens somewhat in the 12 h before the heavy rainfall. In the θ_e field, the gradient is much stronger, there is positive θ_e advection (and a slight increase in θ_e at the extreme rain location over the 12-h period), and the wind shift becomes more pronounced by the peak rainfall time. The combination of the relatively strong north-to-south θ_e gradient, the wind shift near the extreme rainfall location, and the slight trough in the pressure field from west to east suggests that a surface boundary of some sort typically lies just to the south of the location where extreme rainfall occurs in TL/AS MCSs. This is consistent with observations of individual cases, and while the boundary may not always have sufficient temperature contrast to qualify as a "front" (cf. Sanders 1999), it most likely plays a major role in determining the orientation of the convective line in TL/AS systems.

The fact that there is a relatively tight gradient in θ_e at the surface from north to south but a relatively weak thermal/density gradient suggests that there is likely a strong north-to-south moisture gradient. The composite surface dew point field shows this to be true—dew point temperatures are greater than 18 °C (64 °F) to the south of the boundary and then they decrease steadily to the north (Fig. 6.3). Fig. 6.3 also shows an increase in moisture near the centerpoint in the 12 h before the peak rainfall.

This increase is even more dramatic when the upper levels are also considered. The composite precipitable water (PW) in the atmosphere increases from approximately 35 mm to over 40 mm in the 12 h preceding the peak rainfall, and a "bull's eye" of PW develops, centered around the extreme rainfall center (Fig. 6.4). It is not only the *amount* of moisture that is crucial to the production of extreme rainfall, but the relative humidity (RH) as well, and the upper-level RH also increases significantly over the 12 h before the peak rainfall (Figs. 6.5 and 6.6). The increase in RH at upper levels, as evidenced by the 850- and 700-hPa composite RH fields, also indicates a contribution to the overall increase in atmospheric moisture reflected in the PW field.

Another illustration of the moisture increase that leads to extreme rainfall that has been demonstrated in past extreme rainfall studies is low-level moisture convergence.

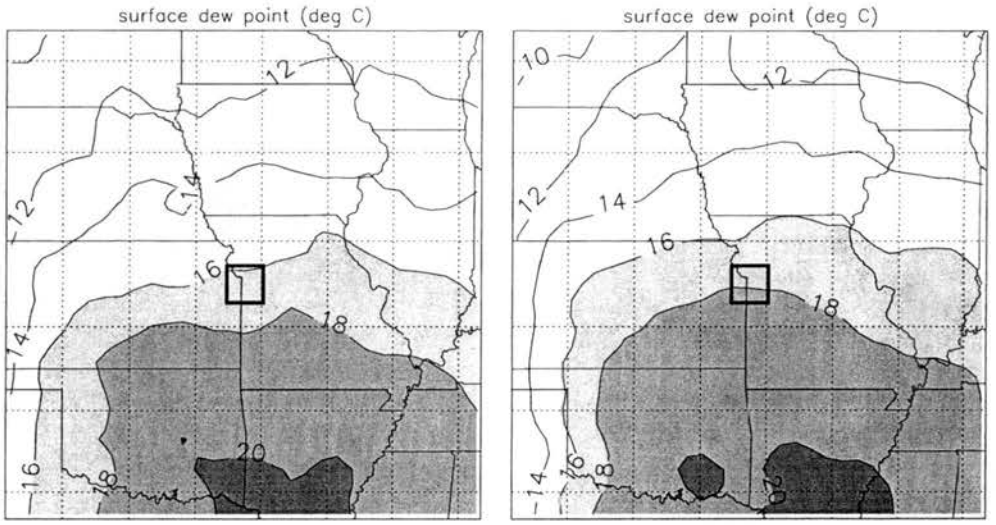

(a) 12 h before peak rainfall

(b) Peak rainfall time

Figure 6.3: As in Fig. 6.1, except for surface dew point temperature. Contour interval is 2 °C, and values greater than 16 °C (61 °F) are shaded.

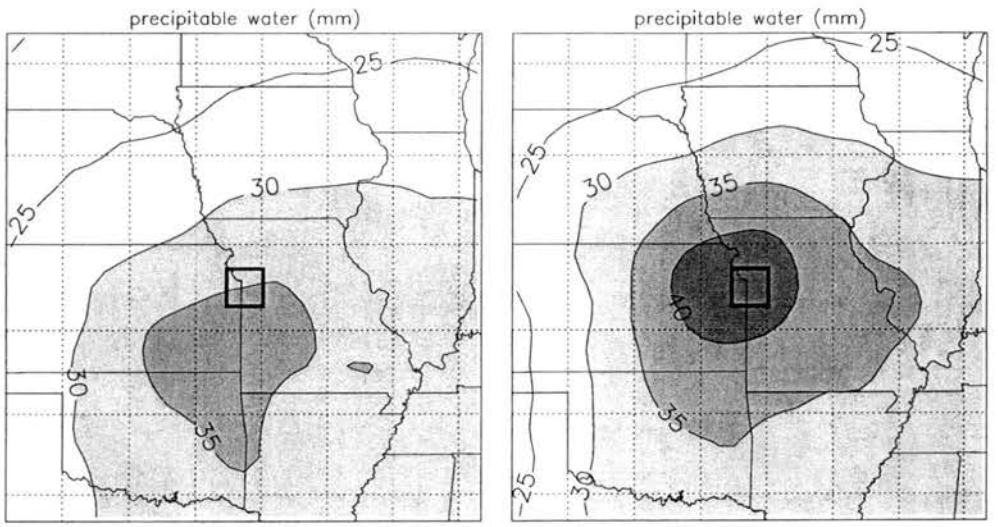

(a) 12 h before peak rainfall

(b) Peak rainfall time

Figure 6.4: As in Fig. 6.1, except for precipitable water (mm). Contour interval is 5 mm, and values greater than 30 mm are shaded.

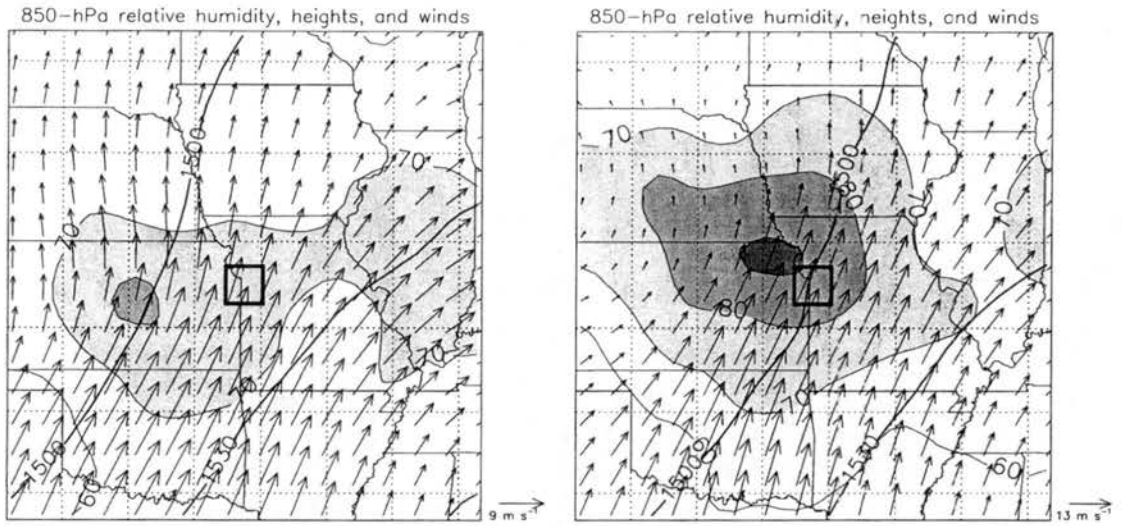

(a) 12 h before peak rainfall

(b) Peak rainfall time

Figure 6.5: As in Fig. 6.1, except for 850-hPa relative humidity, geopotential height (m, thick contours), and winds. Relative humidity contour interval is 10%, and values greater than 70% are shaded.

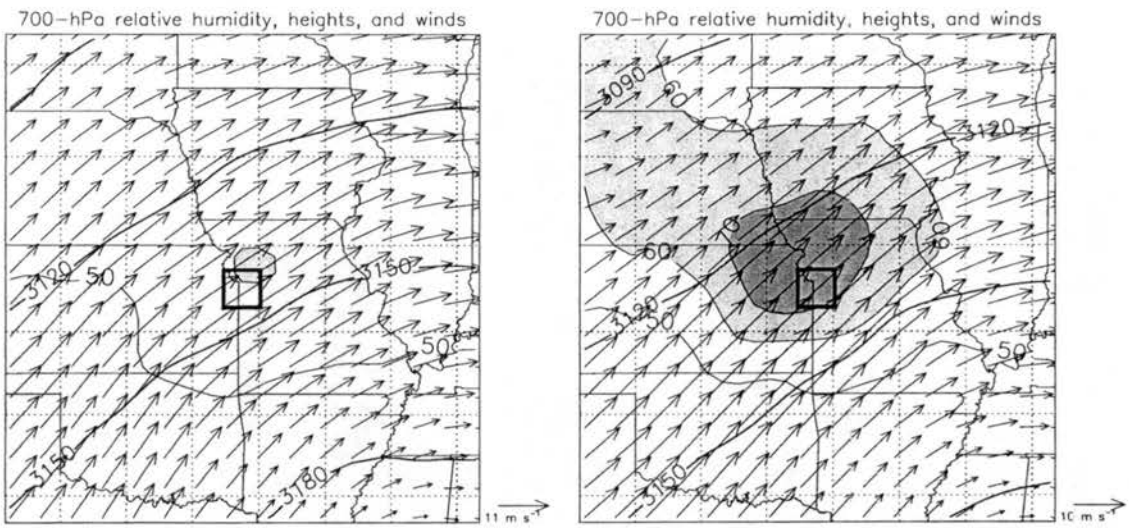

(a) 12 h before peak rainfall

(b) Peak rainfall time

Figure 6.6: As in Fig. 6.1, except for 700-hPa relative humidity, geopotential height (m, thick contours), and winds. Relative humidity contour interval is 10%, and values greater than 60% are shaded.

Junker et al. (1999) found that 850-hPa moisture convergence was maximized to the northwest of the location of heaviest rainfall, and they speculated that this was the case because the initial convection in extreme-rain-producing systems is rooted in the boundary layer near the area of moisture convergence at the surface but south of the moisture convergence at 850-hPa (Fig. 2.7). The composite moisture divergence fields for TL/AS MCSs in this study at the peak rainfall time show a remarkably similar result at 850-hPa, with a convergence maximum (divergence minimum) just to the northwest of the extreme rainfall location (Fig. 6.7a). Supporting Junker et al.'s hypothesis, composite analysis shows that moisture convergence at the surface is maximized to the southwest of the extreme rainfall location, and is maximized at 925-hPa just to the west of the centerpoint (Fig. 6.7b and c). Since new convective development is favored in regions of moisture convergence, these results may indicate that new convective cells often have their bases at around the 925-hPa level and mature as they move downstream, where they produce their heaviest rainfall. These findings, along with the finding that most TL/AS systems form on the cool side of a surface front or boundary, support the idea that the convection in TL/AS MCSs is often elevated (e.g., Colman 1990).

The composite winds for TL/AS MCSs are similar to those previously reported for extreme rainstorms, with veering winds at low levels, an approximately unidirectional profile at mid- and upper-levels, and relatively weak winds throughout the troposphere (Fig. 6.8). This profile shows winds with very similar directions and slightly lower speeds than those found by Junker et al. (1999) for the rain events they studied (Fig. 2.9). There is a strong increase in the 925- and 850-hPa winds in the 12 h prior to the extreme rainfall. The 925-hPa winds at the centerpoint increase from approximately 5 to 8 m s^{-1} and the 850-hPa winds increase from about 6 to 11 m s^{-1}. Part of this increase may be attributable to the average times of day of each of these composites—since the average peak rainfall time is approximately 2100 local time, 12 h earlier would be 0900, or in the morning, when climatologically weaker 850-hPa winds might be expected (e.g., Whiteman et al. 1997). However,

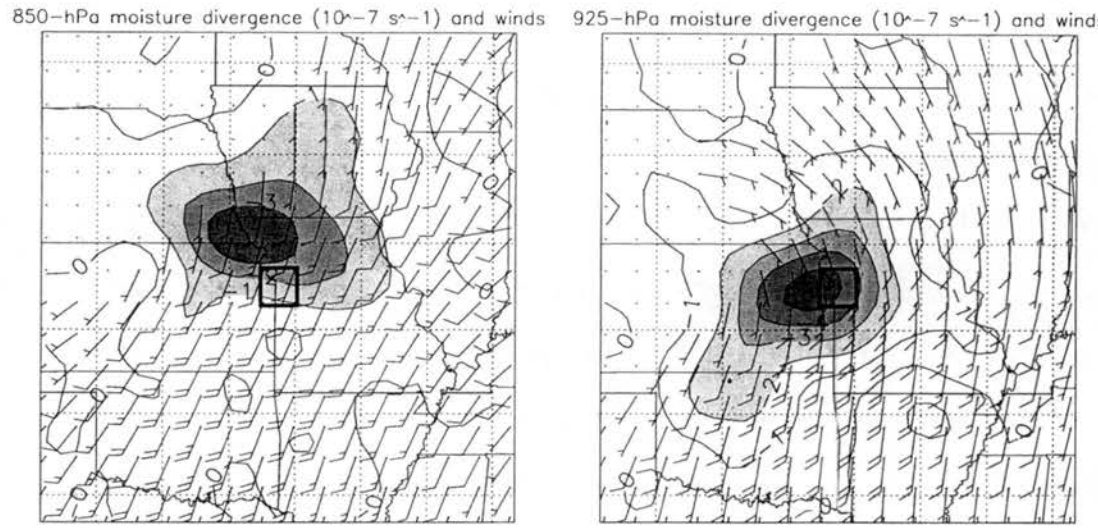

(a) 850-hPa

(b) 925-hPa

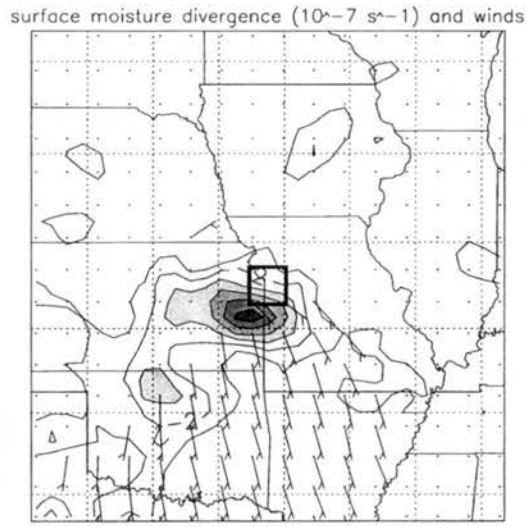

(c) Surface

Figure 6.7: Composite of (a) 850-hPa, (b) 925-hPa, and (c) surface moisture divergence and winds (kt, conventional plotting) for TL/AS MCS extreme rain events at the peak rainfall time. Wind barbs are not plotted where wind speeds are less than 5 kt. Moisture divergence contour interval is $1\times\ 10^{-7}\ s^{-1}$, and values less than -1 are shaded. For clarity, only convergence (negative divergence) contours are shown in panel (c). Map projection is as in Fig. 6.1.

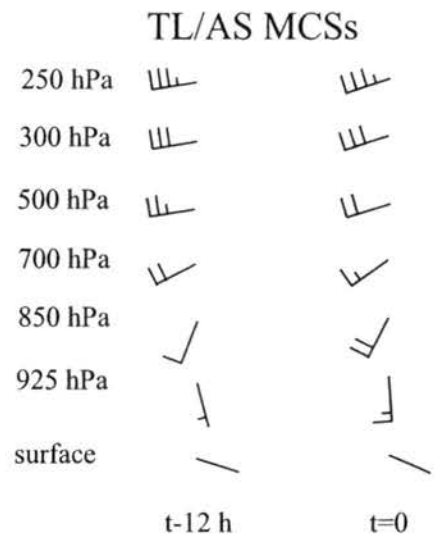

Figure 6.8: Composite wind profile at the grid center for TL/AS MCS extreme rain events at the peak rainfall time and 12 h prior. Wind barbs are plotted conventionally in kt.

it also illustrates the impact that the nocturnal low-level jet has on extreme rainfall events, as discussed in section 2.2.1. As the low-level jet increases after dark, the stronger winds advect moisture northward, which provides a major moisture source for the convection that produces heavy rainfall.

The important role that the low-level jet plays in extreme rain events is also depicted by the composite ageostrophic wind field. Blackadar (1957) suggests that the inertial oscillation is important to the development of low-level jets and that the oscillation leads to an acceleration of the wind to a nocturnal supergeostrophic maximum. The 850-hPa ageostrophic wind composite shows that the winds to the south and west of the centerpoint are subgeostrophic 12 h prior to the extreme rainfall peak, but then become supergeostrophic by the peak rainfall time (Fig. 6.9). North of the centerpoint, evidence of the LLJ is not present, presumably because the 850-hPa surface is often below the sloping frontal boundary. While these fields have a lot of complexity that can not be readily explained, this ageostrophic acceleration seems to support the theory of Blackadar (1957) and to illustrate part of the role that the low-level jet plays in extreme-rain-producing convection.

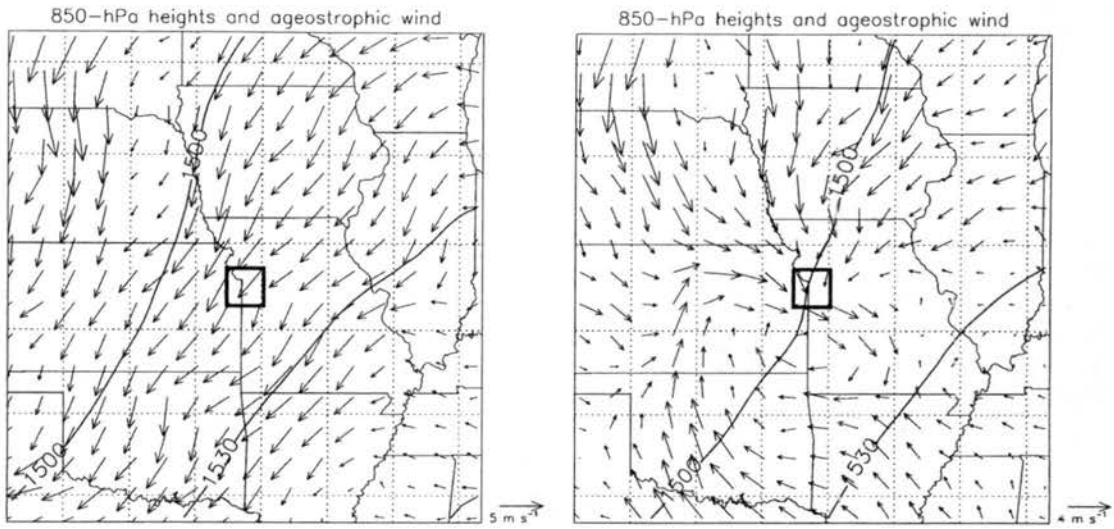

(a) 12 h before peak rainfall

(b) Peak rainfall time

Figure 6.9: As in Fig. 6.1, except for 850-hPa ageostrophic wind and heights (m). Note how the ageostrophic wind to the south and west of the center box reverses direction from panel (a) to panel (b).

The wind profile at upper levels allows for cells to repeatedly develop, for example, to the north of a west-to-east boundary and then move eastward with the mean wind in the cloud layer. The 700- and 500-hPa wind fields change very little in the 12 h preceding the heavy rainfall, aside from a slight decrease in wind speed in the vicinity of the heavy rain location (Figs. 6.10 and 6.11). As MCH79 noted for their "frontal" and "mesohigh" type flash floods, heavy rainfall often occurs under a large-scale upper-level ridge, which these data confirm.

At 250 hPa, a 50-kt jet exists well to the north of the heavy rain location in the composite (Fig. 6.12). The composite of 250-hPa divergence shows a broad region of weak divergence 12 h before peak rainfall, which becomes stronger and more defined by the peak rainfall time (Fig. 6.13). This southwest-to-northeast oriented axis indicates that upper-level divergence may play a role in enhancing the upward motions associated with extreme-rain-producing convection. While some of the divergence represented in the RUC–2 composites may result from convective outflows, the fact that such divergence is present

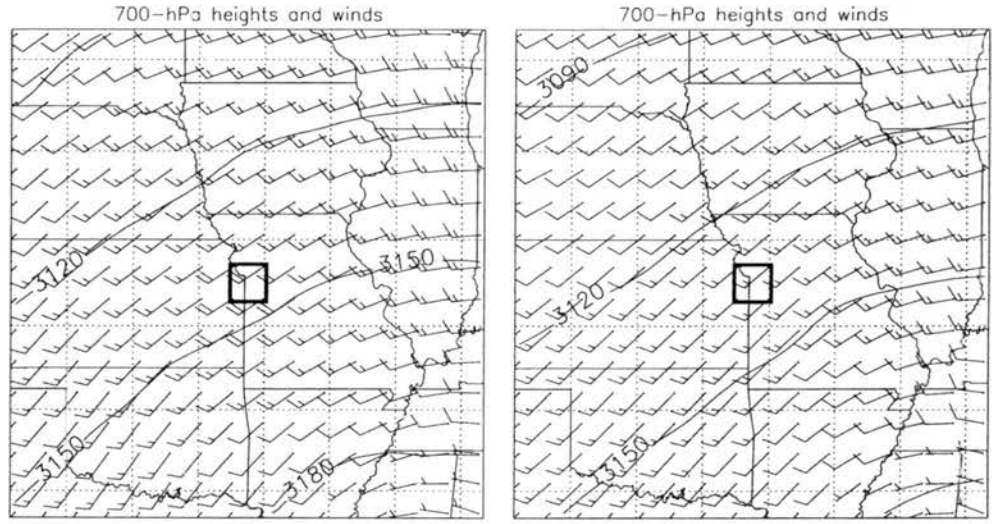

(a) 12 h before peak rainfall

(b) Peak rainfall time

Figure 6.10: As in Fig. 6.1, except for 700-hPa winds (kt) and heights (m).

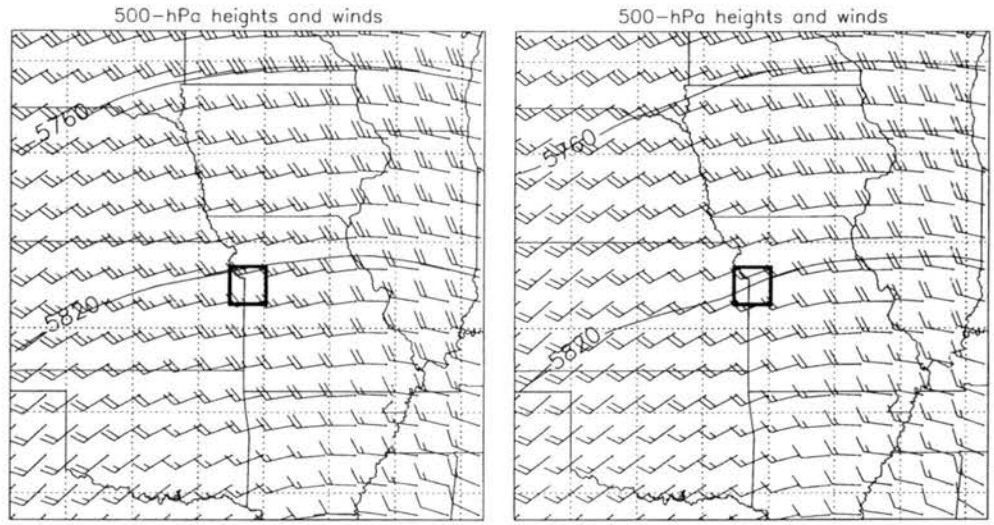

(a) 12 h before peak rainfall

(b) Peak rainfall time

Figure 6.11: As in Fig. 6.1, except for 500-hPa winds (kt) and heights (m).

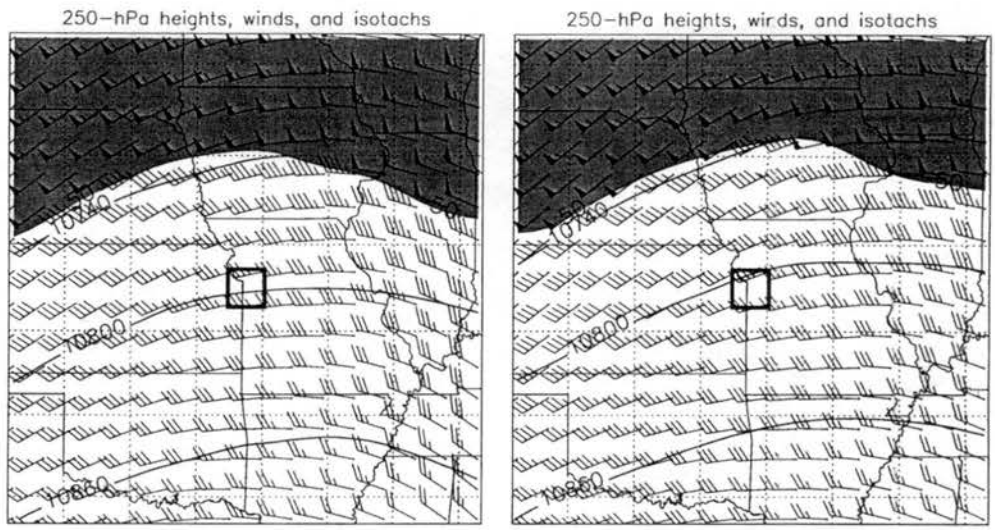

(a) 12 h before peak rainfall

(b) Peak rainfall time

Figure 6.12: As in Fig. 6.1, except for 250-hPa winds (kt), heights (m), and isotachs (wind speeds greater than 50 kt are shaded).

suggests that upper-level dynamical support, in addition to the low-level factors mentioned previously, may be important in the formation of TL/AS MCSs.

An additional variable that is associated with the low-level jet and has been previously found in conjunction with extreme rain events is the advection of θ_e, which represents both temperature and moisture advection, and at low levels is indicative of destabilization of the atmosphere. The composite θ_e advection field at the time of extreme rainfall for TL/AS systems at 850 hPa shows a maximum of positive advection just to the northwest of the extreme rainfall location (Fig 6.14). Even 12 h prior to the heavy rain, there is significant positive advection in the vicinity of the rainfall location. These results confirm the previous findings of Glass et al. (1995) and Junker et al. (1999, cf. Figs. 2.4 and 2.5), that a maximum in θ_e advection is often associated with heavy rainfall. The composite advection of θ (not shown) is positive near the centerpoint (consistent with the veering winds at low levels) but weak. Therefore, it appears that strong moisture advection, with relatively weak thermal advection, is often found in the environments in which extreme-rain-producing TL/AS MCSs form.

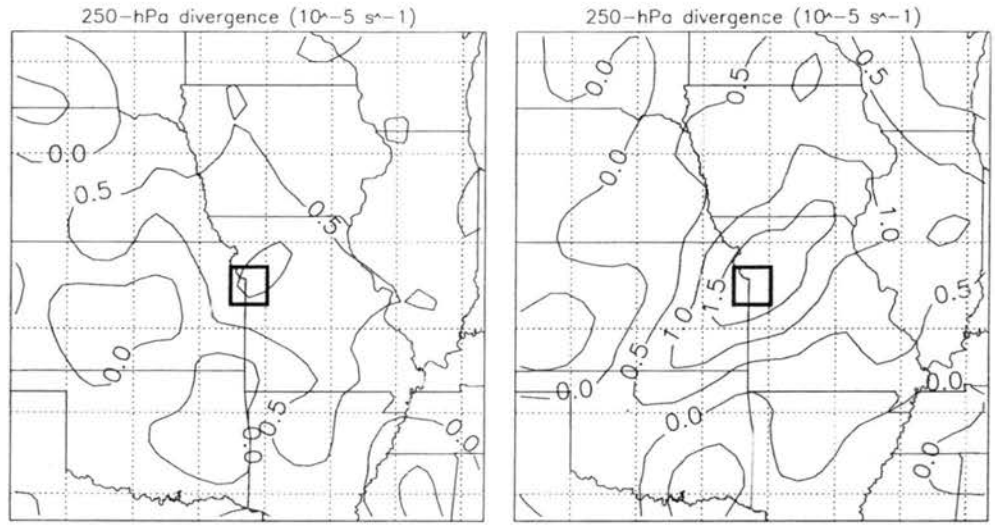

(a) 12 h before peak rainfall (b) Peak rainfall time

Figure 6.13: As in Fig. 6.1, except for 250-hPa divergence. Contour interval is 0.5×10^{-5} s^{-1}.

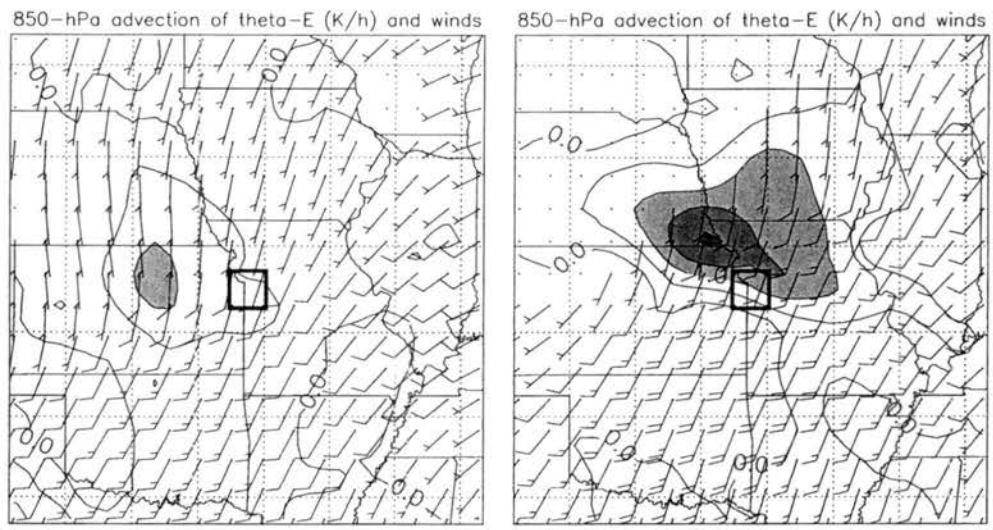

(a) 12 h before peak rainfall (b) Peak rainfall time

Figure 6.14: As in Fig. 6.1, except for 850-hPa equivalent potential temperature advection and winds (kt, conventional plotting). Contour interval is 0.5 K h^{-1}, and values greater than 1.0 K h^{-1} are shaded.

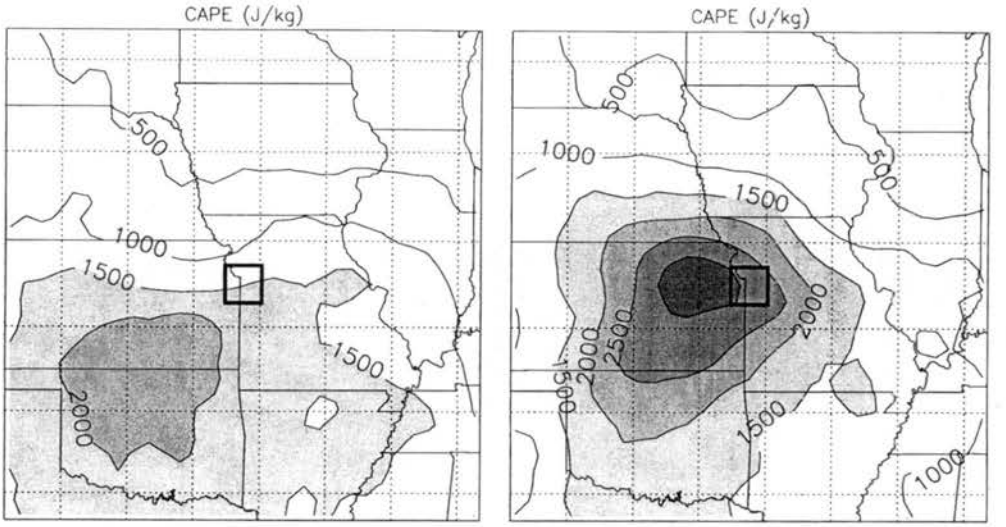

(a) 12 h before peak rainfall

(b) Peak rainfall time

Figure 6.15: As in Fig. 6.1, except for convective available potential energy. Contour interval is 500 J kg^{-1}, and values greater than 1500 J kg^{-1} are shaded.

Finally, while it has been made clear that warm, moist air is typically present in an extreme rain event environment, no mention has been made of the atmospheric stability in this environment. The composite convective available potential energy (CAPE) shows that there is typically more than sufficient instability for strong convection to occur (Fig. 6.15). The maximum in CAPE is just to the west of the extreme rainfall location, which, along with the moisture convergence maxima, is favorable for convective development in this area. The RUC–2 calculates CAPE by using the parcel with maximum buoyancy in the lowest 300 hPa of the atmosphere, so these values do not necessarily represent surface-based available energy (and the storms may indeed be elevated, as discussed above). Therefore, they will typically be larger than the CAPE values found using different calculations. However, the important feature here is that, on average, positive CAPE (at some level in the atmosphere) is present near the heavy rainfall location.

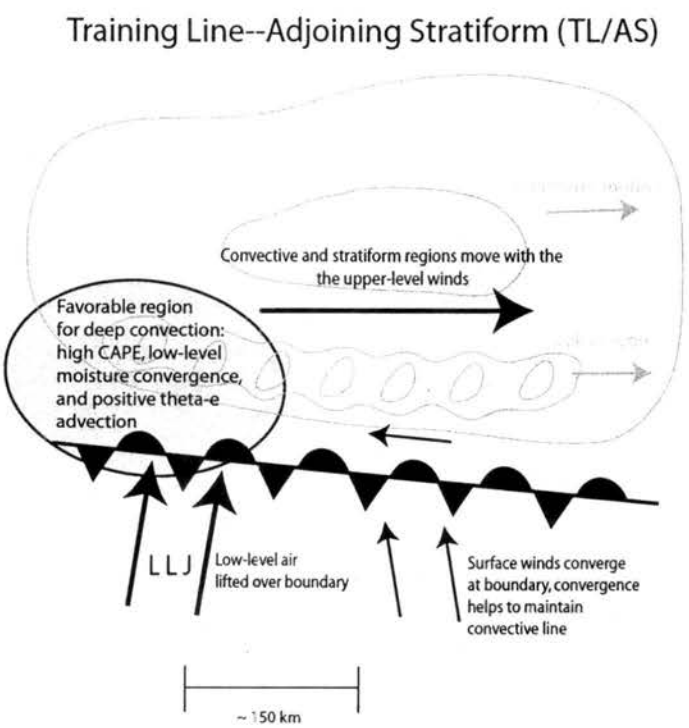

Figure 6.16: Schematic diagram of synoptic and mesoscale features associated with TL/AS MCSs. Typical reflectivity structure is shown in light gray.

6.1.2 Discussion

Synthesizing all of the composite analyses for TL/AS MCSs paints a picture very similar to the synoptic and mesoscale conditions for the "frontal" type flash flood described by MCH79 (Fig. 6.16). In the 12 h prior to the extreme-rain-producing convection, the necessary ingredients for heavy rainfall come together, partly as a result of the diurnal increase in the low-level jet. A dramatic increase in moisture, at both low- and mid-levels, occurs in the area of impending convection during this 12-h period. Relatively strong southerly winds cause this moist, unstable air to be lifted over a slow-moving boundary, which leads to deep convection that becomes linear and is oriented approximately parallel to the boundary. A weak low-pressure center at the surface and an area of upper-level divergence may help to enhance the convergence at low levels, and the high RH inhibits entrainment within the storms. The prevailing upper-level winds also have a large component parallel to the boundary (and hence the convective line), resulting in cell (and stratiform) motion in the

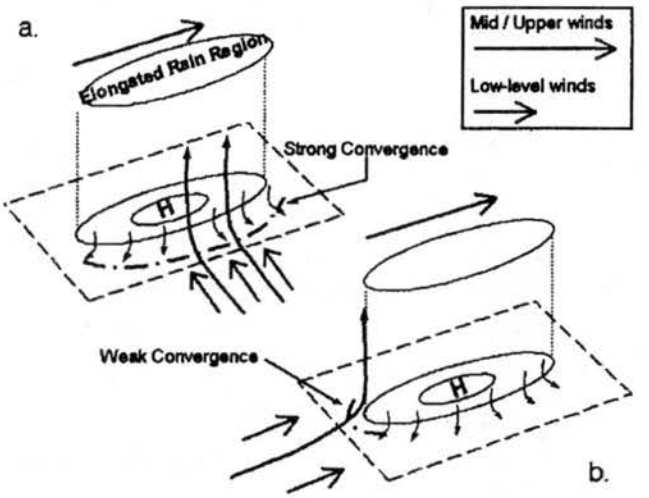

Figure 6.17: Illustration of a multicellular storm growing in an environment where (a) the low-level winds are perpendicular to the mid- and upper-level winds and, (b) the low-level winds are parallel to the mid- and upper-level winds. From Davis (2001).

along-line direction. Such a system produces a "training line" and an elongated region of heavy rainfall, similar to the scenario shown in Fig. 6.17a, where the low-level winds are nearly perpendicular to the upper-level winds. These systems are therefore capable of producing extremely high rainfall totals if this scenario persists for several hours.

A cross-section view of how the low-level jet may lift warm, moist air over a stationary boundary in TL/AS systems is shown in Fig. 6.18 from Trier and Parsons (1993). Somewhat less clear is the reason that the area of stratiform precipitation develops on the cool side of the convective line and behaves as it does. One possibility is that the convective processes transport southerly momentum to upper levels, similar to the processes described by LeMone (1983) and others.

6.2 BPS MCSs

6.2.1 Composite analysis

The surface composite fields for the 26 BPS MCSs are, to first order, quite similar to those for the TL/AS MCS extreme rain events. Winds to the south of the extreme

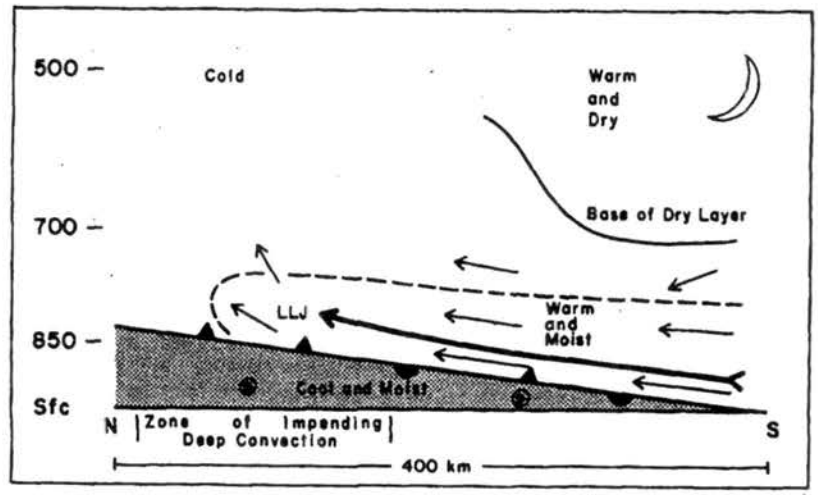

Figure 6.18: An idealized north-south schematic cross section depicting the thermodynamic and flow structure immediately prior to the development of deep convection above the wedge-shaped cold air mass (lightly shaded). The vectors represent the flow in the x–z plane (vertical component is greatly exaggerated). The dot inside the circle represents easterly flow (out of the page) within the cool, moist air mass below the frontal surface. The dashed line represents the boundary of the warm, moist air mass transported northward above the frontal surface by the southerly low-level jet (LLJ) whose axis is denoted by the bold streamline. From Trier and Parsons (1993).

rainfall location are southerly, with weaker winds to the north of this point (Figs. 6.19 and 6.20). There is not a general wind shift across the whole domain as there is in the TL/AS systems, but there is an abrupt shift from southerly to northerly winds at some points west of the extreme rainfall center. The composite surface winds to the north of the centerpoint are very weak. Though weaker than in the TL/AS composite, there is a north-to-south gradient of θ_v. There is a strong gradient of θ_e, suggesting a strong moisture gradient, though the values of θ_e in the vicinity of the extreme rainfall location actually decrease in the 12 h period before peak rainfall. As in the TL/AS composite, the pressure near the centerpoint falls in this 12 h period, but there is no organized east-to-west pressure trough, and the pressure contours do not really indicate an advancing low-pressure center in the BPS composite. While the strong gradient in θ_e suggests that a surface boundary may be present in many of the BPS extreme rain events, the less-uniform wind shift and the lack of an organized low-pressure center or pressure trough suggest that the synoptic

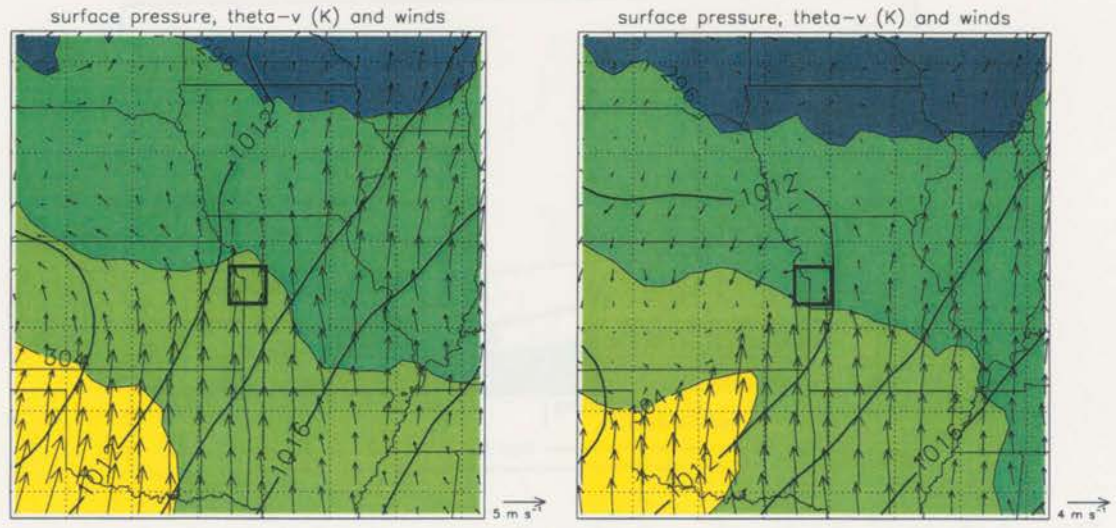

(a) 12 h before peak rainfall

(b) Peak rainfall time

Figure 6.19: Composite of surface virtual potential temperature (K, color contours), winds, and mean sea level pressure (hPa, thick black contours) for BPS MCS extreme rain events. Times shown are (a) 12 h before the peak rainfall and (b) the peak rainfall time. Maximum wind vector is shown in the lower right. Composite is projected onto a map of the central United States, centered near Kansas City, Missouri. The square at the center of the figure indicates the approximate location of the highest rainfall report.

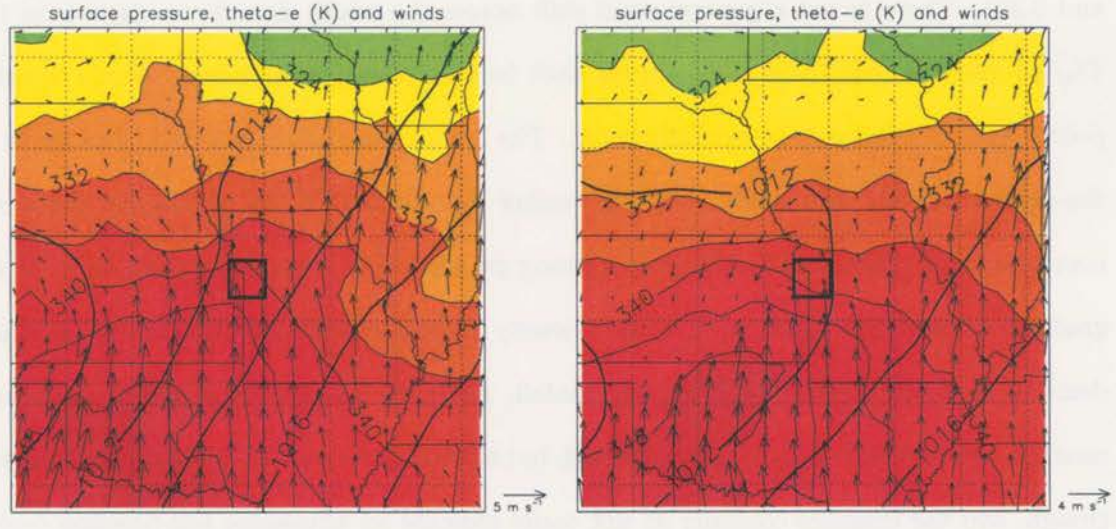

(a) 12 h before peak rainfall

(b) Peak rainfall time

Figure 6.20: As in Fig. 6.19, except for surface equivalent potential temperature, winds, and mean sea level pressure.

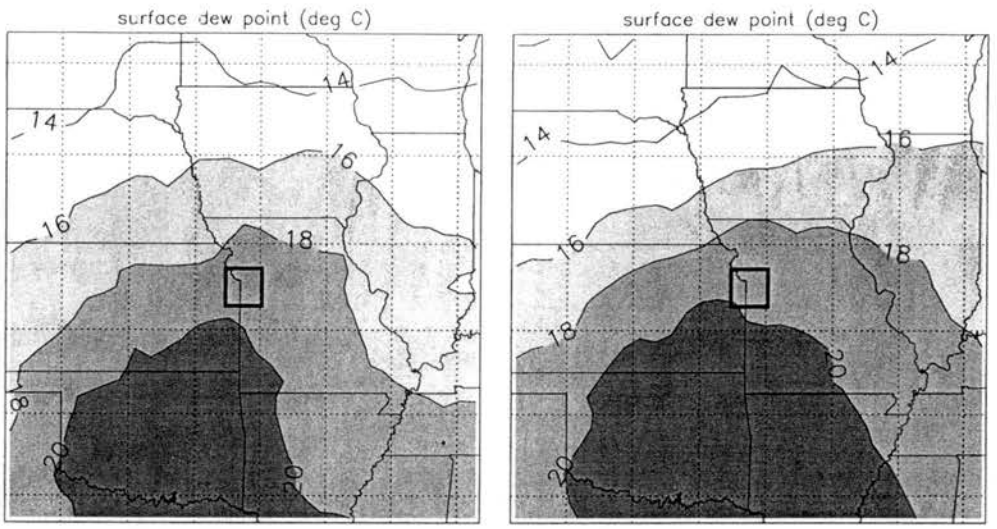

(a) 12 h before peak rainfall

(b) Peak rainfall time

Figure 6.21: As in Fig. 6.19, except for surface dew point temperature. Contour interval is 2 °C, and values greater than 16 °C (61 °F) are shaded.

and mesoscale features at the surface are not as well-defined for BPS systems as they are for TL/AS MCSs. This will be discussed in further detail later.

A major increase in moisture over the 12 h preceding the extreme rainfall is apparent in the BPS composites, and BPS systems tend to occur in environments with even higher quantities of atmospheric moisture than TL/AS systems. Surface dew point temperatures near the centerpoint are greater than 18 °C (64 °F), and PW increases from 35 mm to 45 mm in the 12 h before peak rainfall (Figs. 6.21 and 6.22). The dramatic "bull's eye" of moisture also appears in the composite for PW here, as well as in the 850- and 700-hPa RH fields (Figs. 6.23 and 6.24). In these composites, the axes of moisture are oriented from southwest to northeast.

The moisture divergence fields associated with the BPS events stray considerably from those of the TL/AS systems. At 850 hPa, the maximum of moisture convergence is much weaker and is actually downstream of the extreme rainfall centerpoint (Fig. 6.25a). However, there is a moisture convergence maximum near the centerpoint at 925-hPa, and the surface field looks very similar to that for TL/AS events. The idea that the moisture

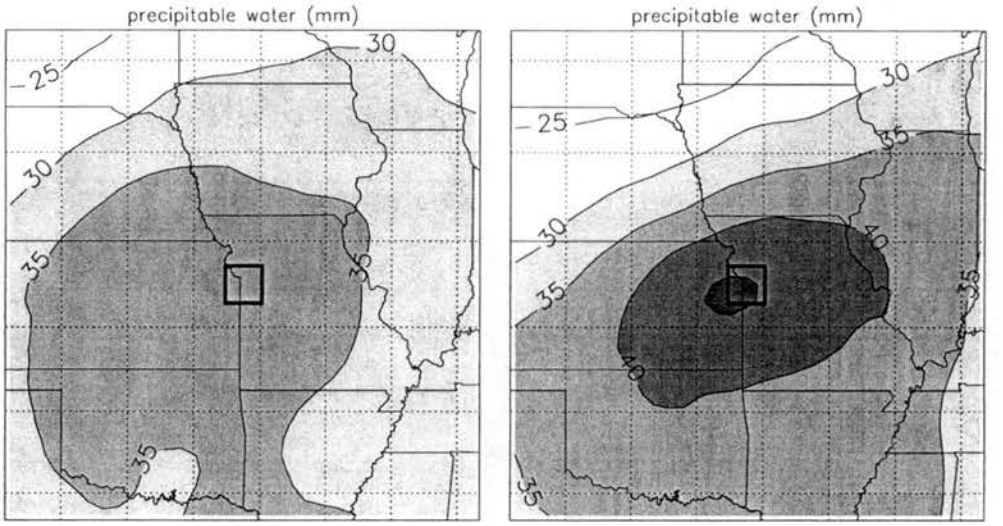

(a) 12 h before peak rainfall

(b) Peak rainfall time

Figure 6.22: As in Fig. 6.19, except for precipitable water (mm). Contour interval is 5 mm, and values greater than 30 mm are shaded.

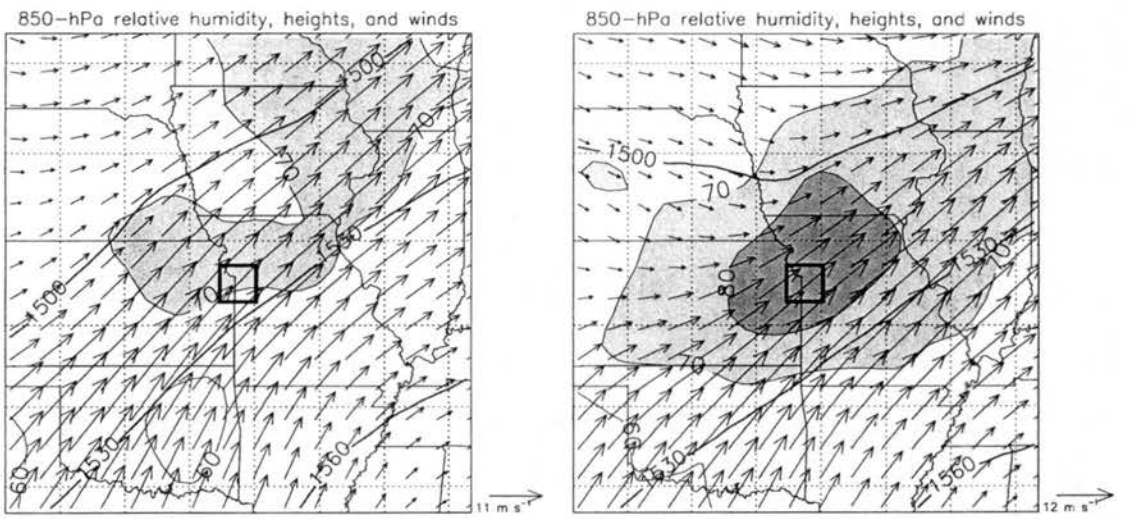

(a) 12 h before peak rainfall

(b) Peak rainfall time

Figure 6.23: As in Fig. 6.19, except for 850-hPa relative humidity, geopotential height (m, thick contours), and winds. Relative humidity contour interval is 10%, and values greater than 70% are shaded.

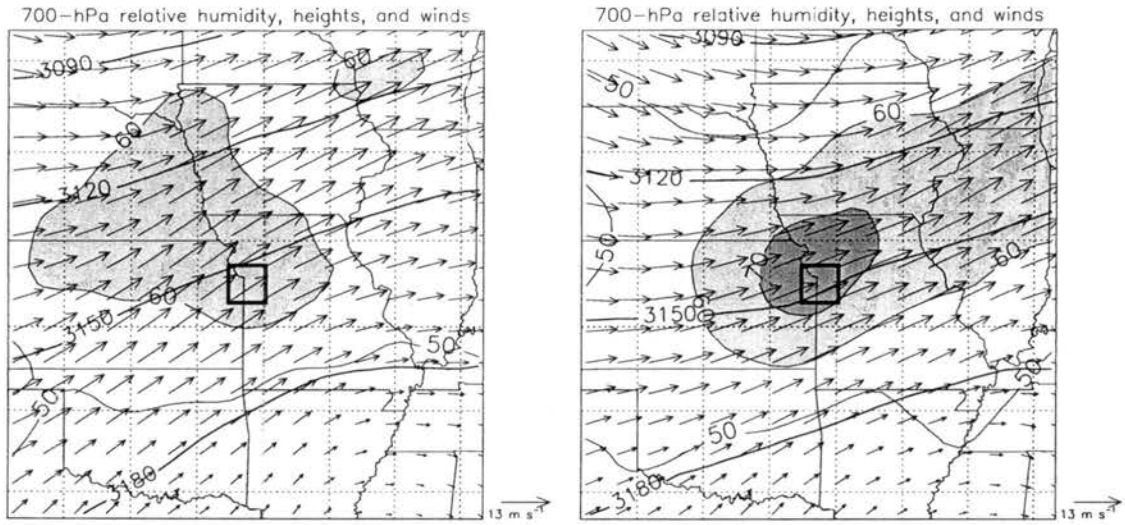

(a) 12 h before peak rainfall

(b) Peak rainfall time

Figure 6.24: As in Fig. 6.19, except for 700-hPa relative humidity, geopotential height (m, thick contours), and winds. Relative humidity contour interval is 10%, and values greater than 60% are shaded.

convergence maxima should be upstream of where the heavy rain falls is called into question here by the locations of these maxima. One possible explanation for this discrepancy lies in the differing organizational characteristics between TL/AS and BPS systems. In TL/AS events, a relatively long convective line is typically responsible for the extreme rainfall. For an extreme amount of rain to fall at a point along such a line, many cells must pass over that point, and the cells forming this line must then form well upstream of that point. In contrast, convective cells in BPS systems often form a very short distance upstream of previous cells. Therefore, the moisture convergence maximum (as a proxy for the location of convective development) can be very close to the location where the extreme rainfall totals are reported, as we see in the 925-hPa composite moisture divergence field.

The composite wind profile for BPS systems is, as a whole, very similar to that for TL/AS events (Fig. 6.26). However, there are a few important differences that should be noted. At the surface, the winds at the centerpoint back from south to southeast and weaken from 2.3 to 1.4 m s^{-1} in the 12 h before the peak rainfall time. This apparent backing,

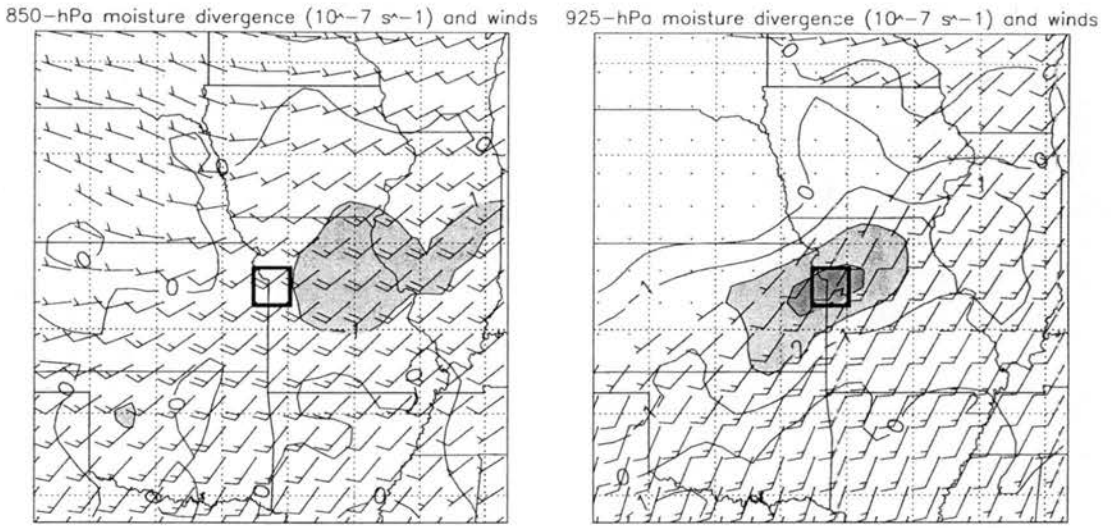

(a) 850-hPa

(b) 925-hPa

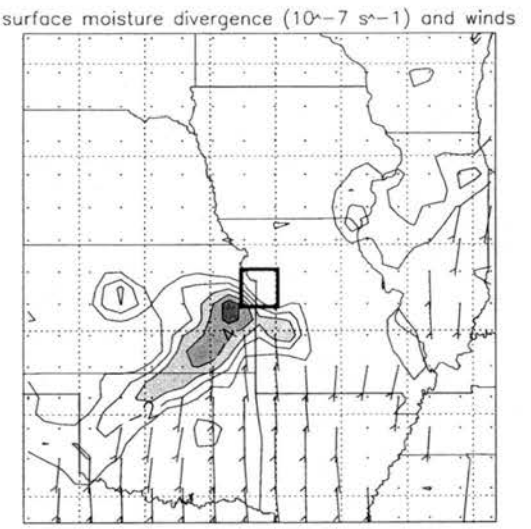

(c) Surface

Figure 6.25: Composite of (a) 850-hPa, (b) 925-hPa, and (c) surface moisture divergence and winds (kt, conventional plotting) for BPS MCS extreme rain events at the peak rainfall time. Wind barbs are not plotted where wind speeds are less than 5 kt. Moisture divergence contour interval is $1\times\ 10^{-7}\ s^{-1}$, and values less than -1 are shaded. For clarity, only convergence (negative divergence) contours are shown in panel (c). Map projection is as in Fig. 6.1.

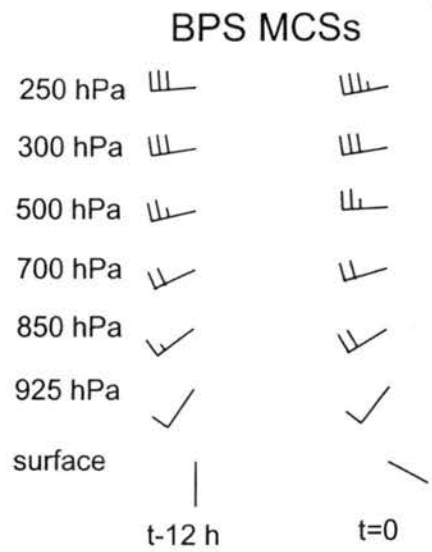

Figure 6.26: Composite wind profile at the grid center for BPS MCS extreme rain events at the peak rainfall time and 12 h prior. Wind barbs are plotted conventionally in kt.

when considered along with the overall surface wind field and the strong θ_e gradient shown in Fig. 6.20, may actually indicate the presence of a boundary at the peak rainfall time that was not there 12 h before, such as a thunderstorm outflow boundary. In Fig. 6.20a, the winds are southerly even to the north of the centerpoint, but 12 h later, the value of θ_e near the centerpoint is lower and the southerlies are no longer apparent. These results suggest that, in many systems, an east-to-west oriented convective outflow boundary may have been established by the convection occurring before the peak rainfall time.

The low-level winds in the BPS composites do not show the strong increases in the 12 h preceding the heaviest rainfall that the TL/AS composites do, and they have a greater westerly component than those in the TL/AS composites (e.g., Figs. 6.23 and 6.26). Since the average time of peak rainfall for BPS events is also after dark (though the distribution is somewhat wider than for TL/AS events), the role that the nocturnal low-level jet plays in BPS systems is less certain. The behavior of the composite ageostrophic wind field is very similar to that of the TL/AS field, with a region of supergeostrophic winds developing to the south of the centerpoint by the peak rainfall time (Fig. 6.27). As discussed in the

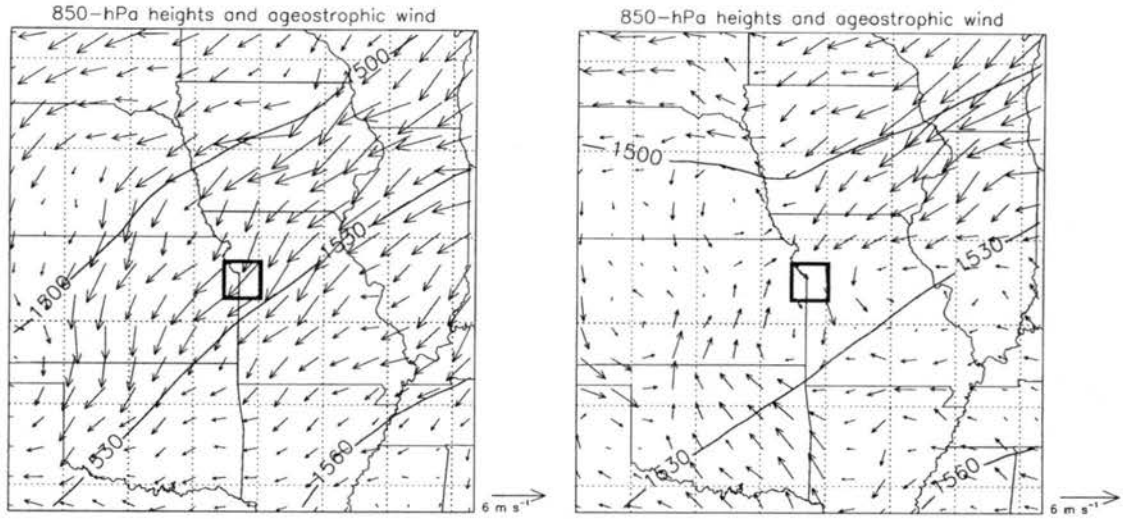

(a) 12 h before peak rainfall

(b) Peak rainfall time

Figure 6.27: As in Fig. 6.19, except for 850-hPa ageostrophic wind and heights (m). Note how the ageostrophic wind to the south and west of the center box reverses direction from panel (a) to panel (b).

previous section, the low-level jet is often associated with positive θ_e advection, which destabilizes the atmosphere and can lead to convective development. However, only very weak positive θ_e advection is associated with these systems (Fig. 6.28). Therefore, while strong southwesterly low-level winds are associated with BPS extreme rain events, and there seems to be some evidence of a low-level jet, the impact that this jet has on the development of BPS systems appears to be less important than it is for TL/AS events. This may help to explain the slightly wider diurnal distribution of BPS events, as they may be just as likely to occur when a low-level jet is absent as when one is present.

The mid- and upper-level wind profile at the centerpoint during BPS systems is similar to that for the TL/AS MCSs, with nearly unidirectional winds above 700 hPa (Fig. 6.26). With the southwesterly low-level winds that are present for BPS systems, the overall veering between low levels and upper levels is small compared to the profile for TL/AS MCSs. In contrast to the TL/AS wind profile, the upper-level wind speeds increase during the 12 h prior to peak rainfall in the BPS profile. The mid- and upper-level wind

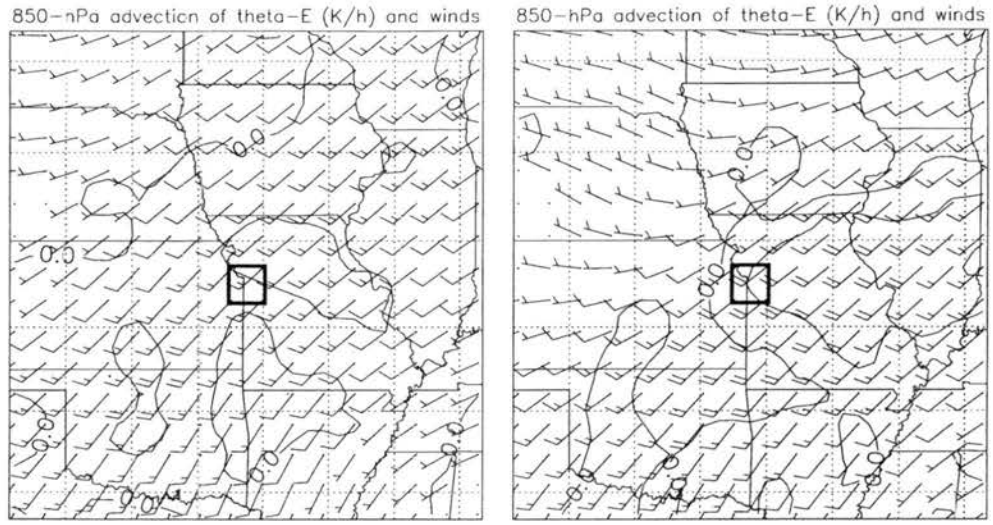

(a) 12 h before peak rainfall

(b) Peak rainfall time

Figure 6.28: As in Fig. 6.19, except for 850-hPa equivalent potential temperature advection and winds (kt, conventional plotting). Contour interval is 0.5 K h^{-1}, and values greater than 1.0 K h^{-1} are shaded.

fields over the entire domain do not show a large-scale trough or ridge near the extreme rainfall location, and the 500- and 250-hPa winds are nearly zonal (Figs. 6.29–6.31). There is once again a jet to the north of the heavy rainfall location in the 250-hPa composite, and a region of upper-level divergence develops by the peak rainfall time (Fig. 6.32). Again, this divergence may be in part related to convective outflows at upper levels, but also may indicate some degree of dynamical support for the extreme-rain-producing convection.

The atmosphere in the vicinity of the centerpoint destabilizes in the 12 h prior to the extreme rainfall, as shown by the composite CAPE field (Fig. 6.33). As in the TL/AS composite, the maximum in CAPE is located just west of the centerpoint. Here, however, the CAPE axis is oriented from southwest to northeast, which is similar to the characteristics of the moisture composites. Though the atmospheric moisture (i.e., precipitable water) in BPS environments is greater than in TL/AS events, the values of CAPE are lower.

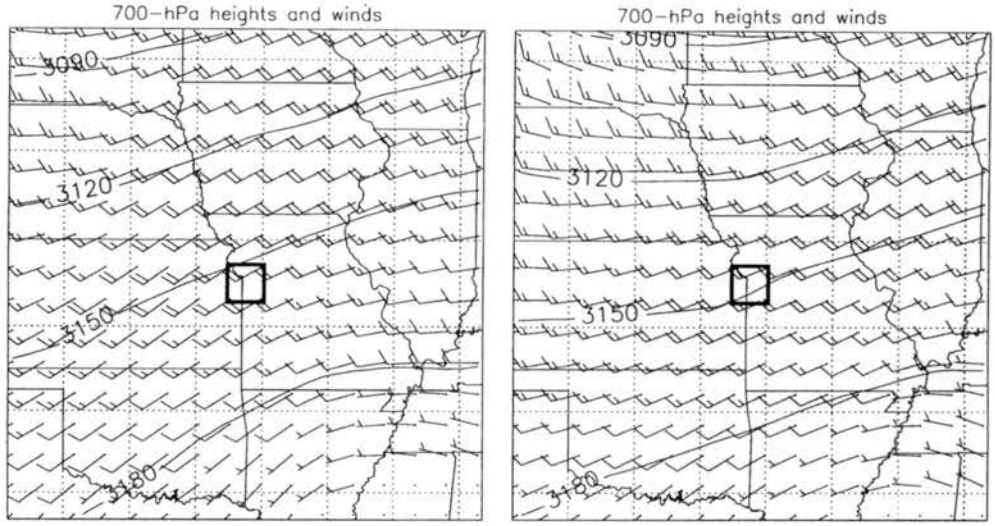

(a) 12 h before peak rainfall (b) Peak rainfall time

Figure 6.29: As in Fig. 6.19, except for 700-hPa winds (kt) and heights (m).

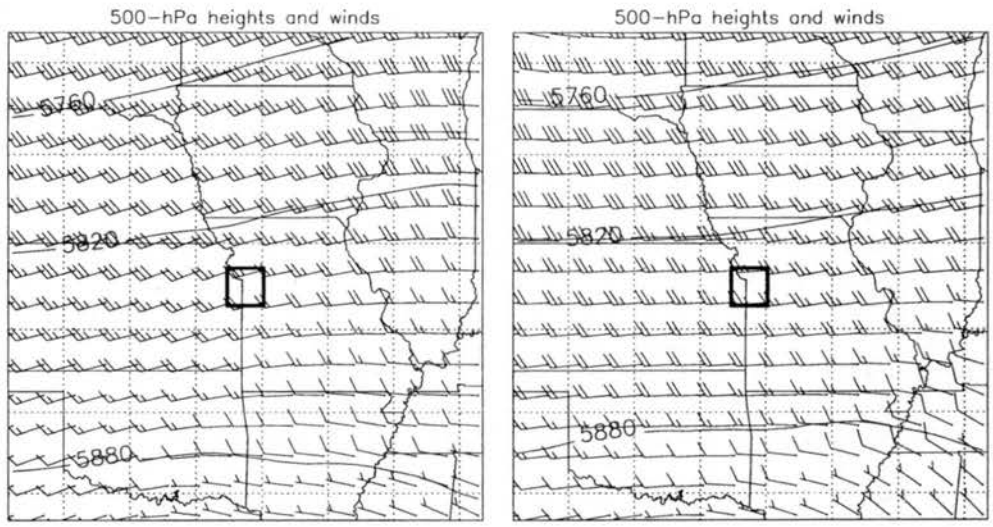

(a) 12 h before peak rainfall (b) Peak rainfall time

Figure 6.30: As in Fig. 6.19, except for 500-hPa winds (kt) and heights (m)

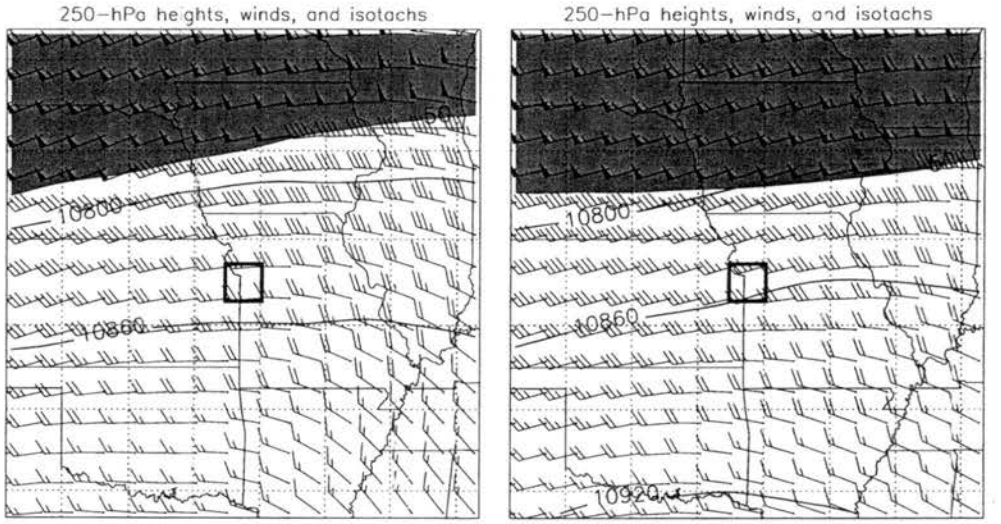

(a) 12 h before peak rainfall

(b) Peak rainfall time

Figure 6.31: As in Fig. 6.19, except for 250-hPa winds (kt), heights (m), and isotachs (wind speeds greater than 50 kt are shaded).

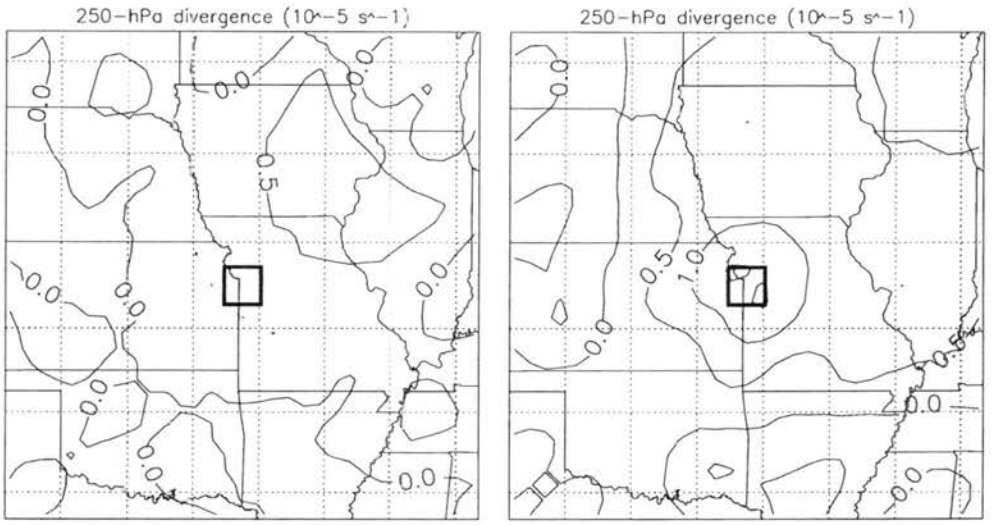

(a) 12 h before peak rainfall

(b) Peak rainfall time

Figure 6.32: As in Fig. 6.19, except for 250-hPa divergence. Contour interval is 0.5×10^{-5} s^{-1}.

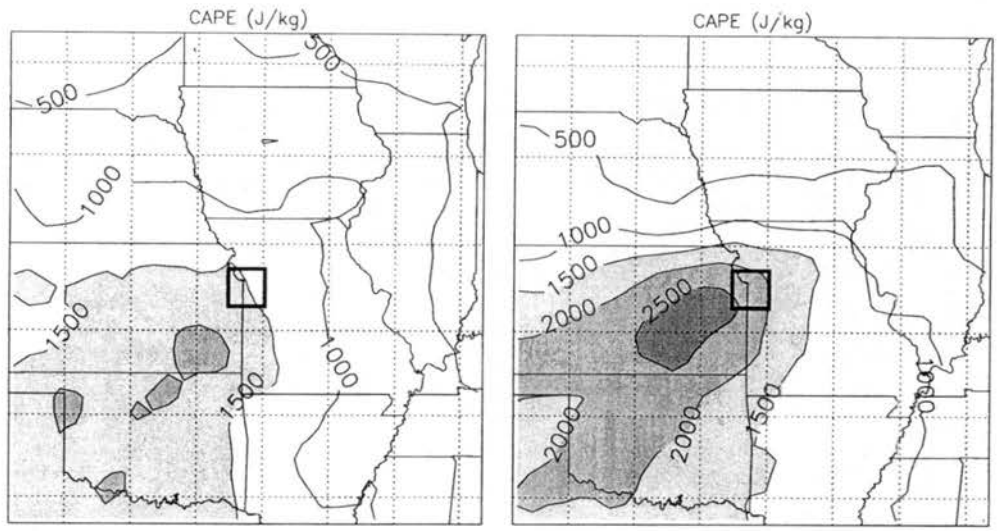

(a) 12 h before peak rainfall

(b) Peak rainfall time

Figure 6.33: As in Fig. 6.19, except for convective available potential energy. Contour interval is 500 J kg^{-1}, and values greater than 1500 J kg^{-1} are shaded.

6.2.2 Discussion

Synthesizing the results of the composite analysis of the environments in which BPS extreme rain events take place reveals a few similarites to the TL/AS composites but several important differences. For BPS MCSs, as in TL/AS systems, the atmospheric moisture increases during the 12 h period prior to the peak rainfall, providing one of the main ingredients necessary for extreme rainfall. Some features, however, such as the poorly-defined wind shift and the lack of organized low-level thermal and moisture advection, suggest that the overall synoptic setup necessary for the development of BPS systems is not as distinct as that for TL/AS systems. These factors, in conjunction with the radar-observed characteristics of BPS systems, imply that certain mesoscale and storm-scale processes are more important to the development and maintenance of a BPS-type MCS than are the large-scale conditions. While the same overall ingredients, such as moisture and instability, must be in place for such a system to occur, it appears that BPS MCSs are less dependent on pre-existing large-scale surface features (i.e., frontal boundaries) than

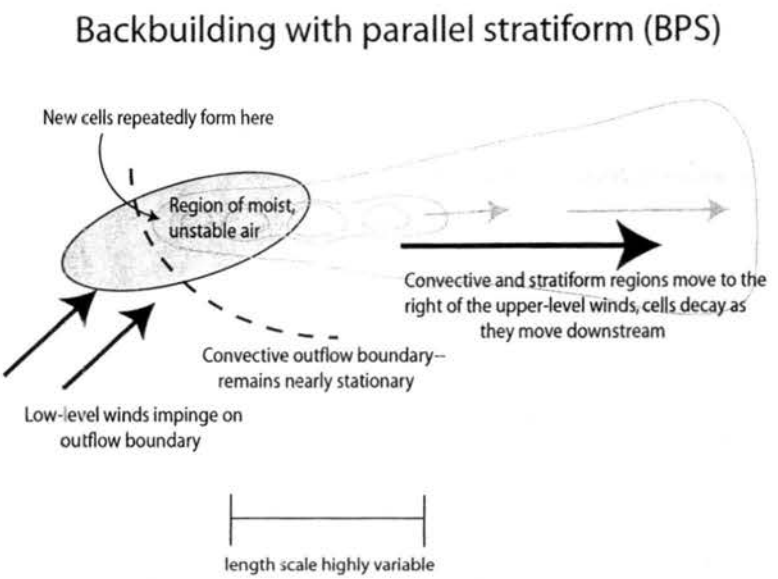

Figure 6.34: Schematic diagram of synoptic and mesoscale features associated with BPS MCSs. Typical reflectivity structure is shown in light gray.

TL/AS systems.

As mentioned in the previous section, the composite fields for TL/AS extreme rain events paint a picture similar to MCH79's "frontal" type flash flood, and they appear to correspond well with the schematics shown in Figs. 6.17a and 6.18. The conditions in place during BPS systems, on the other hand, more closely resemble MCH79's "mesohigh" type and the diagram in Fig. 6.17b, where the low-level winds are approximately parallel to the upper-level winds (Fig. 6.34). As convection begins in these conditions, an outflow boundary develops upstream of the convective cells. (These boundaries are not well-represented in the composites, mainly because they are often not captured by the surface data that are ingested into the model. They are observed in many of the individual cases, however.) The southwesterly low-level winds seen in the BPS composites then impinge on this boundary, which provides the lifting mechanism necessary to trigger new convection, and a backbuilding behavior results as the outflow boundary remains nearly stationary. The mature cells move downstream with the prevailing upper-level winds and this process may continue as long as moisture is available and as long as the outflow boundaries remain viable. Such a

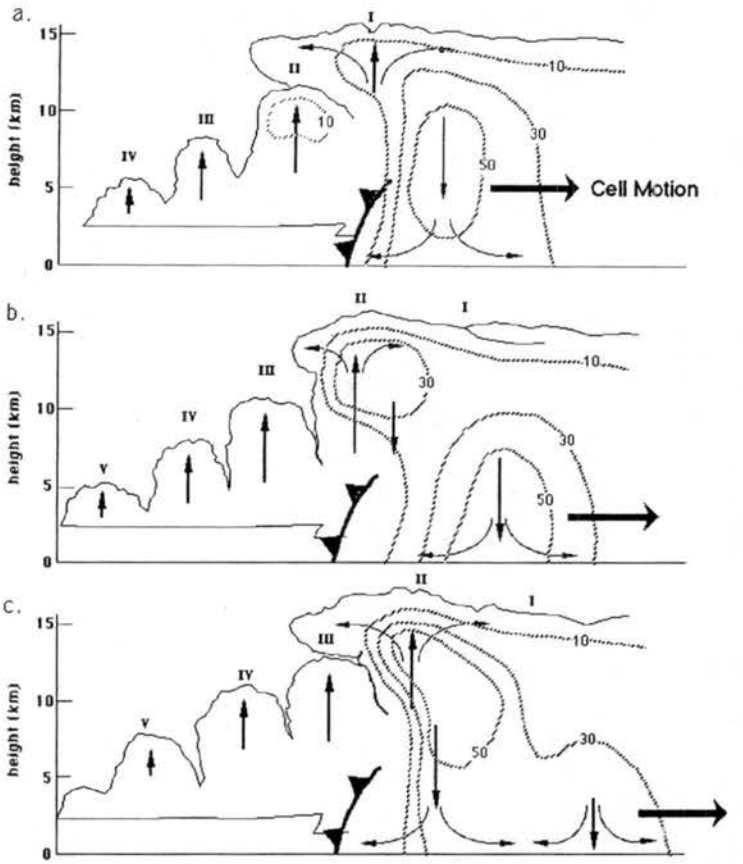

Figure 6.35: Schematic showing three stages in the evolution of a multicell thunderstorm system. Cells are labeled with Roman numerals (I, II, III, etc.); thin arrows indicate the updrafts, downdrafts, and divergence at the storm top and the surface associated with each cell; the frontal symbol indicates the low-level outflow boundary; the cell motion is indicated by the heavy arrow; and hatched lines show radar reflectivity and are labeled in dBZ. Note that the cells are moving left to right while the outflow boundary remains fixed in place. From Doswell et al. (1996)

scenario will not produce an elongated region of heavy rain, but is capable of producing extremely high rainfall totals in a localized area. A cross-section schematic of these processes was developed by DBM96 and was shown previously; it has been reproduced here for the reader's convenience as Fig. 6.35.

The main motivation for using composite analysis in this study was to gain greater understanding of the conditions that lead to the development of the two extreme-rain-producing MCS patterns described above. In addition, connections were made between

previously established atmospheric patterns for heavy rainfall (e.g., those of MCH79, Junker et al. 1999, etc.) and the convective structures that these patterns tend to form. However, a remaining question that applies to all generalizations of MCS environments is: how often do such favorable conditions exist, but no MCSs form? This issue is of even greater importance when considering extreme-rain-producing convection, because favorable conditions may be in place and an MCS may develop, but it will not necessarily produce extreme rainfall at a given location. Predicting convective precipitation remains one of the major unsolved problems in meteorology, and answering the above questions is certainly beyond the scope of this study. However, a continued effort to identify the environments in which convective storms (and in this case, particularly damaging types of convective storms) develop will hopefully provide a slight improvement in our understanding of how they work and in our ability to predict them.

Chapter 7

CASE STUDIES

While composite analysis proved to be a helpful tool to make more general statements about the TL/AS and BPS types of extreme-rain-producing MCSs, the examination of individual cases also provides information about how these systems operate. In this chapter, one TL/AS and one BPS system will be analyzed in greater detail to further illustrate the processes at work in these types of MCSs. These case studies will be relatively brief, as the main goal here is to demonstrate that the individual events making up the composites are representative of those composites, rather than to make specific conclusions about these particular events. In addition, actual atmospheric observations (rather than the RUC–2 analyses) will be the main data utilized in this chapter, to apply yet another perspective to the study of extreme rain events.

7.1 TL/AS MCS: 31 May–1 June 2000

On the evening of 31 May 2000 and the early morning hours of 1 June 2000, an MCS with training line/adjoining stratiform structure developed near the borders of Minnesota, Wisconsin, and Iowa, and produced a widespread area of prolonged heavy rainfall (Fig. 7.1). Six stations reported 24-h rainfall totals over the extreme rain threshold used for this study in this area. The highest 24-h rainfall report was 152 mm (5.98 in) at Platteville in southwestern Wisconsin, and there was an unofficial report of 184 mm (7.25 in) in 3 h at nearby Victory, WI. Flash floods that followed the rainfall caused over $10 million in property damage, and several counties in Minnesota and Wisconsin were declared federal

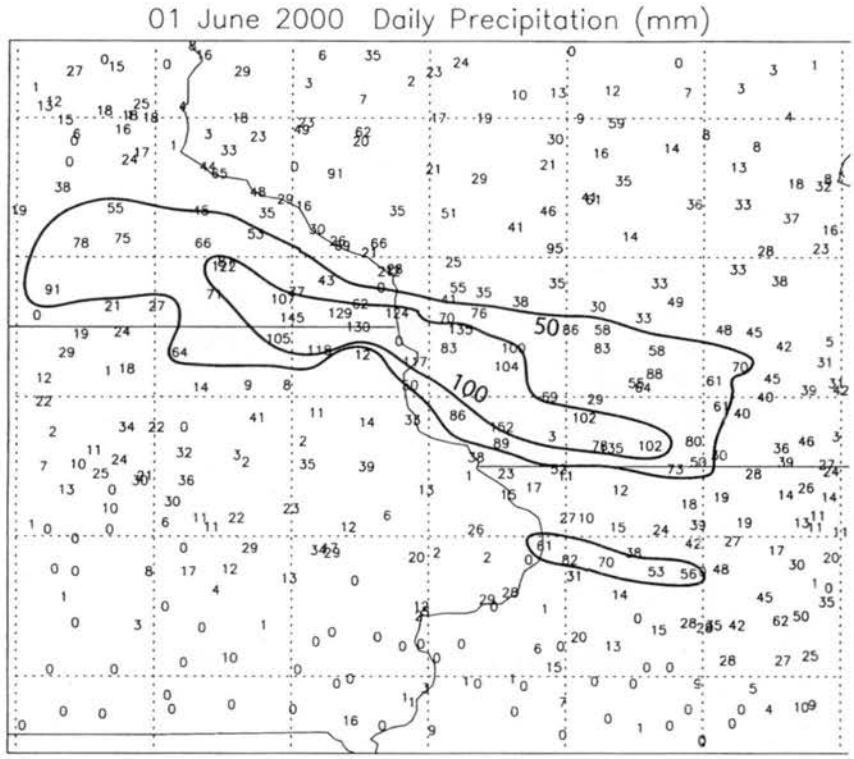

Figure 7.1: Rainfall reports (mm) for the 24-h period ending at 1200 UTC 1 June 2000. 50- and 100-mm isohyets are subjectively analyzed.

disaster areas. There were also a number of severe hail reports and a few severe wind reports associated with the convection.

A summary of the radar reflectivity features associated with this event at selected times is presented in Fig. 7.2. During the morning and afternoon of 31 May, a TS MCS moved through central Iowa and Illinois, which provided a small amount of initial precipitation to the area that would later receive the extreme rainfall. The remnants of this system were still visible in eastern Wisconsin and Illinois at 0100 UTC 1 June, which is when convection began to develop along a line from southwestern Wisconsin westward through northern Iowa (Fig. 7.2a). An hour later, there were two distinct areas of deep convection, one in southwestern Wisconsin, and one in north central Iowa (Fig. 7.2b). The initial training line structure developed in extreme southwestern Wisconsin between 0200 and 0400 (Fig. 7.2b–c), with cells moving toward the east-southeast within a line oriented in approximately the same direction. By 0500 UTC (Fig. 7.2d), a nearly continuous con-

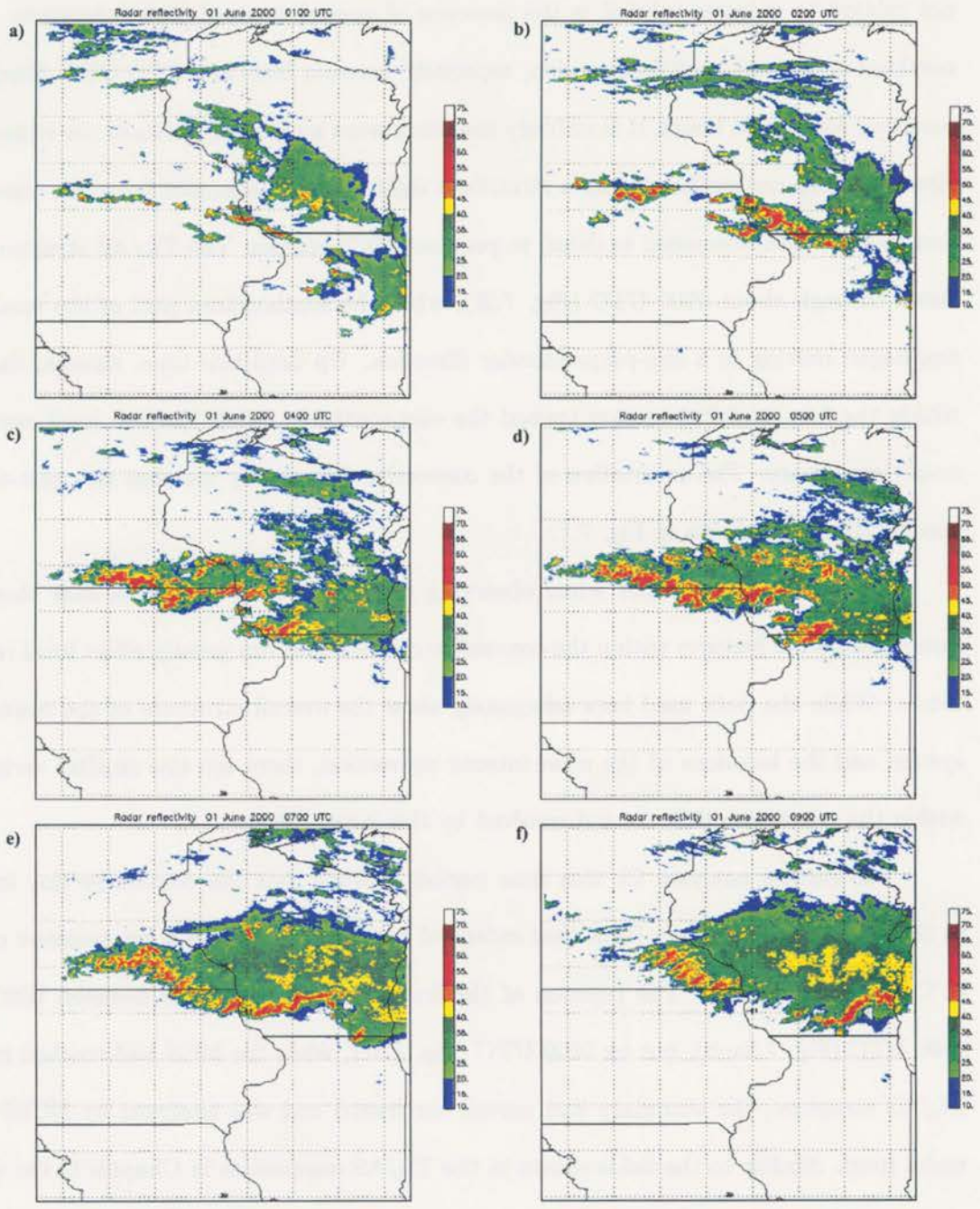

Figure 7.2: Radar reflectivity (dBZ) for the TL/AS MCS extreme rain event at (a) 0100, (b) 0200, (c) 0400, (d) 0500, (e) 0700, and (f) 0900 UTC 1 June 2000.

vective line, with a large adjoining region of stratiform rain to the north and east, existed between southern Minnesota and southwestern Wisconsin. One interesting feature that is not related to extreme rainfall is the presence of several cores of high reflectivity at the northern end of the stratiform region, especially between 0500 and 0700 UTC. Since they persisted for several hours, it is unlikely that they were a result of errors in the radar data. However, deep convection within a stratiform region, so far separated from the convective line, has not been discussed in detail in previous MCS studies. The TL/AS structure persisted through about 0900 UTC (Fig. 7.2f), when the southeastern part of the remaining line began moving in a line-perpendicular direction. Up until this time, though, the cells within the line exhibited motion toward the east-southeast, while the line itself remained nearly stationary. The orientation of the convective line closely matches the west-to-east precipitation axis shown in Fig. 7.1.

One point to remember when observing these reflectivity figures is that there are many small-scale features within the convective clusters that can greatly affect local rainfall totals. While the data used here adequately show the overall structure of the convective system and the locations of the most intense convection, there are also smaller variations within the convective that are not resolved by this 2-km dataset.

The surface analyses for this time period indicate that the convective line formed to the north of a stationary front that extended northeastward from a low-pressure center in Colorado (Fig. 7.3). The position of the front changed very little between 0000 and 0300 UTC (Fig. 7.3a–b), but by 0600 UTC (Fig. 7.3c), when the MCS had reached its full TL/AS structure, the boundary had moved northward and was analyzed by NCEP as a warm front. Similar to the fields shown in the TL/AS composites in Chapter 6, the winds to the south of the boundary were generally from the south while those to the north of the front were from the east and northeast, indicating convergence along the front. Dew point temperatures were in the 60s (°F) and dew-point depressions were small in the vicinity of the boundary, indicating ample moisture and high relative humidity.

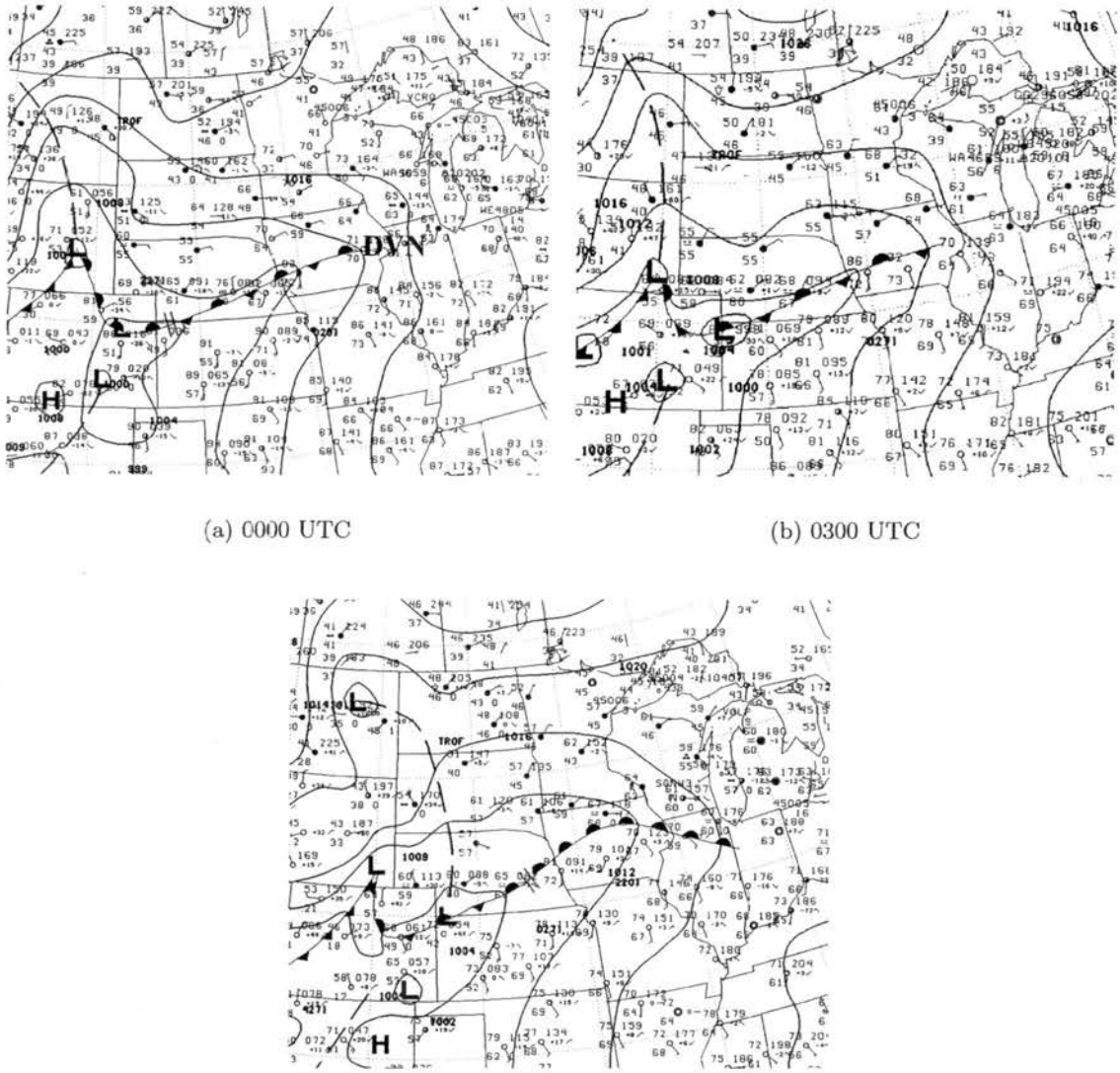

(a) 0000 UTC

(b) 0300 UTC

(c) 0600 UTC

Figure 7.3: NCEP surface analyses for (a) 0000, (b) 0300, and (c) 0600 UTC 1 June 2000. The convective line in this case developed to the north of the stationary front across Iowa. The location of Davenport, IA (DVN) is shown in (a).

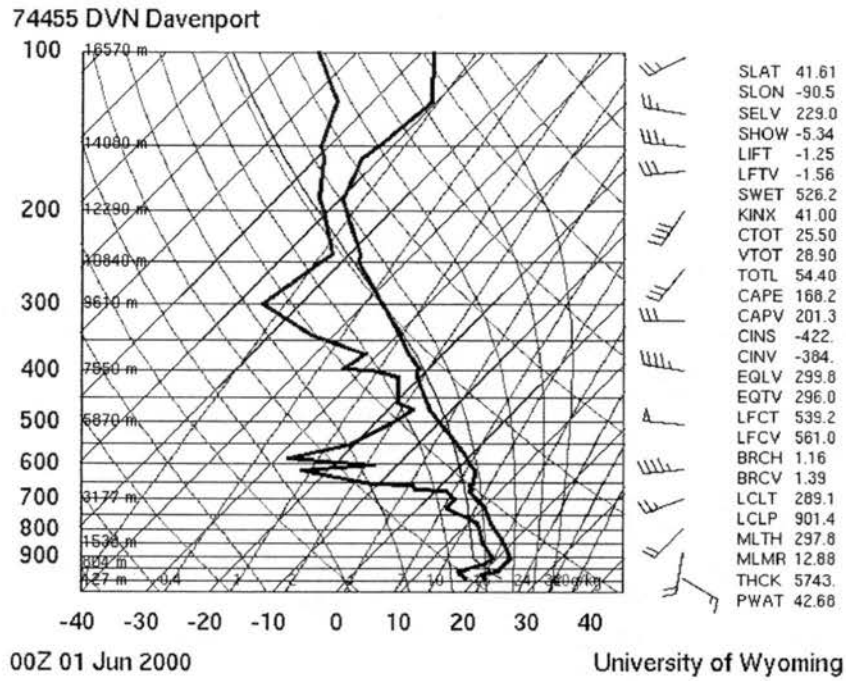

Figure 7.4: Skew–T log p diagram of the sounding from Davenport, IA (DVN) at 0000 UTC 1 June 2000.

The sounding taken at Davenport, Iowa (DVN) at 0000 UTC 1 June, which was very near the location of the surface front at that time, appears to be fairly representative of the environment in which the extreme rainfall occurred. It shows cool air below and a capping inversion at 900 hPa, demonstrating the presence of sub-boundary air at low levels (Fig. 7.4). While the surface-based CAPE is small (168 J kg^{-1}), the available energy of any parcels lifted from above the inversion is quite large. These thermodynamic variables indicate that the convection in this event was most likely rooted above the boundary layer, as was discussed for TL/AS MCSs in the previous chapter. The DVN sounding shows ample moisture, with a moist layer up through 700 hPa, and 42.68 mm of precipitable water. The wind profile from the sounding is also very similar to the composite profile for TL/AS MCSs presented in the last chapter, with veering winds at low levels but little directional shear above 700 hPa.

The upper-level wind fields in the vicinity of the heavy rainfall at 0000 UTC also resemble the composite conditions found for TL/AS MCSs. At 850 hPa, 25-kt winds from

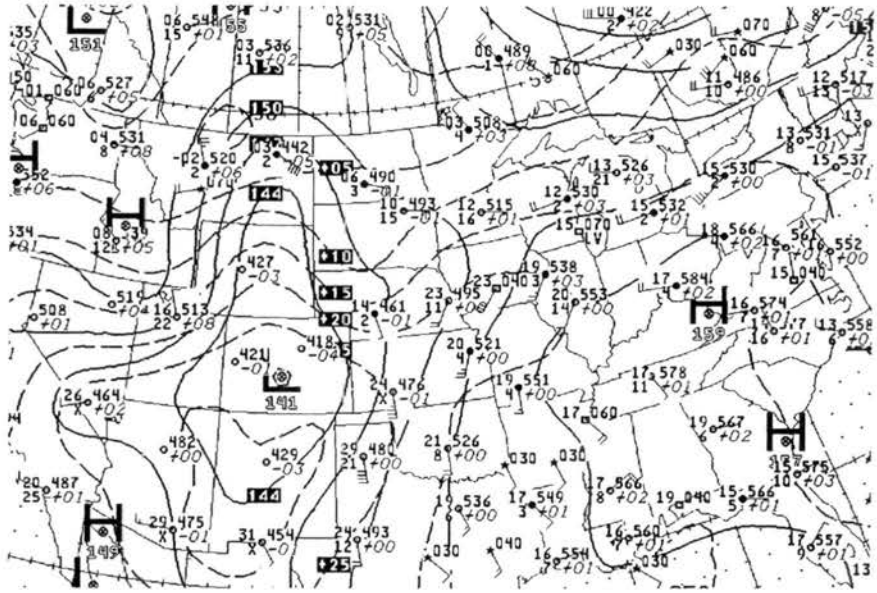

Figure 7.5: NCEP analysis of heights (solid contours) and temperature (dashed contours) on the 850-hPa surface at 0000 UTC 1 June 2000.

the south-southwest in Iowa were advecting warm, moist air northward (Fig. 7.5). There was a relatively strong north-to-south temperature gradient across Iowa, Wisconsin, and Minnesota at this level as well, and the convection that formed a few hours later was likely initiated as this southerly flow was lifted isentropically over the low-level boundary. The 500-hPa analysis shows that the event occurred under the flow around a large-scale ridge that was positioned over the eastern half of the U. S. at the time (Fig. 7.6). The composite upper-level flow field for TL/AS MCS events, as well as past studies by MCH79 and others, show that extreme rain events commonly form under similar positions relative to the upper-level flow. The event also occurred in the right-entrance region of a 110-kt jet streak at the 300-hPa level, an area that is typically associated with upper-level divergence and convective activity (Fig. 7.7). While the composites presented in the previous chapter do not show a jet streak (at least not in the grid that was used), other investigators have shown that extreme rain events often occur in the right-entrance region of a jet streak (e.g., Junker et al. 1999). On the whole, the wind profiles near the convective activity allowed for prolonged convergence and lifting along the boundary and then motion of the convective

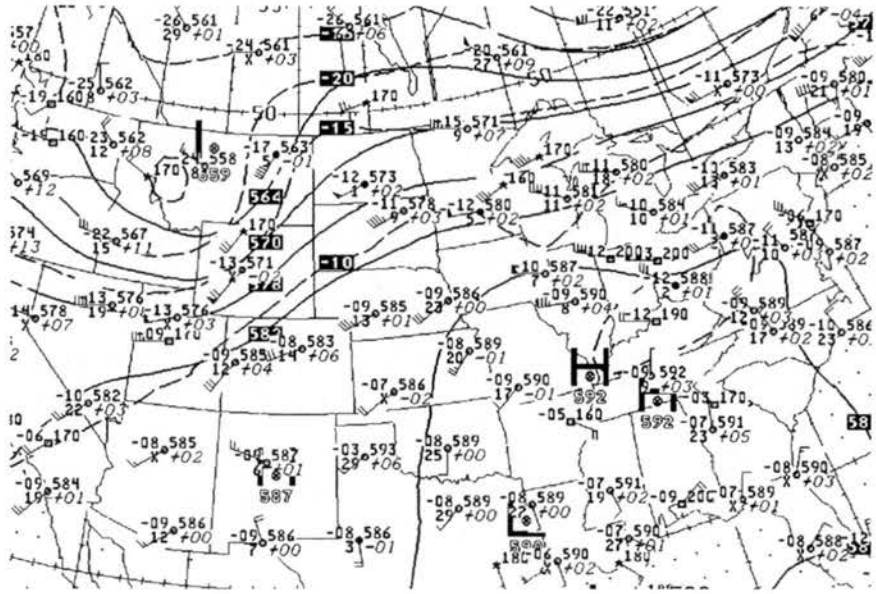

Figure 7.6: NCEP analysis of heights (solid contours) and temperature (dashed contours) on the 500-hPa surface at 0000 UTC 1 June 2000.

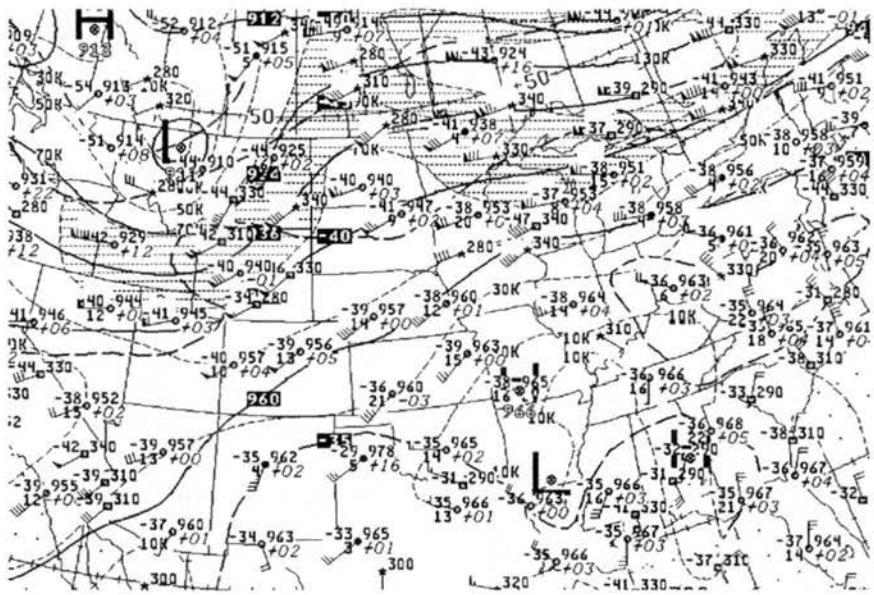

Figure 7.7: NCEP analysis of heights (solid contours) and isotachs (dashed and shaded contours) on the 300-hPa surface at 0000 UTC 1 June 2000.

cells downstream as the low-level winds were nearly perpendicular to the upper-level winds.

This brief overview of the atmospheric conditions attending the 1 June 2000 extreme rain event illustrates how the processes inferred from the composite analyses are consistent with those occurring in actual events. In this case, convection was initiated to the north of a west-to-east oriented stationary front and evolved into a "training line" structure that was responsible for extreme rain totals in Minnesota, Iowa, and Wisconsin. An area of stratiform precipitation developed, and both the convective cells and the stratiform rain moved to the east with the upper level winds. The observed surface and upper-air fields show conditions very similar to those shown by composite analysis to be common to most TL/AS MCSs. Of course, not all such events will develop in exactly the same way, but these results give further insight into how the atmospheric conditions affect the organization of extreme-rain-producing MCSs.

7.2 BPS MCS: 6-7 May 2000

During the overnight hours of 6–7 May 2000 a small area of quasi-stationary convection produced a remarkable amount of rain over several counties just to the southwest of the St. Louis, Missouri metropolitan area (Fig. 7.8). (For a more complete analysis of the mesoscale and storm-scale features of this event, see Glass et al. 2001.) Three stations reported 24-h rainfall totals over the extreme rainfall threshold, including the highest 24-h total of all non-tropical events in the entire population (309 mm, or 12.15 in, at Union, MO). Nearly all of the creeks in the area flooded as a result of the rainfall, and this flash flooding caused 2 fatalities and over $100 million in property damage. There was minor flash flooding around the city of St. Louis, but this event could have been even more devastating had the heaviest rain fallen over the more urbanized and populated areas nearer the city.

The radar reflectivity structure of this event at selected times is shown in Fig. 7.9. Between 0000 and 0300 UTC 7 May, an area of weak rainfall was moving from west to east

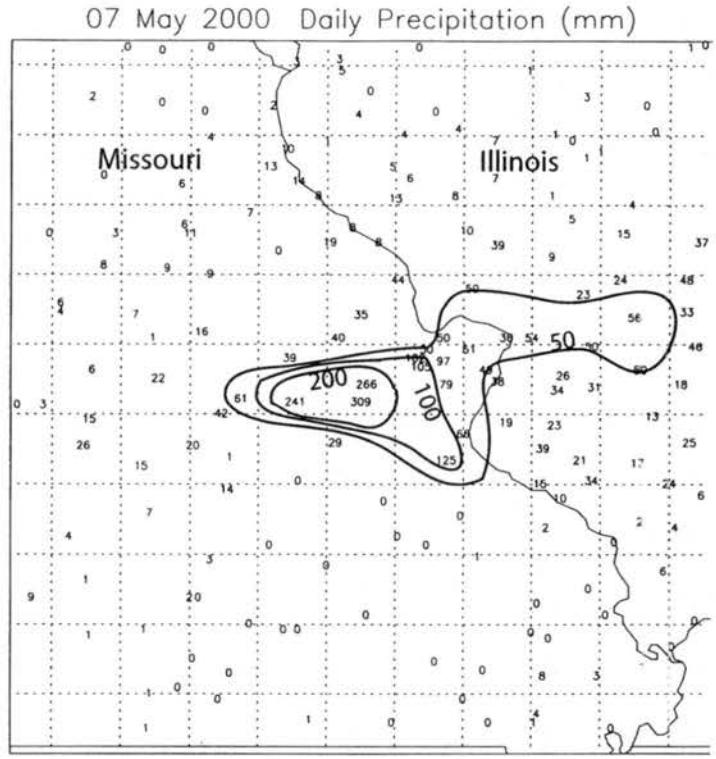

Figure 7.8: Rainfall reports (mm) for the 24-h period ending at 1200 UTC 7 May 2000. 50-, 100- and 200-mm isohyets are subjectively analyzed.

across central Missouri. (This precipitation was likely caused by upward motion associated with a mid-level mesovortex, which is discussed below.) By 0300 UTC (Fig. 7.9a), deep convection began to develop at the western end of this precipitation region. New convective cells formed just upstream of the existing ones after this time, setting up a training effect over east-central Missouri. The MCS continued to backbuild between 0500 and 0900 UTC (Fig. 7.9b–e), which resulted in a nearly stationary region of deep convection and heavy rainfall. Finally, by 1100 UTC (Fig. 7.9f), the system began to move off to the east, and the deep convection dissipated by 1500 UTC. Hourly precipitation observations from Washington, MO (the station reporting 266 mm in Fig. 7.8), show that most of the rain from this event fell in a 6-h period, with rainfall rates of over 25 mm h^{-1} between 0500 and 1100 UTC (Fig. 7.10).

At the surface, there were no analyzed features on the NCEP analysis in the vicinity of the MCS either before or during the heaviest rainfall (not shown). In eastern and central

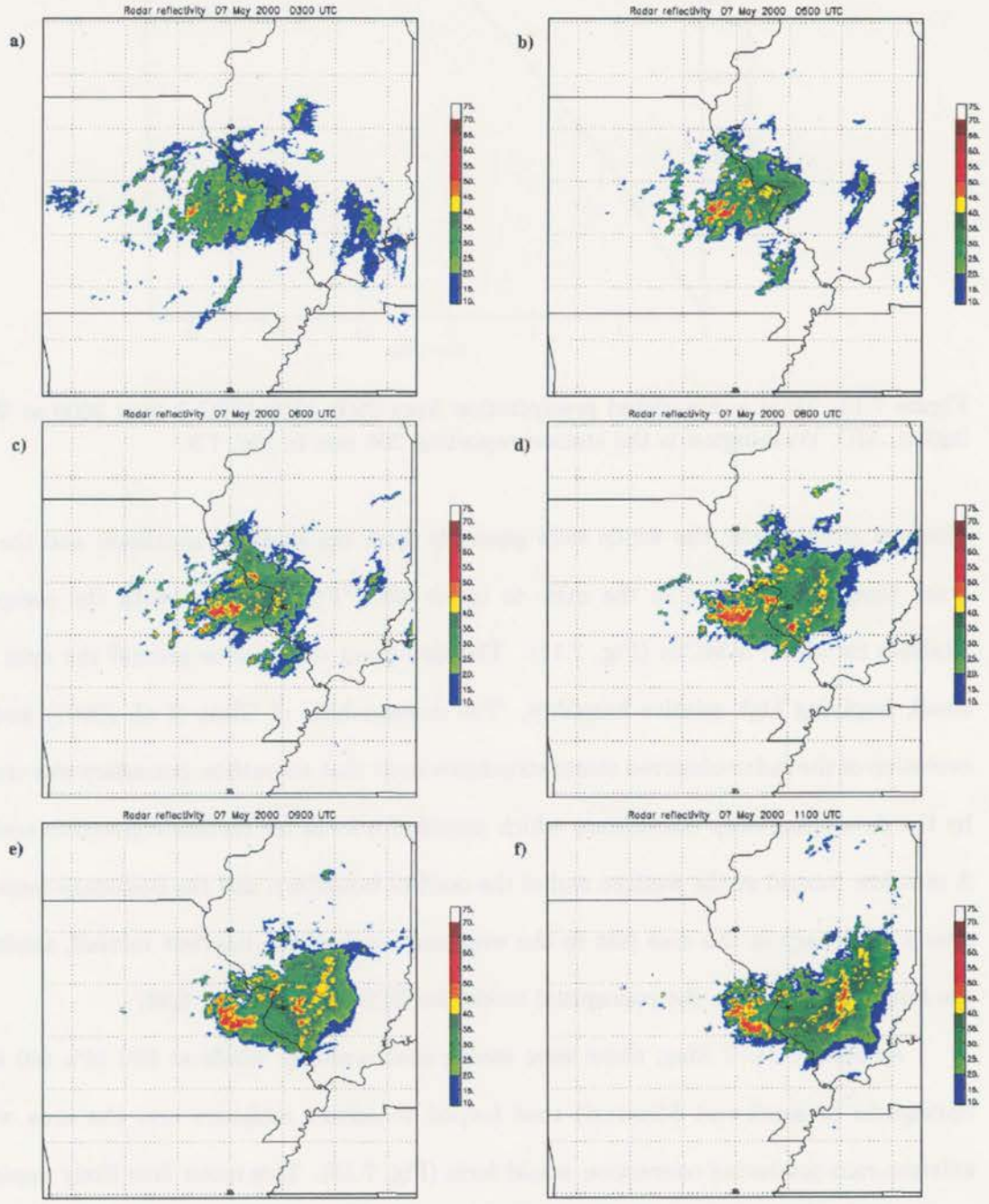

Figure 7.9: Radar reflectivity (dBZ) for BPS MCS extreme rain event at (a) 0300, (b) 0500, (c) 0600, (d) 0800, (e) 0900, and (f) 1100 UTC 7 May 2000. Note that the area of high reflectivity remains nearly stationary between 0500 and 0900 UTC.

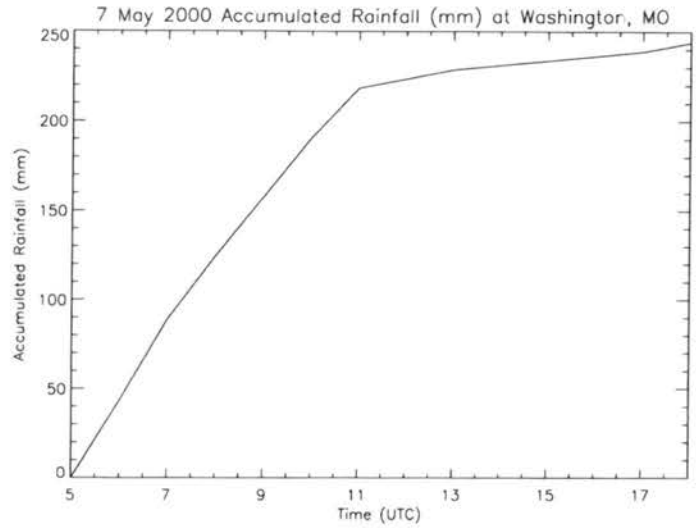

Figure 7.10: Total accumulated precipitation from 0500–1700 UTC 7 May 2000 at Washington, MO. Washington is the station reporting 266 mm in Fig. 7.8.

Missouri at this time, the winds were generally from the south or southeast and the dew point temperatures were in the mid- to upper-60s (°F), consistent with the composite analyses for all BPS MCSs (Fig. 7.11). The dew-point depressions around the area were small, implying high relative humidity. The mesoanalysis of Glass et al. (2001) and the evolution of the radar-observed storm structures show that an outflow boundary was created by the developing deep convection, which provided a focus for further convective activity. A mesolow formed at the western end of the outflow boundary, and the boundary remained nearly stationary in the area just to the west and south of the heaviest rainfall, similar to the boundary shown in the conceptual model for BPS MCSs in Fig. 6.34.

At 0000 UTC 7 May, there were strong southwesterly winds at 850 hPa (40 kt at Springfield in southwest Missouri) that helped to advect moisture into the area where extreme-rain-producing convection would form (Fig. 7.12). This moist flow likely impinged on the outflow boundary described above and provided a continuous moisture source for the convection. At 500-hPa, both the radiosonde analysis and satellite imagery show a mesovortex located just upstream of where the heavy rain would fall (Figs. 7.13 and 7.14). Convection associated with this mesovortex (such as that described by Fritsch et al. 1994)

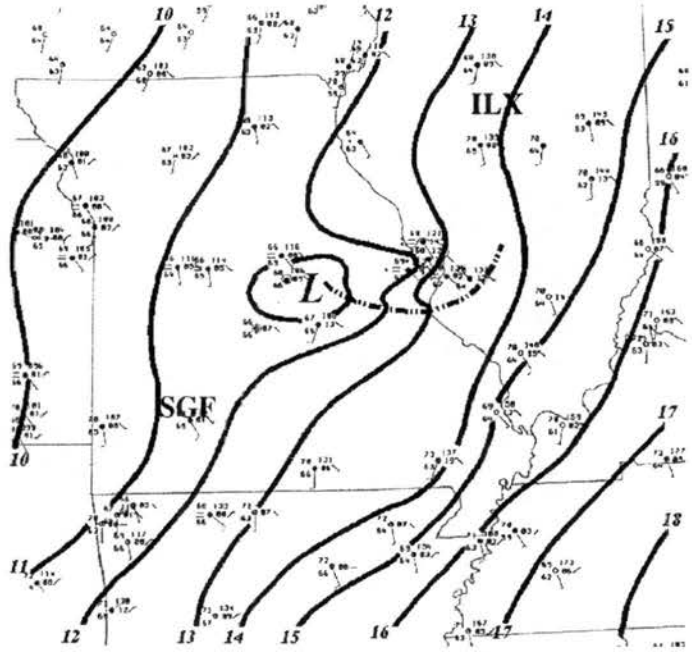

(a) 0600 UTC

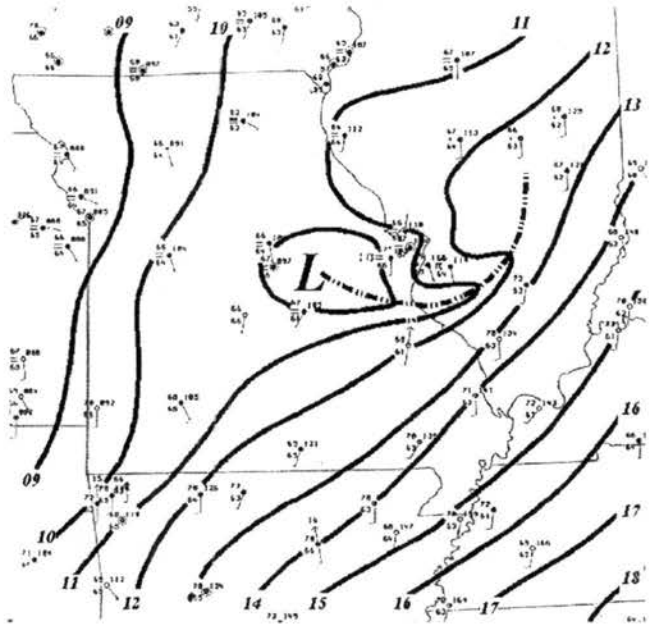

(b) 1000 UTC

Figure 7.11: Surface mesoanalysis at (a) 0600 and (b) 1000 UTC 7 May 2000. Isobars are contoured every 1 hPa, and are marked without the leading "10", so that the contour marked "12" indicates 1012 hPa and so on. Outflow boundary is analyzed with dash-dotted line. Locations of Springfield, MO (SGF) and Lincoln, IL (ILX) are shown in (a). From Glass et al. (2001).

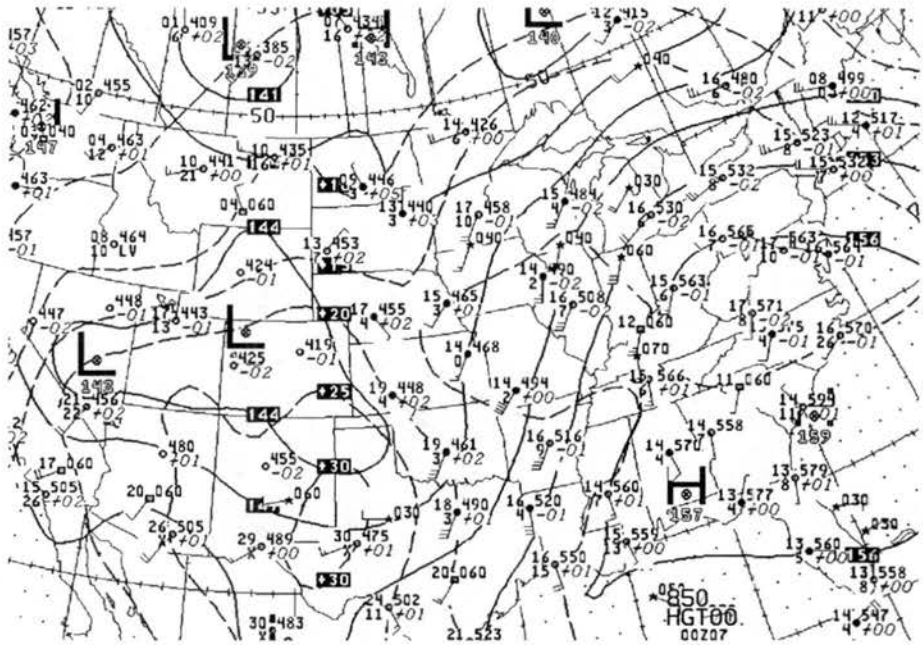

Figure 7.12: NCEP analysis of heights (solid contours) and temperature (dashed contours) on the 850-hPa surface at 0000 UTC 7 May 2000.

produced extreme rainfall in Oklahoma the previous day, and it likely played an important role in the development of the convection in this case as well. The 500- and 300-hPa (not shown) fields for this event varied considerably from the composite fields shown in the previous chapter. While mid-level vortices were present for some BPS systems, they were not represented in the composites. Furthermore, the composite BPS system developed to the south of an upper-level jet (cf. Fig. 6.31), but the winds at upper levels in this event were weak with no nearby jet.

The two nearest soundings to the area where the MCS would develop were taken at Springfield, MO (SGF, in the southwestern part of the state) and Lincoln, IL (ILX, in central Illinois, to the northeast of the extreme rainfall location). Though neither of these soundings was particularly close to the system, they can provide some information about the thermodynamic environment in which it formed. The sounding from each location at 0000 UTC (a few hours before the convection developed) is shown in Fig. 7.15. Both soundings show ample low- and mid-level moisture, a small amount of positive CAPE, and

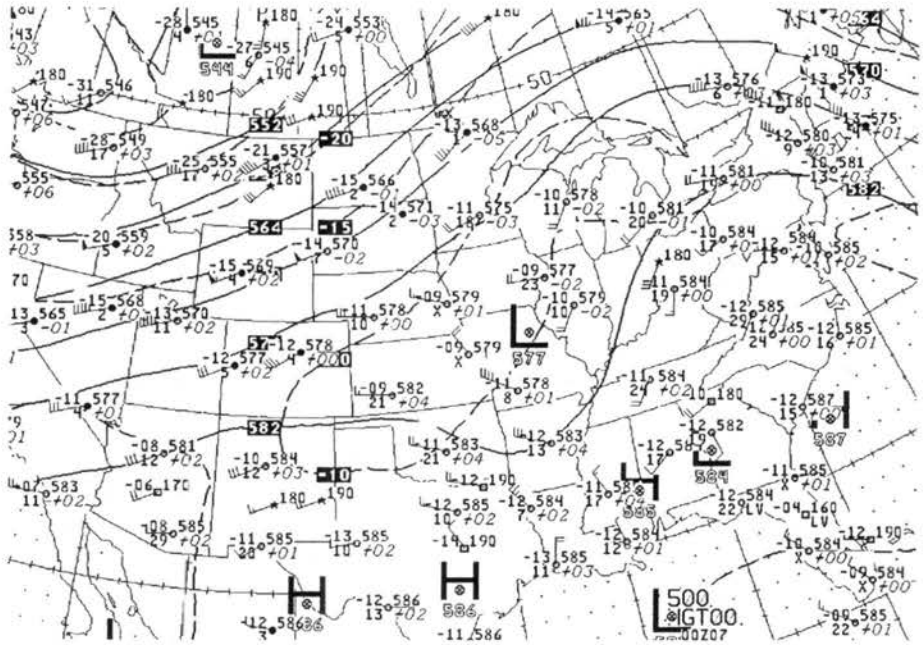

Figure 7.13: NCEP analysis of heights (solid contours) and temperature (dashed contours) on the 500-hPa surface at 0000 UTC 7 May 2000.

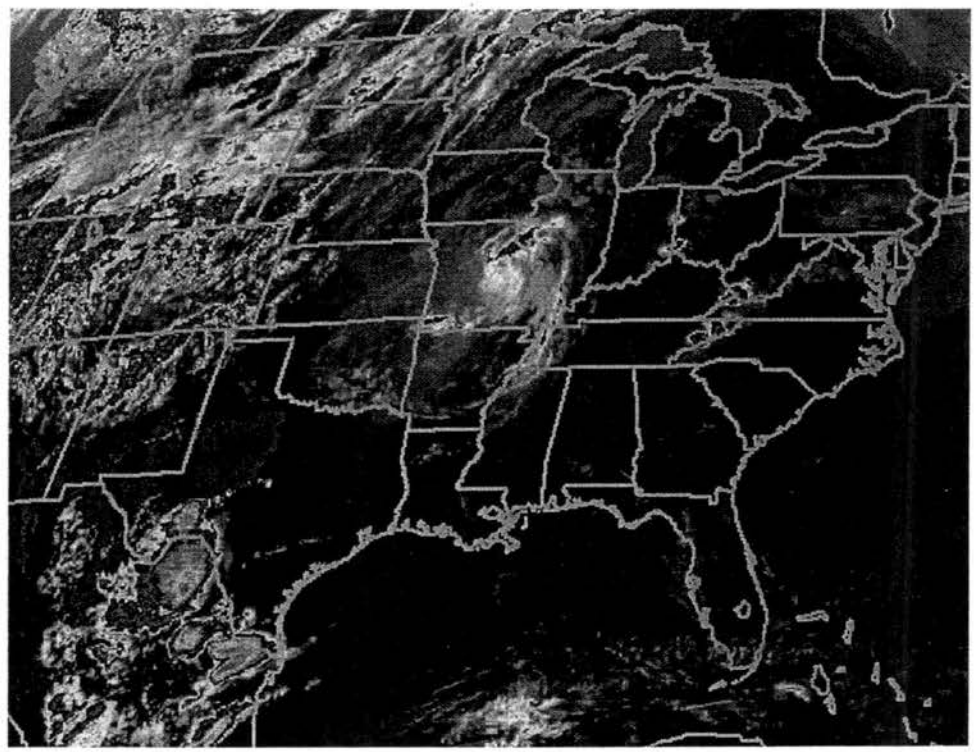

Figure 7.14: Infrared satellite image from 0000 UTC 7 May 2000. Note the cyclonic circulation indicated by the cloud bands associated with the mid-level mesovortex over Missouri.

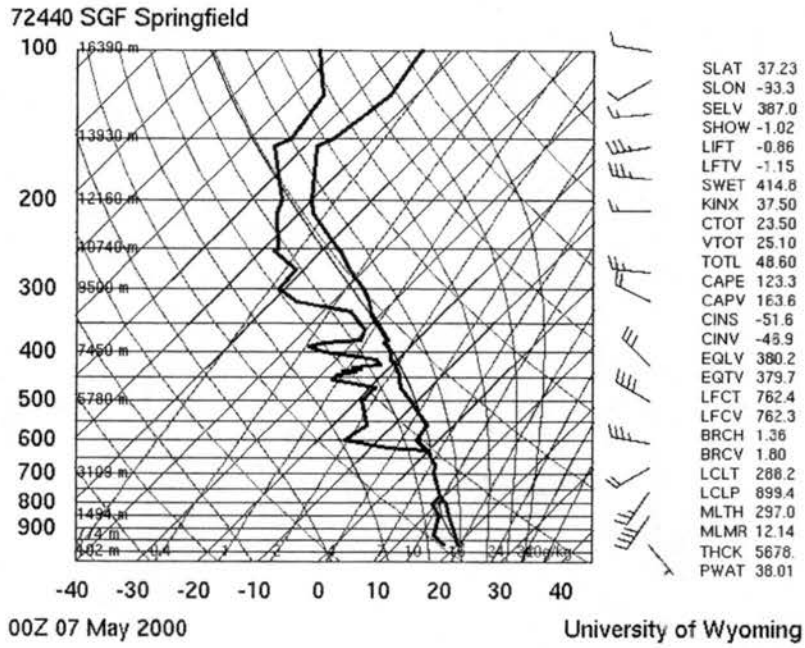

(a) SGF

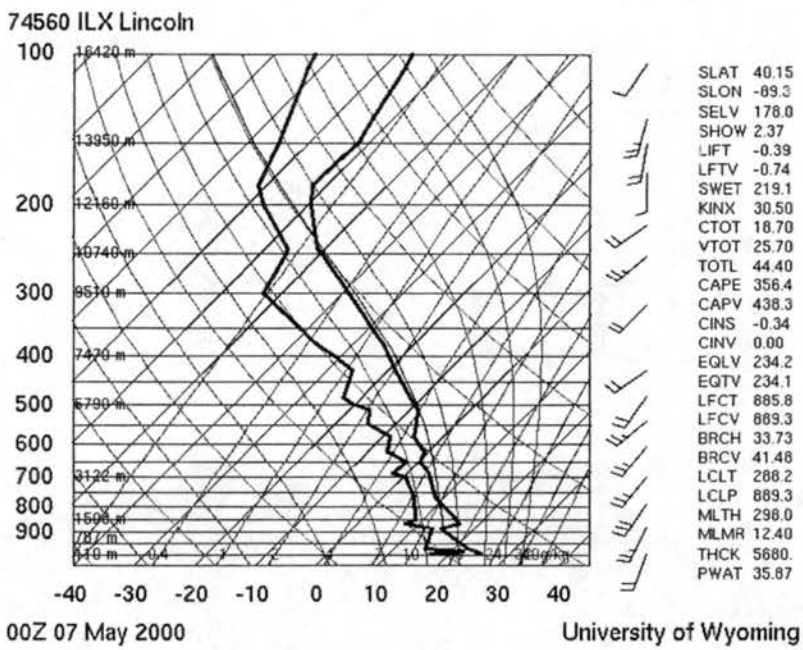

(b) ILX

Figure 7.15: Skew–T log p diagrams of the soundings from (a) Springfield, MO (SGF) and (b) Lincoln, IL (ILX) at 0000 UTC 7 May 2000.

very little convective inhibition. The SGF sounding (Fig. 7.15a) is actually saturated from approximately 775 to 625 hPa, and nearly saturated below that, with a total PW of 38 mm. The ILX sounding (Fig. 7.15b) shows slightly less moisture and no saturated layers, but the PW is still over 35 mm. The wind profile at SGF indicates that a low-level jet may be present to the south of the heavy rain location, as the winds (below 500 hPa) are maximized at the 850-hPa level. This profile has more pronounced veering through the atmosphere than is shown in the composite profile for BPS systems, partly as a result of the midlevel mesovortex. In contrast, the wind profile at ILX is nearly unidirectional throughout the atmosphere. By interpolation, the actual directional shear at the extreme rainfall location is likely somewhere between the two. Using the method of Corfidi et al. (1996) and Corfidi (1998) for estimating the motion of convective elements within an MCS, such a wind profile is supportive of back-building or quasi-stationary convection, though this approach may not have been completely accurate in this event because of the presence of an outflow boundary.

As the composite analyses indicated to be true for most BPS MCSs, the synoptic-scale features responsible for the development of this system are not well-defined. No major surface boundaries were in place before the convection developed. However, a very moist air mass, which can be conducive to high precipitation efficiencies and slow-moving thunderstorm outflows, and a wind profile supportive of backbuilding convection were in place in the area. In this case, mesoscale interactions between a mid-level mesovortex, the low-level jet, and this moist air mass helped to determine where the convection would form. Then, storm-scale processes maintained an outflow boundary that provided the forcing for a quasi-stationary area of convection. While the overall atmospheric conditions were very similar to those shown for all BPS systems in the composite fields, anticipating the formation of a system such as this one would have been a formidable challenge, especially considering that very similar conditions are quite common in the Midwest during the spring and summer.

7.3 Discussion

These two brief case studies illustrate some of the same processes that were inferred from the composite atmospheric fields for extreme-rain-producing TL/AS and BPS MCSs. The actual conditions that were present during the two events described above were very similar to the conditions in the composites and they, along with other cases not shown, indicate that the composite results did not come about by chance or by artifacts of averaging. Furthermore, they confirm the speculation from the previous chapter that TL/AS systems depend heavily on pre-existing synoptic-scale and mesoscale features (especially at the surface), while mesoscale and storm-scale processes are more important for the development and maintenance of BPS MCSs.

Comparing the rain gauge reports to the conceptual models that were shown in Fig. 6.17, we see that the TL/AS system analyzed here (which has low-level winds nearly perpendicular to the upper-level winds) does indeed have an elongated region of heavy rain, while the heavy rainfall area for the BPS system (with low-level winds at a smaller angle to the upper-level winds) is much smaller. However, the BPS system had much higher total rainfall accumulations in this small area. Depending on where the systems are located, both types of rainfall distributions could be extremely damaging.

The characteristics of extreme rain events presented in the last few chapters indicate a number of forecasting challenges for both TL/AS and BPS MCSs (not to mention the other storm types.) While there do appear to be specific situations that favor the development of extreme-rain-producing convection, they are not particularly distinct from other, more benign scenarios. Hopefully these efforts, as well as future work on the subject, will begin to clarify the distinctions that need to be made between systems that produce "everyday" rainfall and the destructive systems described here.

Chapter 8

CONCLUSIONS AND FUTURE WORK

8.1 Conclusions

Using rain gauge observations from the part of the United States east of the Rocky Mountains (excluding Florida) in 1999–2001, 193 events were selected that exceeded a spatially varying threshold for 24-h precipitation accumulation. These cases were deemed "extreme rain events." The climatological characteristics of these events are generally consistent with past studies of heavy precipitation and flash floods:

- Extreme rain events in the complete area of study occurred most frequently in June, July, and August.
- In the northern part of the country, extreme rain events were confined almost exclusively to the warm season, while in the south, such events were generally less dependent on season.

National composite radar reflectivity data were then used to make a quantitative determination about what types of weather systems are most often responsible for producing extreme rainfall totals. These radar data were observed over the life cycle of each extreme rain event to classify it as a synoptic system, a mesoscale convective system (MCS), a tropical system, or an isolated system. Several new findings have emerged from the results of this study:

- The radar analysis showed that 59% of all extreme rain events were associated with

MCSs, and 27% resulted from synoptic weather systems.

- In the Plains and north regions, nearly all of the events were associated with MCSs. In the northeast, synoptic systems were the predominant extreme-rain-producers, while in the southeast, tropical systems played a relatively large role.

- In almost the entire area of study, MCSs were the dominant summertime extreme rain producers. Over 70% of summertime extreme rain events in the entire domain were caused by MCSs. In contrast, synoptically-forced systems produced the most extreme rain events outside the warm season.

Since this analysis showed that MCSs produce many of the extreme rainfall events in the area of study, the radar data from each MCS event were analyzed further to determine the most common modes of convective organization.

- Not surprisingly, there was great variability in the radar-indicated structures of extreme-rain-producing MCSs.

- Many of these systems corresponded to previously established patterns for MCS organization, and many others were not organized into discernable patterns.

- However, two previously unidentified patterns of convective organization were observed most frequently. The first is a "training" convective line with an adjoining region of stratiform rain (TL/AS), and the second is a backbuilding convective line or cluster with a parallel region of stratiform rain downstream (BPS).

Composite analysis of RUC–2 model analyses was then utilized to determine the atmospheric conditions in which TL/AS and BPS MCSs typically form and to compare these results to previous findings on the environments of extreme precipitation systems. In addition, two case studies were presented that further explore the processes responsible for the development of extreme-rain-producing MCSs. These techniques led to the following conclusions:

- Composite analysis showed that extreme-rain-producing TL/AS MCSs usually form in conditions described by the "frontal" flash flood type of Maddox et al. (1979) and others. In this pattern, the convective line forms on the cool side of a pre-existing slow-moving synoptic boundary.

- The conditions in place for BPS MCSs were not as well-defined, and show that these systems are more dependent on mesoscale and storm-scale processes and forcings (such as outflow boundaries) than on larger-scale features.

- Case studies of one TL/AS and one BPS system reinforce these hypotheses about the conditions and processes that are often at work in these types of events.

8.2 Suggestions for future work

This study has considered mainly the overall structures of precipitation systems that produce extreme rainfall as they are observed in the 2-km national composite radar reflectivity dataset. One of the main goals of this work was to determine, for a large number of cases, how such systems are organized. However, many of the processes that determine local rainfall amounts occur on scales smaller than can be resolved by this dataset and require more thorough analysis. As such, several avenues of future research on extreme rainstorms present themselves.

First, radar data can provide much more information than has been used here. Dual-Doppler analysis and information from polarimetric radars could give greater insights into the motion and precipitation characteristics of extreme rainstorms. Radar observations used in conjunction with a high-density network of rain gauges could offer more information about the correlation between certain reflectivity structures and the amount of rainfall they produce.

Second, intensive observations from field projects have been used to greatly increase our understanding of squall lines, MCCs, and other types of convective systems. However, though flash floods cause a great amount of damage and injury each year, very few studies

using such observations have been initiated to analyze the events that cause them. A field study dedicated only to extreme rainfall events may be logistically very difficult since such events are rare and often isolated. However, including extreme-rain-producing systems into a wider-ranging field program that includes a dense network of soundings, radars, surface observations, and rain gauges could greatly increase our understanding of extreme rainfall if a significant event was heavily observed. An exploration of data from past field campaigns may also yield information about extreme rain events that was previously neglected.

Third, a thorough study of extreme-rain-producing weather systems in other parts of the world may increase our understanding of such events as well. While some characteristics of storms that produced flash flooding in the events studied here may be exclusive to the geography and climate of the United States, they certainly have many similar traits to damaging storms across the globe. The ingredients necessary for heavy rainfall (i.e., moisture, upward motion, etc.) are the same everywhere, so applying the criteria used here and examining radar data from other countries may add to the knowledge of the characteristics of extreme rain events as a whole.

Finally, since many of the processes important to heavy rainfall are difficult to observe using conventional methods, numerical modeling may prove useful. Sensitivity studies using numerical simulations may aid in, among other things, our understanding of why some convective systems become quasi-stationary while others that form in similar conditions do not.

All of these suggestions for future work aim toward the goals of both better understanding and better forecasting of heavy precipitation. Since extreme rain events often develop in relatively benign conditions and occur on small scales that are nearly unpredictable outside of a nowcasting timeframe, any work toward this goal will likely represent an improvement over present techniques. With further efforts in this subject, perhaps the processes that govern extreme rainfall will become better known, the signatures that tip off a forecaster to the possibility of extreme rainfall will become more clear, and the

operational numerical weather prediction models will better represent and predict heavy convective rainfall. If any of these goals are accomplished, there can be longer lead times for flash flood watches and warnings, the public can be better informed about the dangers of flash flooding, and life and property can be spared.

REFERENCES

Atkins, N. T., and R. M. Wakimoto, 1991: Wet microburst activity over the southeastern United States: Implications for forecasting. *Wea. Forecasting*, **6**, 470–482.

Augustine, J. A., and F. Caracena, 1994: Lower-tropospheric precursors to nocturnal MCS development over the central United States. *Wea. Forecasting*, **9**, 116–135.

Belville, J. D., and N. O. Stewart, 1983: Extreme rainfall events in Louisiana: The "New Orleans" type. Preprints, *5th Conference on Hydrometeorology*, Tulsa, OK, Amer. Meteor. Soc., 284–290.

Benjamin, S. G., J. M. Brown, K. J. Brundage, B. E. Schwartz, T. G. Smirnova, and T. L. Smith, 1998: The operational RUC–2. Preprints, *16th Conference on Weather Analysis and Forecasting*, Phoenix, AZ, Amer. Meteor. Soc., 249–252.

Blackadar, A. K., 1957: Boundary layer wind maxima and their significance for the growth of nocturnal inversions. *Bull. Amer. Meteor. Soc.*, **38**, 283–290.

Bolton, D., 1980: The computation of equivalent potential temperature. *Mon. Wea. Rev.*, **108**, 1046–1053.

Bosart, L. F., and F. Sanders, 1981: The Johnstown flood of July 1977: A long–lived convective system. *J. Atmos. Sci.*, **38**, 1616–1642.

Bradley, A. A., and J. A. Smith, 1994: The hydrometeorological environment of extreme rainstorms in the southern plains of the United States. *J. Appl. Meteor.*, **33**, 1418–1431.

Brooks, H. E., and D. J. Stensrud, 2000: Climatology of heavy rain events in the United States from hourly precipitation observations. *Mon. Wea. Rev.*, **128**, 1194–1201.

Byers, H. R., and R. D. Coons, 1947: The "bright line" in radar cloud echoes and its possible explanation. *J. Atmos. Sci.*, **4**, 78–81.

Caracena, F., R. A. Maddox, L. R. Hoxit, and C. F. Chappell, 1979: Mesoanalysis of the Big Thompson storm. *Mon. Wea. Rev.*, **107**, 1–17.

Changnon, S. A., Jr., and J. L. Vogel, 1981: Hydroclimatological characteristics of isolated severe rainstorms. *Water Resour. Res.*, **17**, 1694–1700.

Chappell, C. F., 1986: Quasi-stationary convective events. *Mesoscale Meteorology and Forecasting*, P. S. Ray, Ed. Amer. Meteor. Soc., 289–309.

Chappell, C. F., 1993: Dissecting the flash flood forecasting problem. Postprints, *Third National Heavy Precipitation Workshop*, Pittsburgh, PA, (NOAA Tech. Memo. NWS ER–87), 293–297.

Colman, B. R., 1990: Thunderstorms above frontal surfaces in environments without positive CAPE. Part I: A climatology. *Mon. Wea. Rev.*, **118**, 1103–1121.

Corfidi, S. F., 1998: Forecasting MCS mode and motion. Preprints, *19th Conf. on Severe Local Storms*, Minneapolis, MN, Amer. Meteor. Soc., 626–629.

Corfidi, S. F., J. H. Merritt, and J. M. Fritsch, 1996: Predicting the movement of mesoscale convective complexes. *Wea. Forecasting*, **11**, 41–46.

Crysler, K. A., R. A. Maddox, L. R. Hoxit, and B. M. Muller, 1982: Diurnal distribution of very heavy precipitation over the central and eastern United States. *Nat. Wea. Dig.*, **7**, 33–37.

Davis, R. S., 2001: Flash flood forecast and detection methods. *Severe Convective Storms*, *Meteor. Monogr.*, No. 50, Amer. Meteor. Soc., 481–525.

Doswell, C. A., III, 1991: Comments on "Mesoscale convective patterns of the southern High Plains". *Bull. Amer. Meteor. Soc.*, **72**, 389–390.

Doswell, C. A., III, H. E. Brooks, and R. A. Maddox, 1996: Flash flood forecasting: An ingredients–based methodology. *Wea. Forecasting*, **11**, 560–581.

Droegemeier, K. K., and Coauthors, 2000: Hydrological aspects of weather prediction and flood warnings: Report of the Ninth Prospectus Development Team of the U. S. Weather Research Program. *Bull. Amer. Meteor. Soc.*, **81**, 2665–2680.

Foufoula-Georgiou, E., and L. L. Wilson, 1990: In search of regularities in extreme rainstorms. *J. Geophys. Res.*, **95**, 2061–2072.

Fritsch, J. M., and Coauthors, 1998: Quantitative precipitation forecasting: Report of the Eighth Prospectus Development Team, U. S. Weather Research Program. *Bull. Amer. Meteor. Soc.*, **79**, 285–299.

Fritsch, J. M., and G. S. Forbes, 2001: Mesoscale convective systems. *Severe Convective Storms*, *Meteor. Monogr.*, No. 50, Amer. Meteor. Soc., 323–357.

Fritsch, J. M., R. J. Kane, and C. R. Chelius, 1986: The contribution of mesoscale convective weather systems to the warm-season precipitation in the United States. *J. Appl. Meteor.*, **25**, 1333–1345.

Fritsch, J. M., J. D. Murphy, and J. S. Kain, 1994: Warm-core vortex amplification over land. *J. Atmos. Sci.*, **51**, 1780–1807.

Geerts, B., 1998: Mesoscale convective systems in the southeast United States during 1994–1995. *Wea. Forecasting*, **13**, 860–869.

Giordano, L. A., and J. M. Fritsch, 1991: Strong tornadoes and flash–flood–producing rainstorms during the warm season in the Mid–Atlantic region. *Wea. Forecasting*, **6**, 437–455.

Glass, F. H., D. L. Ferry, J. T. Moore, and S. M. Nolan, 1995: Characteristics of heavy convective rainfall events across the Mid-Mississippi valley during the warm season: Meteorological conditions and a conceptual model. Preprints, *14th Conference on Weather Analysis and Forecasting*, Dallas, TX, Amer. Meteor. Soc., 34–41.

Glass, F. H., J. P. Gagan, and J. T. Moore, 2001: The extreme east-central Missouri flash flood of 6–7 May 2000. Preprints, *Symposium on Precipitation Extremes: Prediction, Impacts, and Responses*, Albuquerque, NM, Amer. Meteor. Soc., 174–179.

Heideman, K. F., and J. M. Fritsch, 1988: Forcing mechanisms and other characteristics of significant summertime precipitation. *Wea. Forecasting*, **3**, 115–130.

Holton, J. R., 1992: *An Introduction to Dynamic Meteorology*. 3rd edition. Academic Press, 511 pp.

Houze, R. A., Jr., B. F. Smull, and P. Dodge, 1990: Mesoscale organization of springtime rainstorms in Oklahoma. *Mon. Wea. Rev.*, **118**, 613–654.

Hoxit, L. R., and Coauthors, 1978: Meteorological analysis of the Johnstown, Pennsylvania, flash flood. NOAA Tech. Rep. ERL 401–APCL 43, 71 pp.

Hulson, H. R., 1971: On the relationship between horizontal moisture convergence and convective cloud formation. *J. Appl. Meteor.*, **10**, 765–762.

Junker, N. W., R. S. Schneider, and S. L. Fauver, 1999: A study of heavy rainfall events during the Great Midwest Flood of 1993. *Wea. Forecasting*, **14**, 701–712.

Karl, T. R., and R. W. Knight, 1998: Secular trends of precipitation amount, frequency, and intensity in the United States. *Bull. Amer. Meteor. Soc.*, **79**, 231–241.

Konrad, C. E., II, 1997: Synoptic-scale features associated with warm season heavy rainfall over the interior southeastern United States. *Wea. Forecasting*, **12**, 557–571.

LeMone, M. A., 1983: Momentum transport by a line of cumulonimbus. *J. Atmos. Sci.*, **51**, 281–305.

Maddox, R. A., 1980: Mesoscale convective complexes. *Bull. Amer. Meteor. Soc.*, **61**, 1374–1387.

Maddox, R. A., C. F. Chappell, and L. R. Hoxit, 1979: Synoptic and meso-α scale aspects of flash flood events. *Bull. Amer. Meteor. Soc.*, **60**, 115–123.

Maddox, R. A., L. R. Hoxit, C. F. Chappell, and F. Caracena, 1978: Comparison of meteorological aspects of the Big Thompson and Rapid City flash floods. *Mon. Wea. Rev.*, **106**, 375–389.

Moore, J. T., F. H. Glass, C. E. Graves, S. M. Rochette, and M. J. Singer, 2003: The environment of warm-season elevated thunderstorms associated with heavy rainfall over the central United States. *Wea. Forecasting*, **18**, 861–878.

Moore, J. T., S. M. Nolan, F. H. Glass, D. L. Ferry, and S. M. Rochette, 1995: Flash flood–producing high–precipitation supercells in Missouri. Preprints, *14th Conference on Weather Analysis and Forecasting*, Dallas, TX, Amer. Meteor. Soc., (J4) 7–12.

NOAA, cited 2003: Natural hazard statistics. [Available online at http://www.nws.noaa.gov/om/hazstats.shtml].

Orlanski, I., 1975: A rational subdivision of scales for atmospheric processes. *Bull. Amer. Meteor. Soc.*, **56**, 527–530.

Owenby, J., R. Heim, Jr, M. Burgin, and D. Ezell, cited 2003: Climatography of the U.S. No. 81–Supplement # 3. [Available online at http://lwf.ncdc.noaa.gov/oa/documentlibrary/clim81supp3/clim81.html].

Parker, M. D., 1999: May 1996 and May 1997 linear mesoscale convective systems of the Central Plains: Synoptic meteorology and a reflectivity–based taxonomy. M.S. thesis,

Department of Atmospheric Science, Colorado State University, 185 pp. [Available from Department of Atmospheric Science, Colorado State University, Fort Collins, CO, 80523-1371.]

Parker, M. D., and R. H. Johnson, 2000: Organizational modes of midlatitude mesoscale convective systems. *Mon. Wea. Rev.*, **128**, 3413–3436.

Petersen, W. A., and Coauthors, 1999: Mesoscale and radar observations of the Fort Collins flash flood of 28 July 1997. *Bull. Amer. Meteor. Soc.*, **80**, 191–216.

Pettet, C. R., and R. H. Johnson, 2003: Airflow and precipitation structure of two leading stratiform mesoscale convective systems determined from operational datasets. *Wea. Forecasting*, **18**, 685–699.

Pontrelli, M. D., G. Bryan, and J. M. Fritsch, 1999: The Madison County, Virginia, flash flood of 27 June 1995. *Wea. Forecasting*, **14**, 384–404.

Rogash, J. A., and J. Racy, 2002: Some meteorological characteristics of significant tornado events occurring in proximity to flash flooding. *Wea. Forecasting*, **17**, 155–159.

Rogash, J. A., and R. D. Smith, 2000: Multiscale overview of a violent tornado outbreak with attendant flash flooding. *Wea. Forecasting*, **15**, 416–431.

Sanders, F., 1999: A proposed method of surface map analysis. *Mon. Wea. Rev.*, **127**, 945–955.

Schwartz, B. E., C. F. Chappell, W. E. Togstad, and X.-P. Zhong, 1990: The Minneapolis flash flood: Meteorological analysis and operational response. *Wea. Forecasting*, **5**, 3–21.

Smith, J. A., M. L. Baeck, Y. Zhang, and C. A. Doswell, 2001: Extreme rainfall and flooding from supercell thunderstorms. *J. Hydrometeor.*, **2**, 469–489.

Trier, S. B., and D. B. Parsons, 1993: Evolution of environmental conditions preceding

the development of a nocturnal mesoscale convective complex. *Mon. Wea. Rev.*, **121**, 1078–1098.

Wallace, J. M., 1975: Diurnal variations in precipitation and thunderstorm frequency over the conterminous United States. *Mon. Wea. Rev.*, **103**, 406–419.

Whiteman, C. D., X. Bian, and S. Zhong, 1997: Low-level jet climatology from enhanced rawinsonde observations at a site in the Southern Great Plains. *J. Appl. Meteor.*, **36**, 1363–1376.

Winkler, J. A., 1988: Climatological characteristics of summertime extreme rainstorms in Minnesota. *Annals, Assoc. Amer. Geographers*, **78**, 57–73.

Winkler, J. A., B. R. Skeeter, and P. D. Yamamoto, 1988: Seasonal variations in the diurnal characteristics of heavy hourly precipitation across the United States. *Mon. Wea. Rev.*, **116**, 1641–1658.

Yoshizaki, M., and Y. Ogura, 1988: Two-and three-dimensional modelling studies of the Big Thompson storm. *J. Atmos. Sci.*, **45**, 3700–3722.

Zhang, D.-L., and J. M. Fritsch, 1986: Numerical simulation of the meso–β scale structure and evolution of the 1977 Johnstown flood. Part I: Model description and verification. *J. Atmos. Sci.*, **43**, 1913–1944.

Zhang, D.-L., and J. M. Fritsch, 1987: Numerical simulation of the meso–β scale structure and evolution of the 1977 Johnstown flood. Part II: Inertially stable warm-core vortex and the mesoscale convective complex. *J. Atmos. Sci.*, **44**, 2593–2612.

Zhang, D.-L., and J. M. Fritsch, 1988: Numerical simulation of the meso–β scale structure and evolution of the 1977 Johnstown flood. Part III: Internal gravity waves and the squall line. *J. Atmos. Sci.*, **45**, 1252–1268.

Appendix A

INFORMATION ABOUT EXTREME RAIN EVENTS INCLUDED IN THIS STUDY

Table A.1: Information about each extreme rain event analyzed in this study. The first column is the date(s) on which the event occurred; the second is the state(s) where extreme rainfall totals were reported; the third is the number of stations that reported rainfall over the extreme threshold during the event; the fourth is the maximum 24-h rainfall report (mm); the fifth through seventh are the hours (local standard time) of heavy rain onset, peak rainfall, and rainfall end, respectively, for MCS and isolated events; and the eighth is the storm type classification. Events are in chronological order.

Date	State(s)	rpts	max rain	onset	peak	end	classification
1-2 Jan. 1999	LA	1	181.61	N/A	N/A	N/A	synoptic/convective
3 Jan. 1999	NY	3	124.71	N/A	N/A	N/A	synoptic/convective
21-22 Jan. 1999	IL	1	170.18	N/A	N/A	N/A	synoptic/convective
22-23 Jan. 1999	TN, AL	3	180.34	N/A	N/A	N/A	synoptic/convective
23-31 Jan. 1999	AR, TX, LA, MS, AL	15	250.19	N/A	N/A	N/A	synoptic/convective
11-12 Mar. 1999	LA	2	249.68	13	16	22	TL/AS MCS
13 Mar. 1999	TX	2	229.62	22	2	7	TL/AS MCS
22 Mar. 1999	NY, NH	2	153.16	N/A	N/A	N/A	synoptic/non-convective
3-5 Apr. 1999	AR, LA, TX	5	236.22	N/A	N/A	N/A	synoptic/convective
13-14 Apr. 1999	KS, OK	2	157.99	13	15	0	TL/AS MCS
24-25 Apr. 1999	OK	1	150.11	N/A	N/A	N/A	synoptic/convective
4-5 May 1999	ND	2	152.40	13	15	19	isolated
5-6 May 1999	MS	1	183.64	18	20	1	LL/TS MCS
6-7 May 1999	AL	1	166.37	13	16	8	BPS MCS
16-17 May 1999	IA, WI	3	157.48	12	19	0	TL/AS MCS
18-19 May 1999	PA	1	112.78	15	17	3	LL/TS MCS
1-2 June 1999	IL	1	127.76	19	22	3	LL/TS MCS
3 June 1999	SD	1	101.60	19	20	1	disorganized MCS
4 June 1999	NE	1	139.95	22	0	3	TL/AS MCS
6 June 1999	ND	1	110.49	N/A	N/A	N/A	synoptic/convective
10 June 1999	NE	1	123.19	18	20	2	TL/AS MCS
13 June 1999	IL	1	130.81	N/A	N/A	N/A	synoptic/convective
13-14 June 1999	MI	1	106.68	N/A	N/A	N/A	synoptic/convective
20 June 1999	OK	2	141.99	1	5	12	TL/AS MCS
25-26 June 1999	AR	1	163.07	19	23	3	disorganized MCS
25-27 June 1999	LA	3	282.70	N/A	N/A	N/A	synoptic/convective

Table A.1 continued.

Date	State(s)	rpts	max rain	onset	peak	end	classification
27 June 1999	KY	1	135.64	0	2	6	isolated
27-28 June 1999	KS	2	139.70	6	14	0	BPS MCS
28 June 1999	TN	1	167.89	22	0	2	LL/TS MCS
29-30 June 1999	GA, SC	3	194.31	6	10	20	sea-breeze front
1 July 1999	IL	1	152.40	7	14	17	BPS MCS
1-2 July 1999	OH	1	100.58	15	20	0	disorganized MCS
2-3 July 1999	IA	3	166.37	17	20	2	LS MCS
4 July 1999	NY	1	124.46	2	7	9	BPS MCS
5 July 1999	MN	4	154.18	20	22	3	TL/AS MCS
6 July 1999	MI	2	112.78	20	22	2	LL/TS MCS
7-8 July 1999	VA	1	114.30	14	16	20	LL/TS MCS
9-10 July 1999	KS	1	165.10	18	19	2	LL/TS MCS
10-11 July 1999	GA	1	151.13	17	19	0	disorganized MCS
13 July 1999	MN	1	127.51	21	23	3	BPS MCS
15 July 1999	MI	2	132.08	20	0	2	BPS MCS
18-19 July 1999	IA, WI, MN	4	146.05	18	1	6	BPS MCS
19-20 July 1999	NE	2	148.59	19	21	3	TL/AS MCS
20-21 July 1999	IA, WI	4	180.34	16	1	7	BPS MCS
25-26 July 1999	KS	1	175.77	15	17	0	isolated
25-26 July 1999	WI	2	142.24	17	19	23	LL/TS MCS
6-7 Aug. 1999	IA, NE	11	221.49	17	23	4	BPS MCS
8 Aug. 1999	MO	1	164.34	19	21	5	BPS MCS
12 Aug. 1999	SD, ND	8	128.02	20	22	2	LL/TS MCS
12-13 Aug. 1999	IL	1	129.03	19	22	2	PS MCS
20-21 Aug. 1999	PA	2	141.22	12	16	20	isolated
22-24 Aug. 1999	TX	4	406.40	N/A	N/A	N/A	tropical
24-25 Aug. 1999	IN, OH, WV, TN	7	147.32	N/A	N/A	N/A	synoptic/convective
26 Aug. 1999	NC	1	162.05	22	1	4	TL/AS MCS
29-31 Aug. 1999	NC	6	220.73	N/A	N/A	N/A	tropical
30 Aug. 1999	SD	2	181.36	20	22	5	LS MCS
3 Sept. 1999	SD	4	136.14	18	20	5	TL/AS MCS
3-4 Sept. 1999	SD	4	148.59	N/A	N/A	N/A	multiple MCSs
4-7 Sept. 1999	VA, NC, PA	10	195.07	N/A	N/A	N/A	tropical
10-11 Sept. 1999	MA, NH, ME	27	175.26	N/A	N/A	N/A	synoptic/non-convective
14-18 Sept. 1999	all eastern states	268	464.82	N/A	N/A	N/A	tropical
27 Sept. 1999	KS	1	146.81	20	0	5	BPS MCS
27-28 Sept 1999	NC	1	183.90	N/A	N/A	N/A	multiple MCSs
29-30 Sept 1999	VA	1	113.79	N/A	N/A	N/A	synoptic/convective
8-9 Oct. 1999	KY, LA, TN	3	186.69	N/A	N/A	N/A	synoptic/convective
17-18 Oct. 1999	VA, NC, SC	12	198.63	N/A	N/A	N/A	tropical
1-2 Nov. 1999	TN	1	153.67	N/A	N/A	N/A	synoptic/non-convective
2-4 Jan. 2000	IL, IN, KY	5	182.88	N/A	N/A	N/A	synoptic/convective
24-25 Jan. 2000	SC	1	203.20	N/A	N/A	N/A	synoptic/non-convective
18-19 Feb. 2000	KY	1	127.51	N/A	N/A	N/A	synoptic/convective
10-11 Mar. 2000	TN	1	145.54	14	16	22	BPS MCS
21-22 Mar. 2000	NJ, PA	4	132.84	N/A	N/A	N/A	synoptic/non-convective
22-23 Mar. 2000	KS, TX	3	153.67	17	22	10	TL/AS MCS
1-3 Apr. 2000	MS, AL	2	200.91	N/A	N/A	N/A	synoptic/convective

Table A.1 continued.

Date	State(s)	rpts	max rain	onset	peak	end	classification
17-18 Apr. 2000	VA	1	116.84	12	15	3	disorganized MCS
19 Apr. 2000	SD	2	128.52	N/A	N/A	N/A	synoptic/non-convective
20-21 Apr. 2000	MI	1	101.60	N/A	N/A	N/A	synoptic/convective
21-22 Apr. 2000	NY, ME	3	119.38	N/A	N/A	N/A	synoptic/convective
24 Apr. 2000	GA	1	176.53	10	13	19	PS MCS
3 May 2000	LA	1	181.86	2	8	13	BPS MCS
6 May 2000	OK	1	170.18	20	4	11	TL/AS MCS
7 May 2000	MO	3	308.61	22	2	9	BPS MCS
17-18 May 2000	MN, MI	2	128.78	N/A	N/A	N/A	synoptic/convective
19-20 May 2000	TX	1	223.52	21	0	6	LL/TS MCS
24-25 May 2000	KY, TN	3	147.32	17	20	4	BPS MCS
1 Jun. 2000	IA, MN, WI	6	151.89	19	23	9	TL/AS MCS
4 June 2000	TX	3	281.43	18	22	8	LS MCS
5-7 June 2000	NY, MA	10	135.89	N/A	N/A	N/A	synoptic/non-convective
12-14 June 2000	ND	6	164.59	15	21	5	BPS MCS
16-17 June 2000	MO, IL	6	175.26	N/A	N/A	N/A	synoptic/convective
16-17 June 2000	OH	1	127.00	18	21	6	LL/TS MCS
19-20 June 2000	ND, MN	4	150.62	18	23	3	BPS MCS
23-24 June 2000	KS, MO, IA, NE, IL	11	165.35	15	20	4	TL/AS MCS
3-4 July 2000	NE	3	133.35	15	22	8	LS MCS
5 July 2000	IL	1	133.35	19	0	9	disorganized MCS
5-6 July 2000	IA	1	135.38	22	0	5	TL/AS MCS
8 July 2000	WI	1	210.06	23	5	15	TL/AS MCS
8-9 July 2000	WI	1	207.77	14	20	3	BPS MCS
10 July 2000	IA	5	158.75	23	2	6	LL/TS MCS
10 July 2000	IL	1	133.35	22	1	8	TL/AS MCS
12 July 2000	MO	1	139.70	1	3	8	TL/AS MCS
15-16 July 2000	NY, MA, VT, NH, ME	11	155.45	N/A	N/A	N/A	synoptic/convective
23-24 July 2000	VA, NC	3	183.90	16	20	7	disorganized MCS
29-30 July 2000	OH	1	123.70	12	17	3	disorganized MCS
30-31 July 2000	PA	1	114.30	18	19	0	isolated
3-4 Aug. 2000	NY	1	111.51	11	15	17	BPS MCS
5 Aug. 2000	SD	3	140.97	19	0	5	disorganized MCS
6-7 Aug. 2000	PA	2	121.92	N/A	N/A	N/A	multiple MCSs
11-12 Aug. 2000	MA	2	146.05	18	20	3	disorganized MCS
12 Aug. 2000	NJ	1	137.67	8	12	21	isolated
14-15 Aug. 2000	WI	2	136.40	16	20	0	TL/AS MCS
26-27 Aug. 2000	KY	1	172.72	N/A	N/A	N/A	multiple MCSs
1 Sept. 2000	AL	2	173.23	5	8	14	isolated
1-2 Sept 2000	MI	3	190.50	14	17	23	BPS MCS
6 Sept. 2000	GA	1	157.48	N/A	N/A	N/A	synoptic/non-convective
11 Sept. 2000	WI	3	171.20	20	0	4	PS MCS
11-12 Sept. 2000	MD	1	121.92	17	18	21	isolated
11-12 Sept. 2000	MI	1	121.41	N/A	N/A	N/A	multiple MCSs
15 Sept. 2000	NH	1	100.33	N/A	N/A	N/A	synoptic/non-convective
18 Sept. 2000	NC, SC	3	181.61	N/A	N/A	N/A	tropical
22-23 Sept 2000	SC	1	203.71	N/A	N/A	N/A	tropical
4-5 Oct. 2000	IL	2	163.32	14	21	8	TL/AS MCS
22-23 Oct. 2000	OK	5	232.41	13	22	6	TL/AS MCS

Table A.1 continued.

Date	State(s)	rpts	max rain	onset	peak	end	classification
23-24 Oct. 2000	TX	1	172.47	7	11	3	disorganized MCS
24-25 Oct. 2000	OK	2	150.37	16	20	13	disorganized MCS
26 Oct. 2000	OK	1	144.78	2	7	13	disorganized MCS
27-28 Oct. 2000	OK	1	149.10	14	16	20	isolated
2-4 Nov. 2000	TX	2	205.74	N/A	N/A	N/A	synoptic/convective
5-6 Nov. 2000	OK	3	152.40	N/A	N/A	N/A	synoptic/convective
18-19 Nov 2000	LA	1	252.73	N/A	N/A	N/A	synoptic/non-convective
24 Nov. 2000	AR	2	161.29	N/A	N/A	N/A	synoptic/non-convective
16 Dec. 2000	TN	1	139.70	N/A	N/A	N/A	synoptic/convective
15-17 Feb 2001	AR, AL	2	154.18	N/A	N/A	N/A	synoptic/convective
1-4 Mar. 2001	MS, AL	4	194.31	N/A	N/A	N/A	synoptic/convective
21-22 Mar. 2001	MA, NH	9	126.75	N/A	N/A	N/A	synoptic/non-convective
27-28 Mar. 2001	TX	2	223.27	N/A	N/A	N/A	synoptic/non-convective
29-30 Mar. 2001	NY, MA	3	150.37	N/A	N/A	N/A	synoptic/non-convective
4-5 Apr. 2001	MS	2	253.24	N/A	N/A	N/A	TL/AS MCS
4-5 May 2001	TX	4	234.95	16	22	5	TL/AS MCS
4-5 May 2001	NE	1	147.83	N/A	N/A	N/A	synoptic/convective
6-7 May 2001	AR	1	223.77	15	17	2	isolated
14-16 May 2001	MI	4	123.44	22	2	9	TL/AS MCS
30 May 2001	OK	2	151.38	23	2	9	LL/TS MCS
31 May 2001	LA	1	178.31	10	12	18	sea-breeze front
1-2 June 2001	VA	1	113.54	N/A	N/A	N/A	synoptic/convective
3 Jun. 2001	MO	1	139.19	2	4	12	TL/AS MCS
5-6 June 2001	NC	1	165.10	21	23	2	LL/TS MCS
5-11 June 2001	TX, LA, MS, AL	87	497.33	N/A	N/A	N/A	tropical
6 June 2001	MO	1	144.78	1	5	11	LL/TS MCS
12-13 June 2001	IA	1	125.48	16	20	3	TL/AS MCS
12-14 June 2001	SC, GA	2	177.80	N/A	N/A	N/A	tropical
15-16 June 2001	VA, NC	3	239.27	N/A	N/A	N/A	tropical
16-18 June 2001	PA, NY, MA	13	128.02	N/A	N/A	N/A	synoptic/convective
19-20 June 2001	KS	1	209.55	12	18	3	BPS MCS
27-28 June 2001	GA	1	149.86	16	20	1	isolated
8 July 2001	WV	3	124.71	6	12	14	BPS MCS
17-18 July 2001	OH	3	132.33	17	22	3	PS MCS
19 July 2001	MO	1	147.57	6	10	13	TL/AS MCS
25 July 2001	GA	2	158.50	2	3	11	disorganized MCS
25 July 2001	OH	1	101.35	2	5	11	isolated
26 July 2001	KY	1	137.16	21	4	8	BPS MCS
26 July 2001	MS	2	182.88	7	9	17	sea-breeze front
26-27 July 2001	NE	1	150.62	16	17	21	LS MCS
26-27 July 2001	ND	2	114.81	16	21	3	disorganized MCS
26-27 July 2001	WV	3	134.87	6	14	19	disorganized MCS
28-30 July 2001	KY, WV	4	170.69	N/A	N/A	N/A	synoptic/convective
1 Aug. 2001	MN	3	165.10	12	19	23	TL/AS MCS
1-2 Aug. 2001	WI	7	154.18	20	0	7	BPS MCS
2 Aug. 2001	MI	1	113.79	19	21	1	BPS MCS
3-4 Aug. 2001	MA	1	106.93	15	17	23	isolated
4-5 Aug. 2001	PA	1	121.92	11	15	22	isolated
11 Aug. 2001	VA, MD, DC	2	136.14	14	16	21	disorganized MCS
11-12 Aug. 2001	OH	1	116.08	19	21	0	isolated

Table A.1 continued.

Date	State(s)	rpts	max rain	onset	peak	end	classification
12-13 Aug. 2001	MD, PA	2	147.32	16	18	23	disorganized MCS
19 Aug. 2001	MI	1	104.14	N/A	N/A	N/A	synoptic/convective
22-23 Aug 2001	IA, IL	6	220.22	16	22	3	BPS MCS
25-26 Aug. 2001	MI	1	102.11	18	23	1	disorganized MCS
27 Aug. 2001	TX	1	184.15	17	19	6	disorganized MCS
30-31 Aug. 2001	TX	12	251.46	9	21	5	sea-breeze front
1 Sept. 2001	VT	1	134.37	16	19	2	LL/TS MCS
3 Sept. 2001	AL	1	159.51	1	8	13	disorganized MCS
4 Sept. 2001	TX	1	191.01	6	10	16	isolated
7-8 Sept 2001	IA	1	130.30	N/A	N/A	N/A	multiple MCSs
8-9 Sept 2001	AR, TX	4	221.49	15	21	5	LL/TS MCS
18-19 Sept 2001	NE	1	115.06	4	6	11	isolated
24-25 Sept 2001	PA, NY	7	127.51	N/A	N/A	N/A	synoptic/convective
10-11 Oct 2001	AR, TX, MS	6	244.09	N/A	N/A	N/A	synoptic/convective
12-13 Oct 2001	LA	1	186.69	N/A	N/A	N/A	multiple MCSs
13-14 Oct 2001	TN	1	142.24	N/A	N/A	N/A	synoptic/convective
15-17 Nov 2001	TX	11	235.46	N/A	N/A	N/A	synoptic/convective
24-25 Nov 2001	AL	2	196.60	18	22	8	LS MCS
27-30 Nov 2001	KY,AR,LA,TN,TX,MS	21	304.80	N/A	N/A	N/A	synoptic/convective
15-17 Dec 2001	KY, TN, TX	8	221.74	N/A	N/A	N/A	synoptic/convective